Modeling the Transient Behavior of a Run-around Heat and Moisture Exchanger System

A Thesis Submitted to the College of

Graduate Studies and Research

In Partial Fulfillment of the Requirements

For the Degree of Master of Science

In the Department of Mechanical Engineering

University of Saskatchewan

Saskatoon

By

Mehran Seyed Ahmadi

© Copyright Mehran Seyed Ahmadi, November, 2008. All rights reserved.

Permission to Use

In presenting this thesis in partial fulfilment of the requirements for a Postgraduate degree from the University of Saskatchewan, I agree that the Libraries of this University may make it freely available for inspection. I further agree that permission for copying of this thesis in any manner, in whole or in part, for scholarly purposes may be granted by the professor or professors who supervised my thesis work or, in their absence, by the Head of the Department or the Dean of the College in which my thesis work was done. It is understood that any copying or publication or use of this thesis or parts thereof for financial gain shall not be allowed without my written permission. It is also understood that due recognition shall be given to me and to the University of Saskatchewan in any scholarly use which may be made of any material in my thesis.

Requests for permission to copy or to make other use of material in this thesis in whole or part should be addressed to:

Head of the Department of Mechanical Engineering

University of Saskatchewan

57 Campus Drive

Saskatoon, Saskatchewan (S7N 5A9)

ABSTRACT

In this thesis, a numerical model for coupled heat and moisture transfer in a run-around membrane energy exchanger (RAMEE) with a liquid desiccant as a coupling fluid is developed. The numerical model is two dimensional, transient and is formulated using the finite difference method with an implicit time discretization. The model for the case of only heat transfer for a single heat exchanger is compared to an available analytical solution and good agreement is obtained. It is shown that the discrepancy between the numerical and theoretical dimensionless bulk outlet temperature of the fluids is less than 4% during the transient period. The model is also validated for the case of simultaneous heat and moisture transfer using experimental data measured during the laboratory testing of a RAMEE system. The results for both sensible and latent effectiveness showed satisfactory agreement at different operating conditions. However, there are some discrepancies between the simulation and the experimental data during the transient times. It is proposed that these discrepancies may be due to experimental flow distribution problems within the exchanger. The maximum average absolute differences between the measured and simulated transient effectivenesses were 7.5% and 10.3% for summer and winter operating conditions, respectively.

The transient response of the RAMEE system for step changes in the inlet supply air temperature and humidity ratio is presented using the numerical model. In addition, the system quasi-steady state operating conditions are predicted as the system approaches its steady state operating condition. The effect of various dimensionless parameters on the

transient response is predicted separately. These included: the number of heat transfer units, thermal capacity ratio, heat loss/gain ratio, storage volume ratio and the normalized initial salt solution concentration. It is shown that the initial salt solution concentration and the storage volume of the salt solution have significant impacts on the transient response of the system and the heat loss/gain rates from/to the circulated fluid flow can change the system quasi-steady effectiveness substantially. The detailed study of the transient performance of the RAMEE is useful to determine the transient response time of the system under different practical situations.

ACKNOWLEDGMENTS

I would like to express my deep and sincere gratitude to my supervisors Professor R.W. Besant and Professor C. J. Simonson. Thank you for your help and inspiration throughout this research. It was not possible to accomplish this work without your support and guidance. I wish to thank my family for their love and encouragement.

I would like to acknowledge financial assistance from the Natural Science and Engineering Research Council of Canada (NSERC) and Venmar CES, Saskatoon.

Dedication

I dedicate this thesis to my parents, Mojtaba and Maryam
Thank you very much for your love and support throughout my life

TABLE OF CONTENTS

page

LIST OF TABLES

LIST OF FIGURES

NOMENCLATURE

ACRONYMS

AHRI	Air-conditioning Heating and Refrigerating Institute
ASHRAE	American Society of Heating, Refrigerating and Air-Conditioning Engineers
HVAC	Heating, Ventilation and Air-Conditioning
LCC	Life-Cycle Cost
LAMEE	Liquid-to-Air Membrane Energy Exchanger
IAQ	Indoor Air Quality
RMSE	Root Mean Square Error
RAMEE	Run-Around Membrane Energy Exchanger
RAMEETA	Run-Around Membrane Energy Exchanger Testing Apparatus

ENGLISH SYMBOLS

A	ratio of water mass to mass of salt solution, kg/kg
A_c	cross section area of a channel, m^2
B	coefficient used for salt solution heat capacity correlation
b	coefficient used for salt solution density correlation
C	heat capacity rate, W/K
C_{Salt}	concentration of salt solution (kg of salt per kg of solution), %
$C_{Salt,Initial}$	initial salt solution concentration, (%)
$C_{Salt,Steady\ state}$	salt solution concentration at steady state condition, (%)
c_p	specific heat capacity, J/(kg·K)

D	coefficient used for salt solution density correlation
D_h	hydraulic diameter, m
d	channel thickness, mm
E	coefficient used for salt solution heat capacity correlation
F, G	Anzelius - Schuman functions
f	general function
H	enthalpy, J/kg
H^*	operating condition factor that represents the ratio of latent to sensible energy differences between the inlets of airstreams
h	convective heat transfer coefficient, $W/(m^2 \cdot K)$
h_{fc}	net heat of phase change
h_m	convective mass transfer coefficient, $kg/(m^2 \cdot s)$
I	ionic strength, mol/kg
I_r	modified Bessel functions of the first kind r^{th} order
K	electrolyte parameter
k	thermal conductivity, W/(m·K)
k_m	water vapor permeability of membrane, kg/(m·s)
Le	Lewis number
M	mass, kg
M_s	molecular weight of solvent, g/mol
m	number of spatial nodes in x (or y) direction
$\dot{m}$	mass flow rate, kg/s
m'	molality, mol/kg

N	number of data points in the transient solution used to compare numerical results with experimental data
NTU	number of heat transfer units for each exchanger
NTU_m	number of mass transfer units for each exchanger
Nu	Nusselt number
n	number of liquid desiccant (or air channels)
P	total pressure, Pa
Pe	Peclet number
Pr	prandtl number
p	partial pressure, Pa
Q	pump volume flow rate, m^3/s
q	heat loss/gain rate, W
Re	Reynolds number
Sh	Sherwood number
T	temperature, K
T_0	reference temperature, K
t	time, s
t^*	dimensionless time defined relative to time required for the resident fluids to be replaced by the incoming fluids within a exchanger
U	overall heat transfer coefficient, $W/(m^2 \cdot K)$
U_m	overall mass transfer coefficient, $kg/(m^2 \cdot s)$
U^1	Heaviside step function

V	velocity, m/s
v	number of moles of cation (or anion)
W	humidity ratio, kg_v/kg_{Air}
X	ratio of water mass to mass of pure salt, kg/kg
X'	the mass content of a component in a binary isopiestic solution in kilograms of the substance per kilogram of solution, kg/kg
Z	charge of cation (anion)
x, y, z	coordinates
x_0, y_0, z_0	exchanger dimensions, m
x^*, y^*	dimensionless coordinates

GREEK SYMBOLS

α	dimensionless parameter which represents different dwell time for each fluid within a single heat exchanger
β	empirical coefficient used for salt solution thermal conductivity correlation
δ	thickness of membrane, mm
Δ	difference
ΔH_{Sol}	heat of solution, J/kg
ε	effectiveness
$\bar{\varepsilon}$	average effectiveness
η	number of liquid desiccant circulation within both exchangers of a run-around system required to reach quasi-steady state condition

η'	time required for the RAMEE to reach quasi-steady state condition, min.
θ	dimensionless temperature used for the analytical/numerical comparison of a single heat exchanger
μ	initial ratio of mass of salt (or solution) in the two exchangers to total mass of salt (or solution) in the system
ρ	density, kg/m^3
ρ_{Salt}	mass of salt (kg) per unit volume (m^3) of salt solution
σ	heat loss/gain ratio which represents heat loss/gain rate relative to energy transfer rate within a exchanger
τ	dimensionless time of a run-around system defined relative to the transport time for the bulk solution to flow through both exchangers
τ'	time required for the bulk salt solution to flow through both exchangers once in a run-around system, min.
τ^*	dimensionless time used for the analytical/numerical comparison of a single heat exchanger
φ	uncertainty
ψ, ω	general properties

SUBSCRIPT

Air	air side
a	fluid "a" in the analytical comparison of a single heat exchanger
b	fluid "b" in the analytical comparison of a single heat exchanger

E	exhaust side
ex	exchanger
f	fluid
g	moist air
Indoor	indoor condition
i	component "i" in multi component solution
in	inlet
L	liquid
l	latent
out	outlet
S	supply side
Salt	pure salt
Sol	salt solution
s	sensible
st	storage tank
t	total
v	water vapor
w	water

SUPERSCRIPT

i	value of a variable at the current node
j	value of a variable at the current iteration
k	value of a variable at the current time step

CHAPTER 1
INTRODUCTION

1.1 Overview

In developed countries, most people spend more than 90% of their time in buildings where it is necessary to maintain the indoor environment within comfortable conditions for the occupants (ANSI/ASHRAE Standard 55-2004). Recently several studies have shown a strong relationship between ventilation rate, which impacts indoor air quality, and occupant productivity (Fang et al., 2000; Kosonen and Tan, 2004). Adequate fresh outdoor air is required to maintain satisfactory indoor air quality and to provide a healthy and comfortable environment. ANSI/ASHRAE Standard 62.1-2004 recommends at least 8.5 L/(s person) of outdoor air for most occupied office buildings. Conditioning outdoor ventilation air can comprise a large part of the total space-conditioning load. Without exhaust air energy recovery, the energy required to condition ventilation air typically constitutes 20 to 40 % of the annual thermal load for typical commercial buildings (ASHRAE, 2005) and this can be even higher in hospitals, schools and recreational facilities that require 100% fresh air and no circulated air to meet ventilation standards. These facts combined with the increasing cost of energy and environmental concerns imply that new ways should be developed for energy use in buildings to be conserved or made more efficient.

Energy can be recovered from the exhaust air of the ventilation system to increase the energy efficiency of buildings. Since both the temperature and relative humidity should

be controlled in buildings to provide comfortable conditions for the people, recovery of both thermal or sensible energy and moisture or latent energy is important. Air-to-air energy recovery in buildings has been shown to provide considerable energy savings and can decrease the required size of heating and cooling equipment by transferring heat and moisture between the supply side and the exhaust side of the ventilation system (Fauchoux et al., 2007).

There are many devices commercially available that have the ability to transfer energy between the supply and exhaust air ducts of a building. According to (ASHRAE, 2004), the ideal air-to-air energy recovery system is one that has the following characteristics:

- Allows heat transfer between exhaust and supply air streams (i.e. sensible energy transfer as indicated by a temperature change).
- Allows moisture transfer between exhaust and supply air streams (i.e. latent energy transfer as indicated by a vapor pressure change).
- Allows no significant transfer of air which includes other gases, pollutants, biological contaminants and particulates.

There are several different ways to classify air-to-air exchangers. As shown in Figure 1-1 (Larson, 2006), currently available air-to-air energy exchangers can be divided into four main groups. First, air-to-air energy exchangers can be categorized based on their ability to transfer both heat and moisture which are named energy recovery systems or only heat which are named heat recovery systems.

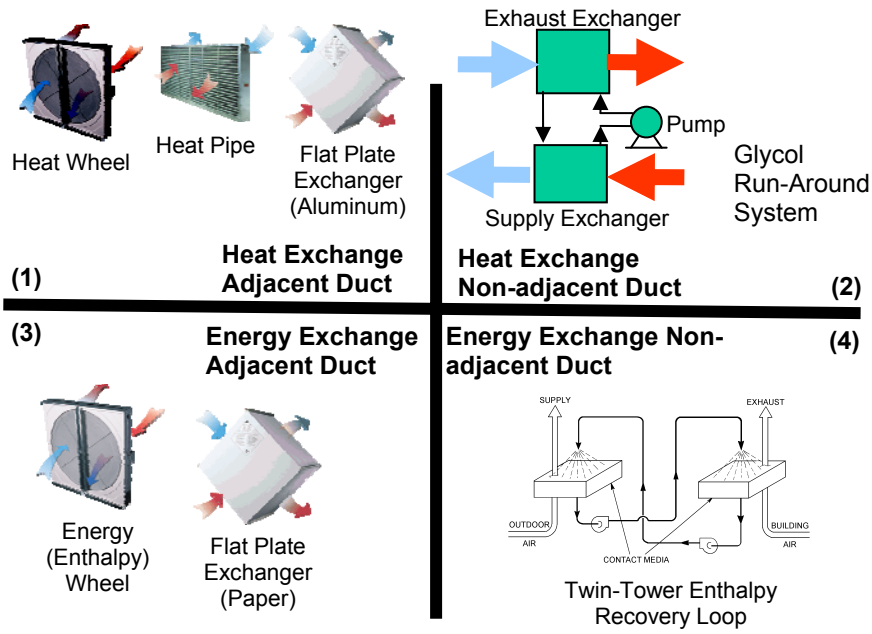

Figure 1-1. Four Main Categories of Air-to-Air Energy Exchangers and their samples (Larson, 2006).

The heat and energy recovery devices or systems are split by the horizontal line in Figure 1-1 with heat recovery only on the top and both heat and moisture recovery on the bottom. In general, energy recovery devices are more desirable than heat recovery devices because of their capability to transfer latent energy as well as sensible energy. As shown in Figure 1-2, during (AHRI, 2005) hot and humid summer test conditions, the total energy recovered by a 75 % effective heat and moisture exchanger is almost three times higher than energy recovered by a 75% effective heat exchanger for the same conditions. The implication is that the total energy savings achieved from an energy recovery system is significantly greater than heat recovery alone for summer conditions. During winter, this figure shows the savings to be large for sensible energy but smaller for both heat and moisture recovery compared to summer test conditions.

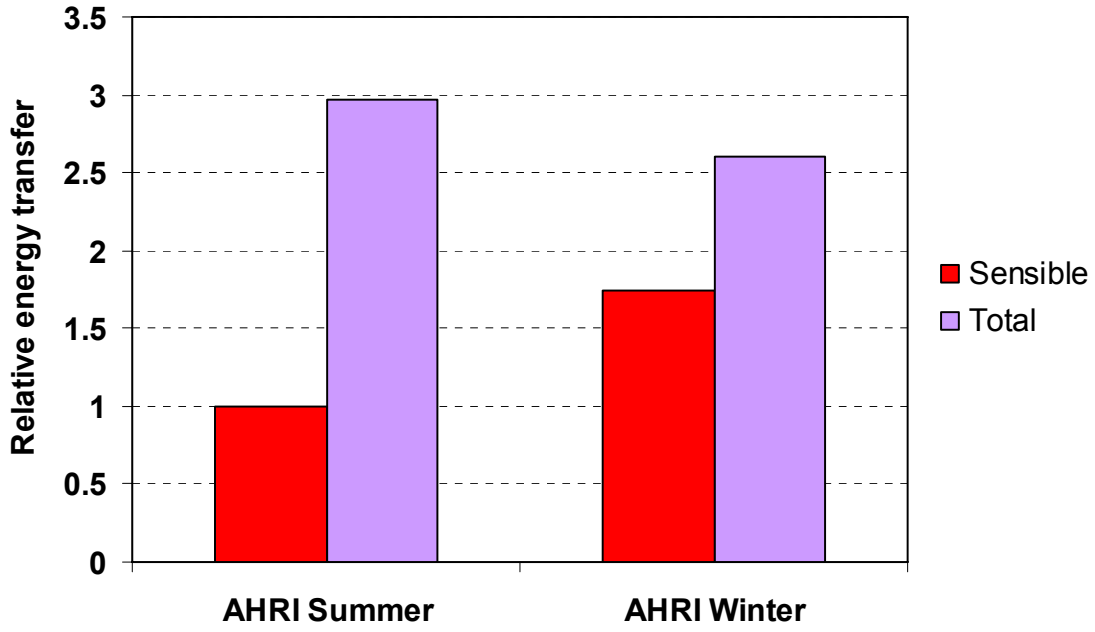

Figure 1-2. Comparison between sensible and total energy recovery during AHRI summer and winter test conditions normalized so that the AHRI summer sensible energy recovery = 1.

The second method to classify air-to-air energy recovery systems is according to their ducting arrangement. As shown in Figure 1-1, the left side of the vertical line represents devices or systems that require the supply and exhaust ducts to be side-by-side. Systems that allow the supply and exhaust ducts to be located remotely from each other are shown on the right hand side. The remote exchangers, one in the ventilation air stream and the other in the exhaust air stream, allow this type of system to be applied in retrofit applications without large additional ducting costs. In addition, carryover and cross-flow leakage of air through seals, which are concerns for their possible health effects for some applications such as health care facilities, can be avoided when the exhaust and supply air ducts are far apart.

All of the exchangers shown in Figure 1-1 have their advantages and limitations. They are usually chosen based on the criteria of performance, initial cost and operating and maintenance cost. The heat exchangers with adjacent ducts such as heat pipes, fixed plates and heat wheels shown in quadrant 1 are the most common type of air-to-air energy recovery systems due to their low first costs and good performance. A heat pipe exchanger (Wu et al., 1997) has no moving parts, however, the effectiveness is limited and the pressure drop of the air side is often quite large [up to 500 Pa (2 inches of water)] (Besant and Simonson, 2003). Heat wheels are compact and have a low pressure drop but some contaminant transfer from one air stream to the other may occur due to adjacent ducting. Flat (fixed) plate exchanges have no moving parts and may recover up to 80% of the available waste exhaust heat (ASHRAE, 2004) however 60 to 70% is common. As well, plate exchangers need to be manufactured in large sizes where higher flow rates are required and this increases the pressure drop.

The run-around heat recovery system shown in quadrant 2 of Figure 1-1 is a system that contains two liquid-to-air heat exchangers (e.g. coil exchangers) where one is located in the supply airstream and the other one is in the exhaust air stream. The coupling liquid is typically aqueous-glycol which is pumped in a closed loop between the exchangers to transfer sensible heat. Non-adjacent ducting allows this type of exchanger to be applied conveniently in retrofit applications.

As shown in quadrant 3, flat plate heat exchangers can be made from water vapor permeable membranes to transfer both heat and moisture (Niu and Zhang, 2001). The other devices in this category are energy wheels that have been studied for two decades and are well established technology (Simonson and Besant, 1999a, Simonson and

Besant, 1999b). Energy wheels can transfer both heat and moisture between supply and exhaust airstreams in buildings, but are limited to applications where the supply and exhaust air ducts are adjacent. As shown in quadrant 4 of Figure 1-1, there is only one system named the twin-tower enthalpy recovery system that is commercially available and is able to transfer both heat and moisture between remotely located supply and exhaust air streams. However, the lack of published performance data, the large size of this system and the problem of liquid droplets including desiccant salts transported downstream by the air flow present limitations for the application of the twin-tower enthalpy recovery loop for HVAC applications.

Based on an ideal air-to-air recovery system criteria, all the aforementioned energy recovery systems have some disadvantages along with their advantages. This implies the need for a system that is capable of heat and moisture transfer between remotely located air streams without cross contamination. The desire to develop such a system resulted in the research proposal for a run-around energy recovery system that consists of exchangers constructed with semi-permeable membranes and coupled with a liquid desiccant pumped in a closed loop between the exchangers to transfer simultaneously both heat and water vapor.

1.2 Background of the Run-around Membrane Energy Exchanger (RAMEE)

Plate exchangers, made with water vapor permeable membranes to transfer both heat and moisture, have been proposed as a recent alternative to energy wheels to transfer heat and water vapor between two air streams (Niu and Zhang, 2001; Zhang and Niu, 2002), but require the supply and exhaust ducts to be located side-by-side. A Run-Around

Membrane Energy Exchanger (RAMEE), shown schematically in Figure 1-3, has been suggested as a new system for energy recovery (Fan et al., 2006).

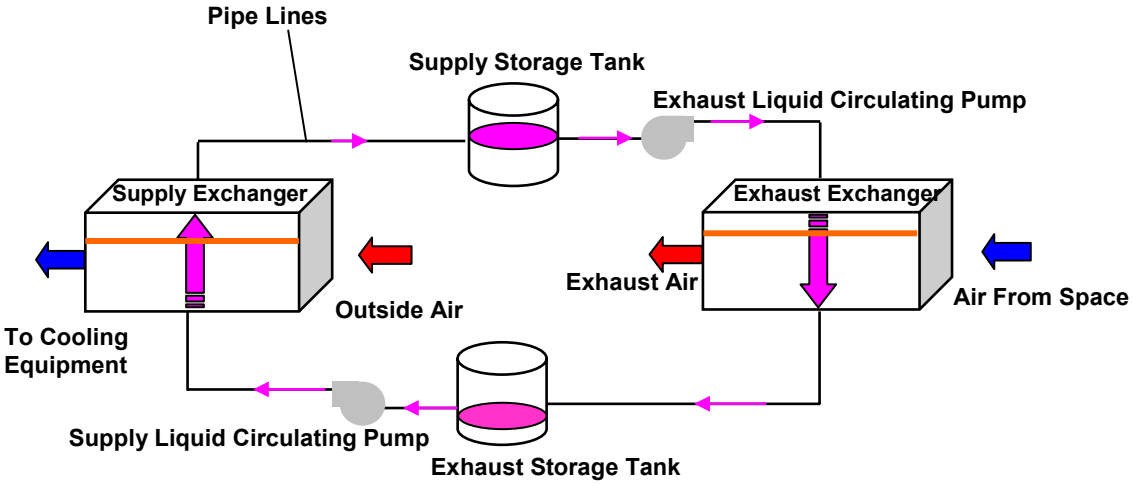

Figure 1-3. Schematic of the run-around membrane energy exchanger (RAMEE) system.

The RAMEE system uses semi-permeable membranes in each exchanger with an aqueous salt solution used as a coupling liquid pumped between the exchangers to transfer heat and water vapor simultaneously between the supply and exhaust air streams (Larson et al., 2007). The liquid desiccant is continuously circulated between the supply and exhaust exchangers as shown in Figure 1-3. The salt solution transports heat or sensible energy, as well as water vapor, between the two air streams. In a typical ventilation system, building supply air is heated and humidified during winter operation and cooled and dehumidified during summer operation. Compared to rotary energy or enthalpy wheels, which recover both heat and moisture between adjacent ducts, the RAMEE system may be more convenient to apply in retrofit applications where supply and exhaust ducts are remotely located. The only moving parts are liquid pumps and the

run-around fluid. Carryover and cross flow leakages of air, which are a concern for rotary wheels, should be negligible in the RAMEE system.

The system described above has been numerically modeled by Fan (2005). A two dimensional, steady-state mathematical model was developed to study the heat and water vapour transport in a RAMEE system with a lithium bromide salt solution for heat and moisture recovery. The system is comprised of two cross flow exchangers, one in each air stream. It was shown that an overall effectiveness of 70% can be achieved when the run-around exchanger sizes and operating conditions are correctly chosen.

Based on promising results obtained from the numerical model of Fan (2005), an initial prototype was built (Hemingson, 2005) using Tyvek as the membrane as shown in Figure 1-4. The testing of this prototype was unsuccessful because of excessive membrane deflection due to the liquid desiccant pressure which resulted in blockage of the air flow channels and a low effectiveness values. The penetration of liquid desiccant through the membrane to the air was another issue in this design. Larson (2006) addressed problems with the first prototype by focussing on the material properties of semi-permeable membranes required for each liquid-to-air membrane energy exchanger (LAMEE) in the RAMEE system. The characteristic such as the air permeability and the liquid penetration of different membranes were determined.

Figure 1-4. RAMEE Prototype 1 (Hemingson, 2005).

Erb (2006) and Erb (2007) used the findings of the previous researchers to design and build new exchanger prototypes shown in Figure 1-5. The performance of the RAMEE system with two identical cross flow heat exchangers was measured under laboratory testing conditions (Erb, 2006; Erb, 2007). The laboratory testing results showed that the system effectiveness was lower than the predicted values by Fan et al. (2006) at AHRI summer operating conditions. In addition, large transient times were observed especially during AHRI winter operating conditions. These unforeseen problems and discrepancies between the numerical and experimental results have implied the need for more research on topics such as new exchanger designs, experimental testing and simulation studies for the RAMEE system.

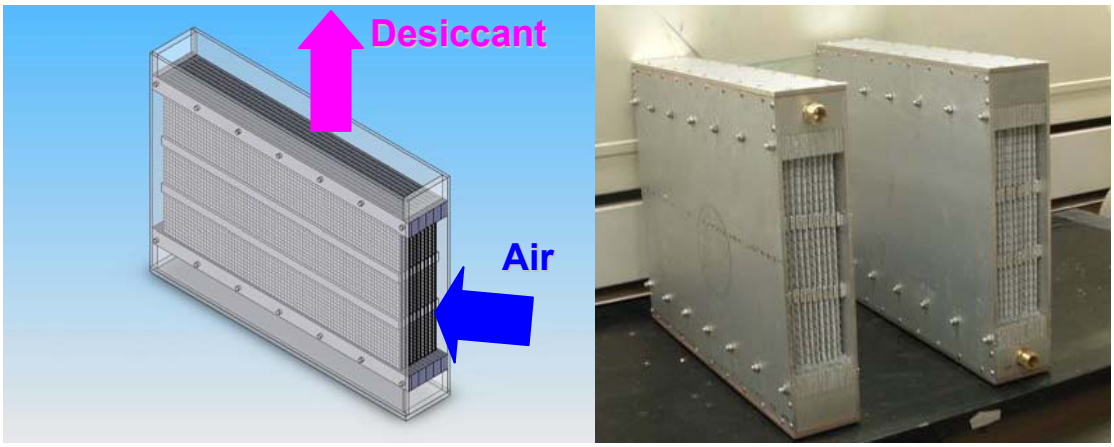

Figure 1-5. RAMEE Prototype 2 (Erb, 2006; Erb, 2007).

1.3 Literature Review

Many research papers have been written on the performance of flat-plate heat exchangers and their transient response in transferring heat. Also, there are quite a few studies on the run-around heat recovery system. The performance of direct-contact cross-flow exchangers with the ability of transferring both heat and water vapour as a humidifier/regenerator is also presented in the published literature. In recent years, the behaviour and performance of these types of exchangers using semi-permeable membranes in run-around energy recovery applications has attracted more researchers. A brief literature review for the abovementioned devices or systems is presented in the following sections.

1.3.1 Cross Flow Plate Heat Exchangers

Cross flow heat exchangers have been widely used in industry. Therefore, accurate prediction of the steady-state thermal performance of these exchangers is required. Many research papers have been written on modeling the performance of heat exchangers, especially for simple configurations, such as plate exchangers. Correlations are readily available in heat transfer textbooks (Incropera and Dewitt, 2002) for design proposes.

The simulation of cross flow heat exchangers based on the assumption of ideal plug flow may significantly deviate from a real case in which the flow field has large axial heat or sensible energy dispersion. Luo and Roetzel (1998) developed an analytical solution for the sensible effectiveness and temperature distribution in cross flow heat exchangers with axial dispersion in one fluid. Constant thermal properties, heat transfer coefficients and dispersion coefficients were assumed in their work. This investigation showed that the influence of axial dispersion on temperature effectiveness is significant for low Peclet numbers (i.e. $Pe < 20$) and this effect increases as the Number of Transfer Units (NTU) increases. In the current study, the effect of axial dispersion in the exchanger has been neglected, because in most of the simulations, Pe is greater than 20.

The transient response of heat exchangers is required to develop control strategies for different HVAC systems. Operational difficulties caused by start-up, shutdown and system failure have motivated investigations of the transient response of cross flow heat exchangers. Several analytical and numerical studies have analyzed the transient response of cross flow heat exchangers. Romie (1983) analyzed the transient outlet temperature of two unmixed fluids leaving a cross flow exchanger. Using Laplace transforms, the response was found with large wall capacitance effects with respect to that for the fluids for a step change in the inlet temperature of either fluid. In another study, Spiga and Spiga (1987) developed an analytical solution for the transient two-dimensional temperature distribution for the exchanger wall and both gases, for cross flow heat exchangers with neither gas mixed using the Laplace transform method. The solutions are applicable for the case of a large wall capacitance and are presented as integrals of the modified Bessel function in time and space for the response to a step,

ramp and exponential excitations. Spiga and Spiga (1988) presented solutions for the two-dimensional transient temperatures following a deltalike excitation at the inlet of the primary fluid. The assumption of large wall capacitance was no longer made in this analysis and with finite wall capacitance the solutions were provided as integrals of Green's function using the threefold Laplace transform method.

Romie (1994) gave the transient response of cross flow heat exchangers for which the thermal capacitance of the wall is negligible compared to the ones for the fluids. A step input disturbance was provided in the hot fluid inlet temperature where a threefold Laplace transform was used to solve the energy balance equations for two fluids. The analytical solution developed by Romie (1994) is employed to verify the numerical model for a single heat exchanger in the current study.

Mishra et al. (2004) studied the transient behavior of cross flow heat exchangers by solving a mathematical model using the finite difference method. The thermo-physical properties of the fluids were assumed to be constant. Also, the model was based on the bulk temperature of fluids within the channels. The dynamic performance of the heat exchanger was investigated in response to step, ramp, and exponential excitations of the inlet temperature of the hot fluid. Their model results for the case of no axial dispersion and longitudinal heat conduction can be used to validate the transient model of a single heat exchanger where the wall capacitance can not be neglected. Their results showed that the longitudinal heat conduction in the wall of the heat exchanger influenced the performance of the heat exchanger during the transient period significantly when the capacitance of the separating sheet was considerable. It had been shown that the longitudinal conduction in the exchanger wall plays an important role on the transient

behavior of the system when NTU increases from 2 to 8. Similarly, fluid axial dispersion is important when Peclet number is smaller than 20. Mishra et al. (2008) also investigated the transient response of the three-fluid cross flow heat exchangers with both large and finite wall capacitance using a finite difference method. In their model, all the fluids were unmixed and step, ramp, exponential, and sinusoidal disturbances of the inlet temperature were provided in the central fluid entrance.

Srihari and Das (2008) carried out experimental tests and theoretical analysis to study the effect of port to channel flow mal-distributions on the transient response for U-type and Z-type plate exchangers separately when the axial dispersion term in the governing equations only deal with fluid back mixing within the channels. It was found that flow maldistribution could affect the performance of the Z-type plate heat exchangers more than the U-type exchangers, during both the transient time and the final steady state condition. Their numerical model, using the finite difference method, predicted the expected changes in initial delay and response time observed in their experimental results in the presence of non-uniform flow.

This literature review shows that there have been a substantial number of research papers on the performance of the single exchangers.

1.3.2 Run-around Heat Recovery Systems

Sufficient outdoor air ventilation rate is one of the requirements for a comfortable and healthy indoor environment. The run-around heat recovery system is an economically attractive way of allowing the ventilation rates in buildings to be increased

(Dhital et al., 1995). The run-around heat recovery system, also called a liquid-coupled indirect transfer-type exchanger system, has been utilized in industry for several decades.

A pioneering effort to study run-around heat recover systems was done by London and Kays (1951). It was shown that to achieve the optimum condition of operation for the system, the heat capacity rate of the coupling liquid should be equal to the heat capacity rate of the air.

A procedure for analyzing and optimizing the design of a run-around heat recovery system with two coils was developed by Forsyth and Besant (1988a; 1998b). They proposed that many design parameters should be taken into account rather than only the overall effectiveness. The work has been extended by Zeng et al. (1992) using a numerical simulation based on energy balances for each exchanger. Temperature dependent properties were considered in the model. The results indicated that when the temperature difference between the inlet supply and exhaust air streams is large and the Reynolds number is low for the coupling fluid in the coil tubes, the assumption of constant properties is no longer valid and temperature dependent properties of the aqueous-glycol coupling fluid must be included. Bennett et al. (1994a; 1994b) made extensions to Forsyth and Besant (1988a; 1988b) work by considering liquid bypass to control part load conditions, thermal contact resistance between the fins and coils and wavy-fin coil geometry. A numerical model including hourly weather data for performing yearly simulation was developed and verified using measured data. They also developed a life-cycle cost (LCC) design procedure. Implementation of LCC optimized design resulted in substantial enhancement of the performance of the run-around heat recovery system. It was concluded that the net savings over the life

cycle were expected to increase by more than 45% in the optimized system compared to the installed system that was monitored.

The run-round heat recovery system still has remained an appealing research area because of its high reliability and flexibility in HVAC design and retrofit applications and many research papers have been written on run-around systems in recent years. Fan et al. (2005) developed a two dimensional steady-state mathematical model to study heat transport of a run-around heat recovery system for air-to-air heat recovery in HVAC applications using cross flow flat plate heat exchangers. It was assumed that the airflow and liquid flow were fully developed and unmixed when they flow through the channels of the heat exchanger. A finite difference method was used to solve the governing equations and its accuracy was verified by comparing the results with the known theoretical solution in heat transfer textbooks. It was shown that the number of transfer units (NTU) and thermal capacity ratio needed to be selected carefully in order to achieve a high overall effectiveness.

Ranong et al. (2005) analyzed the steady state and transient behavior of the system consisting of two exchangers coupled by a circulating fluid. The transient response of the system to a step change in the coupling fluid mass flow rate was studied. The system response calculated by the method of Laplace transforms and explicit finite difference method showed that the outlet temperature of the external flows oscillates with reducing amplitude after a step change in mass flow rate of coupling fluid to reach a new steady state condition. This finding implied that the transient behavior of a coupled system was different than single heat exchanger where no oscillations are observed.

1.3.3 Cross Flow Enthalpy Exchangers

In recent years, some research has been performed on liquid desiccant systems due to their potential ability to handle the latent loads of buildings. Liquid desiccants include aqueous salt solutions such as lithium bromide, lithium chloride, calcium chloride and magnesium chloride in water. Liquid desiccants are able to absorb moisture from air (dehumidification) and then this absorbed moisture can be removed from the liquid desiccant by using waste energy from the exhaust air stream or another process to regenerate the desiccant liquid.

1.3.3.1 Direct contact or open systems

Park et al. (1994) studied coupled heat and mass transfer between air and a triethylene glycol solution in a cross flow configuration through a detailed numerical analysis. A direct contact between the liquid desiccants and air as well as a constant liquid film thickness were considered and it was assumed that thermodynamic equilibrium exists at the air-triethylene glycol solution interface. Laminar and steady air and liquid desiccant flows, constant physical properties and large Peclet numbers were assumed in their work. The governing equations were solved using a finite difference method. This numerical solution gives the three-dimensional temperature and concentration distributions in both the liquid desiccant and air streams. Comparison between the mathematical/numerical model and experimental data indicated that the simulation predictions were satisfactory. It was shown that a decrease in the mass flow rate of the air causes a better control of air humidity ratio as well as lower air temperatures for cooling applications.

Ali et al. (2004) evaluated the influence of the addition of Cu-ultrafine particles in the liquid desiccant for a system similar to the system of Park et al. (1994). They aimed to

investigate the augmentation of heat and mass transfer within the salt solution in the presence of solid metal particles. The liquid desiccant flow was laminar, fully developed and smooth (not wavy). They also assumed that Peclet number was large enough to neglect the diffusion in the direction of flow. It was found that a higher volume fraction of Cu-ultrafine particles provided better dehumidification and air cooling. Through a parametrical study they also showed that a decrease in air Reynolds number offers better dehumidification and cooling for air, while the effect of salt solution Reynolds number was negligible. In addition, an increase in the residual time and contact surface area between air and the falling solution film resulted in enhancement of dehumidification and cooling process.

Mesquita et al. (2006) developed a numerical model to analyze the combined heat and mass transfer in parallel flow (co-current and counter current) liquid-desiccant dehumidifiers. The liquid desiccant and the air flow were laminar and fully developed and the desiccant flow was not wavy. They used three different approaches to investigate the problem for internally cooled dehumidifiers. In the first approach, a constant value for the temperature of the liquid desiccant was assumed, also the bulk temperature of the air was considered across the channel. The energy and mass balance equations were solved for the air stream using correlations for convective heat and mass transfer coefficients. The second approach was based on the assumption of constant desiccant film thickness. The governing differential equations were solved using the finite difference method. The third approach introduced a variable thickness for the desiccant film; however it used the same equations and assumptions as the second approach. The only difference was that the thickness of the desiccant film was recalculated in the

direction of flow due to the change in the liquid mass flow rate. The results from the third approach compared well with experimental data for air outlet temperature. However, there were discrepancies at the higher desiccant flow rates in air humidity ratio results that remained to be investigated.

Liu et al. (2007) developed a theoretical model to simulate the heat and mass transfer process in a cross flow dehumidifier/generator as a key component in a liquid desiccant air conditioning system. In their model, the liquid desiccant directly contacted the moist air and coupled heat and moisture transfer occurred between the two fluids. It was assumed that the desiccant flow rate was unaffected by absorbing/desorbing moisture. Also, constant thermo-physical properties of the fluids were assumed. The model could express the temperature and concentration field distributions inside the dehumidifier/generator. The average absolute discrepancy between the calculated results and experimental findings for enthalpy effectiveness and moisture effectiveness were 7.9% and 8.5%, respectively.

1.3.3.2 Closed or membrane systems

Air-to-air enthalpy, or heat and moisture plate exchangers constructed with water vapour permeable membranes are a more recent development and only a few research papers have been published. Air-to-air enthalpy exchangers result in a reduction in energy consumption and the size of cooling and heating equipment. With air-to-air enthalpy exchangers, both heat and moisture are recovered from the exhaust air stream in winter. In summer, the excess heat and moisture are transferred to the exhaust air stream to cool and dehumidify the supply air.

Niu and Zhang (2001) studied the coupled heat and moisture transfer in a cross flow air-to-air enthalpy exchanger with hydrophilic membrane cores. Axial dispersion in the two air streams was neglected. Also, the heat of sorption was assumed constant and equal to the heat of vaporization. Based on the above assumptions, they developed a mathematical model which was solved using the finite difference method. The model was validated by experimental data from a laboratory experiment on a cross-flow membrane-based enthalpy exchanger. The effect of the membrane material and the outside operating conditions on the sensible, latent, and enthalpy effectivenesses were discussed. It was found that the latent effectiveness was influenced by both the membrane material selected and the operating conditions. They defined a coefficient of moisture diffusion to consider the effect of these parameters on water vapour permeability of the membrane. Zhang and Niu (2002) expanded their study by developing an analogy between the number of mass transfer units and that for heat transfer, and developed a correlation for latent effectiveness very similar to the empirical correlation for sensible effectiveness. Simonson and Besant (1999a; 1999b) had used the same approach to establish correlations to determine effectiveness of energy wheels.

Sparrow et al. (2001) investigated the mass transfer characteristics of new type air-to-air exchangers through an experimental study. The membrane used in the exchanger consisted of a very thin, continuous polymer layer on top of an ordinary polymer. The presence of a thin polymer film allows the transfer of water vapor while preventing the transfer of other gases. Transferring of moisture takes place by dissolving the water vapor in the thin layer of polymer. Then, the dissolved water vapor moves across the thin-film coating of the membrane due to the presence of a partial pressure

between the surfaces of the film. The experiments on the exchanger were carried out both in a wind-tunnel test facility and in a simulated field test. It was demonstrated that an effectiveness as high as 50% is achievable by using composite polymer membranes as the exchanger wall. In addition to water vapor, the permeability of the membrane to carbon dioxide (to represent a typical contaminant gas) was measured. It was shown that the effectiveness of the exchanger based on testing with CO_2 gas, is 21 to 61 times less than water vapor. The similar behavior was expected using other gases such as formaldehyde, sulfur hexafluoride, and propane. The practical implication is that the membrane wall can be used in the case where indoor air quality (IAQ) is a concern.

1.3.4 Run-around Membrane Energy Exchanger (RAMEE)

Fan et al. (2006) developed a two dimensional steady-state mathematical model to study the heat and water vapour transport in a RAMEE system with a lithium bromide solution as the coupling fluid. A finite difference method was employed to numerically solve the governing equations for heat and moisture exchange. Their results showed that the factors that affect the distribution of the temperature and moisture content in an air-to-liquid heat and moisture exchanger are the inlet airflow rate, temperature and humidity ratio, the number of heat transfer units, number of mass transfer units, heat capacity ratio and mass flow rate ratio. They found that the results were different from those of the run-around heat recovery system with no moisture transfer. The maximum effectiveness of a run-around heat and moisture recovery system operating at the AHRI summer test conditions (AHRI, 2005) occurs approximately at $C_{Sol}/C_{Air} = 3$ (C_{Sol}/C_{Air}, heat capacity ratio of salt solution to that for air) for balanced airflow rates, while a

run-around heat recovery system has a peak effectiveness at $C_{Sol}/C_{Air} = 1$ according to Zeng (1990) and Fan et al. (2005).

Erb (2007) tested the performance of a RAMEE system under laboratory testing conditions. Testing under AHRI winter conditions showed that the desiccant requires a very long time (many hours or even days) to reach its equilibrium concentration in the system. This extremely long time taken for the desiccant to reach equilibrium is linked to the capacitance of the desiccant. At AHRI summer conditions, the experimental test results showed an increase in effectiveness with an increase in NTU, which was confirmed by the numerical model prediction by Fan et al. (2006). However, the test results did not show an effectiveness peak at $C_{Sol}/C_{Air} = 3$ while the numerical model predicted that the effectiveness peaks at $C_{Sol}/C_{Air} = 3$. Experimental results presented an increasing effectiveness throughout the entire range of C_{Sol}/C_{Air}, approaching a constant value at high values of C_{Sol}/C_{Air}. As shown in Figure 1-6, at high C_{Sol}/C_{Air} values, the experimental effectiveness was up to 5% lower than the numerical results. The difference was attributed to non-uniform flow distribution of the desiccant (Shang and Besant, 2005; Shang and Besant, 2006; Srihari and Das, 2008). As the desiccant flow rate increases (corresponding to an increase in C_{Sol}/C_{Air}), the flow becomes more uniform. This is why the experimental and numerical data show better agreement when C_{Sol}/C_{Air} is high than when C_{Sol}/C_{Air} is low.

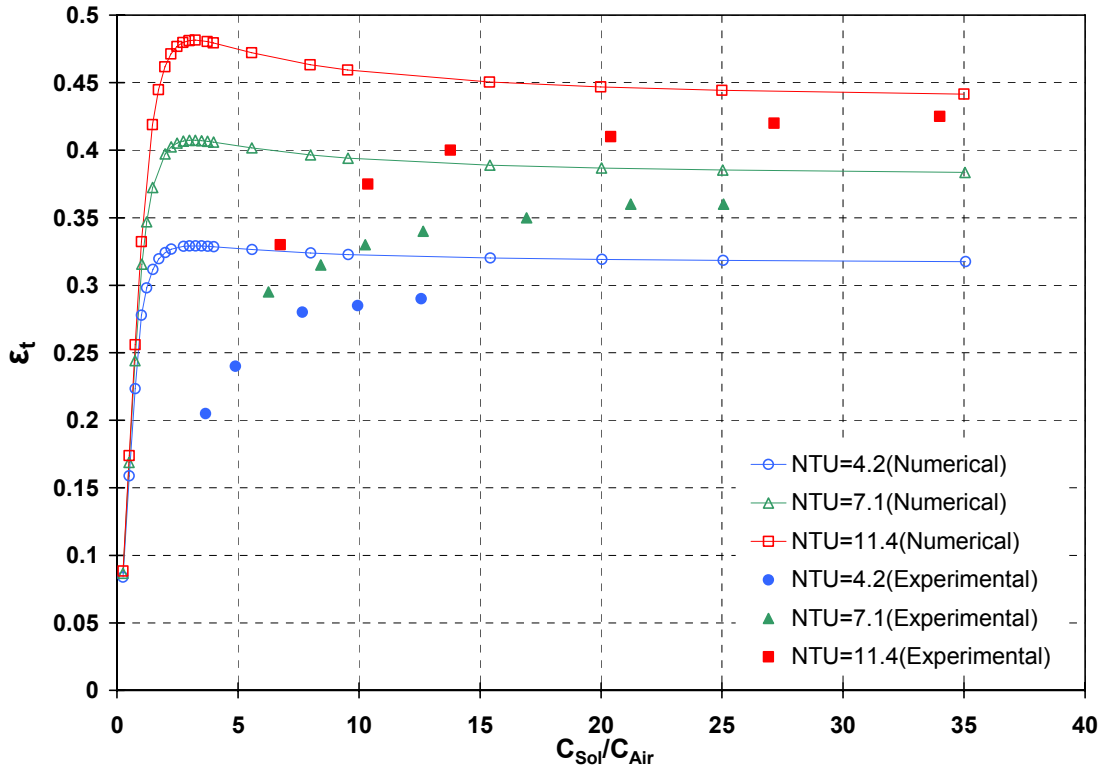

Figure 1-6. Comparison of the overall total effectiveness of the RAMEE system between Fan's numerical model (2006) and Erb's laboratory testing (2007) (AHRI summer operating condition).

There appears to be no analytical or numerical research on the transient behaviour of the heat and moisture cross flow plate exchanger in the literature. Besides, there is no published literature that investigates the effect of the desiccant capacitance and concentration on the transient response of run-around energy recovery systems. Moreover, to increase the understanding of real system characteristics, this thesis includes results concerning heat loss/gain between the system and its surroundings, which has been neglected in all previous works.

1.4 Objectives

The main propose of the present research is to develop and verify a transient numerical model for a run-around membrane energy recovery (RAMEE) system using cross-flow exchangers with liquid desiccant as a coupling fluid. The goal is to determine the dynamic performance of a RAMEE system, considering the thermal and mass transfer capacitance effects of the salt solution in the system. The explicit objectives are to:

- develop a numerical model for simultaneous heat and mass transfer in the RAMEE system considering transient effects and heat loss/gain from/to the liquid desiccant loop,
- validate the numerical model for two cases: (a) plate-type cross flow heat exchanger considering only heat transfer using published literature and (b) a RAMEE system with both heat and moisture transfer using experimental data; and
- apply the validated model to identify the RAMEE design characteristics to allow the designer of this system to rapidly modify the rate that the RAMEE system moves toward steady state conditions.

1.5 Thesis Overview

To address first objective, a theoretical/numerica1 model of the RAMEE system is developed in detail in Chapter 2. The model is developed based on the conservation of mass and energy principles. This numerical model for the exchangers is two dimensional and transient, and is formulated using the finite difference method with an implicit time discretization.

The analytical and experimental verification of the mathematical/numerical model (second objective) is presented in Chapter 3. The analytical comparison is for the transient temperature response of a single exchanger with heat transfer only. The experimental validation of the numerical model is presented for the RAMEE system considering simultaneous heat and moisture transfer in the RAMEE system operating under both summer and winter operating conditions.

In Chapter 4, the verified model for the run-around energy recovery system is used to investigate the dynamic performance of the system during simultaneous heat and moisture transfer (third objective). To make the results of general use, dimensionless parameters are used throughout this chapter to present the simulation results.

Chapter 5 provides a summary and the conclusions from this study. The thesis is concluded with some suggestions for future research work.

CHAPTER 2
NUMERICAL MODEL

2.1 Introduction

The purpose of this chapter is to develop a transient numerical/mathematical model for a run-around heat and moisture recovery system. The assumptions, governing equations and boundary conditions used to develop the numerical model are presented in detail.

A run-around heat and moisture recovery system, shown schematically in Figure 2-1, has been suggested as a new system for energy recovery (Fan et al., 2006). The run-around membrane energy exchanger (RAMEE) uses semi-permeable membranes in each exchanger with an aqueous salt solution coupling liquid pumped between the exchangers to transfer heat and water vapor simultaneously between the supply and exhaust air streams (Larson et al., 2007). Compared to rotary enthalpy wheels, which recover both heat and moisture between adjacent duct air flows, the RAMEE system may be more convenient to apply in retrofit applications where supply and exhaust ducts are remotely located. The only moving parts are liquid pumps and the run-around fluid. Carryover and cross-flow leakages of air, which can be a concern for some rotary wheel applications, should be negligible in the RAMEE system. The steady state performance of a RAMEE system has been simulated by Fan et al. (2006), but there have been no research publications on the transient performance of run-around systems that transfer both heat and moisture between supply and exhaust airstreams. It is expected that these

transient effects will be important during the operation of these systems because the thermal and mass capacity of the liquid is large compared to that of the air.

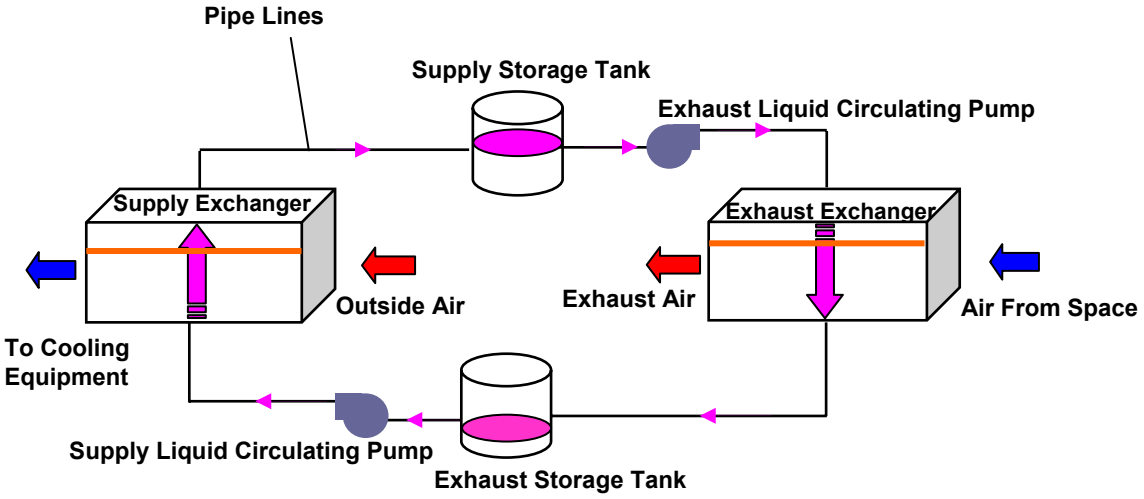

Figure 2-1. Run-around membrane energy exchanger (RAMEE).

The purpose of this chapter is to develop a numerical model with a finite difference formulation to investigate the transient performance of a run-around system for exchanging heat and moisture between two air streams using two cross-flow flat plate heat exchangers, one in each air stream at different operating conditions.

2.2 Mathematical Formulation

A run-around membrane energy exchanger (RAMEE) system is comprised of two liquid-to-air membrane energy exchangers (LAMEE), two storage tanks, connecting tubing and pumps as shown in Figure 2-1. Each LAMEE has multiple air and liquid flow channels, each separated by a semi-permeable membrane. The geometry of one pair of flow channels for a cross-flow flat plate LAMEE and the coordinate system used for the mathematical model are shown in Figure 2-2. Flow channels adjacent to these two shown are assumed to be identical, implying that only one exchange surface need be

modeled. The channel sizes of the air side (d_{Air}) and liquid desiccant side (d_{Sol}) are not necessarily the same. Within a LAMEE, the salt solution flows vertically through the exchanger in the positive y direction and air flows horizontally through the exchanger in the positive x direction. In this exchanger, the semi-permeable membranes allow water vapor to diffuse normal to the plane of the membrane (in the z direction) and the air and desiccant streams transport this water vapor and heat downstream (in the positive x and y directions). Liquid water is prevented from entering the air channels by the microporous membrane. Propore^{TM} consisting of microporous polypropylene is chosen in this study. The approximate pore size for this microporous membrane is in the range of 0.1 μm (Larson et al., 2007).

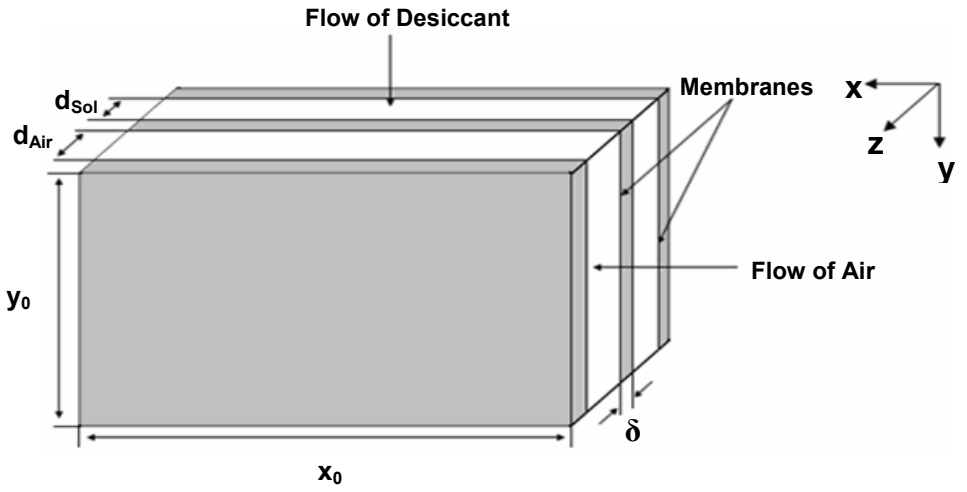

Figure 2-2. Schematic of a cross-flow liquid-to-air membrane energy exchanger (LAMEE).

2.2.1 Assumptions

The following assumptions are made for the mathematical analysis.

1. In order to model heat and mass transfer, the bulk mean temperatures and moisture concentrations of each fluid flow within a channel are used. These flows are assumed to be laminar and fully developed (i.e. entrance effects are negligible).

2. The heat and mass transfer processes occur only normal to each membrane in the z direction and the membrane properties are constant.

3. Axial and lateral heat conduction and water vapor molecular diffusion in the two fluids are negligible.

4. Heat gain or loss due to adsorption/desorption of water vapor at the membrane surface occurs only in the liquid component.

5. The membrane thermal and mass transfer capacitance effects are negligible.

6. The desiccant liquid in the storage tanks is well mixed at all times.

The first assumption avoids the problem of determining the lateral temperature and moisture concentration distributions in each channel and simplifies the problem to one dimensional for the bulk fluid variables. Entrance effects will be negligible for these exchangers because the inverse heat and mass transfer Graetz numbers are greater than 0.05, resulting in constant heat and mass transfer coefficients (Iskra and Simonson, 2007). It is observed that the entrance regions of the air and the liquid desiccant flows are less than 6% of the exchanger length in the pertinent direction for typical operating conditions. Therefore, for most operating conditions, the effect of entry

length will be negligible. As well, the Reynolds numbers for both fluids in the exchanger remain in the laminar flow range for most operating conditions.

The second assumption is valid because the membrane is thin and has a higher thermal and moisture transfer resistance compared to convective heat and mass transfer resistance in the fluid stream, respectively. As well, the surface area to volume ratio for the exchanger is high. Therefore, one-dimensional diffusion through the semi-permeable membrane occurs normal to each surface. Assumption 3 arises because Pe is greater than 20 in most of the operating conditions in this study. The effects of axial dispersion and lateral diffusion are generally neglected for $Pe > 20$ (Luo and Roetzel, 1998) and are quite small even for $Pe > 10$ (Mishra et al., 2004). These effects are only important for very slow liquid metals that have high thermal diffusivity.

The energy of phase change is assumed to be delivered to or obtained from the liquid desiccant (Simonson and Besant, 1997) in assumption 4 because the convective heat and mass transfer coefficients on the air side are typically an order of magnitude smaller than the convective heat and mass transfer coefficients on the liquid side. In addition, the phase change between the liquid and vapor states occurs at the interface between the liquid and the membrane. The fifth assumption simplifies the analysis; however, it is valid since the membrane has negligible thermal capacity and mass compared to thermal and mass transfer capacitance of desiccant fluid in the system (Iskra, 2007). Assumption 6 implies that the outlet properties of the salt solution in the storage tanks are the same as the average reservoir conditions at any time due to fluid mixing.

2.2.2 Analysis of a Cross Flow Channel between Air and Solution (LAMEE)

Based on the above assumptions, the governing equations for the coupled heat and moisture transfer through the permeable membrane in a LAMEE are now presented. The set of governing equations at any point (x, y) on the membrane surface consists of a pair of heat and moisture transfer equations for the air side and another pair for the liquid side. The detailed development of the governing equations for a cross flow heat and moisture exchanger is presented in Appendix B.

2.2.2.1 Moisture balance in the air stream

The change of water vapor content with time at any point (x, y) in the air side within the exchanger is determined by knowing mass gain/loss in the air flowing in the x direction and water vapor flux through the membrane in the z direction:

$$\rho_{Air} d_{Air} \frac{\partial W_{Air}}{\partial t} + \frac{\dot{m}_{Air}}{y_0} \frac{\partial W_{Air}}{\partial x} + 2U_m (W_{Air} - W_{Sol}) = 0, \qquad (2.1)$$

where $\dot{m}_{Air}$ is the mass flow rate of dry air through a single channel, W_{Air} is the bulk humidity ratio of the air and W_{Sol} is the humidity ratio of the air that is in equilibrium with the bulk salt solution. The equilibrium humidity ratio of the salt solution depends on the bulk temperature and concentration of the salt solution:

$$W_{Sol} = f(X_{Sol}, T_{Sol}). \qquad (2.2)$$

according to the analytical expression developed by (Cisterance and Lam, 1991) and presented in Appendix A. The symbol d_{Air} is the air channel thickness and, y_0 is the exchanger length along the desiccant flow direction, and the symbol U_m is the overall

mass transfer coefficient for water vapor flux between the air and salt solution and is defined as:

$$U_m = \left[\frac{1}{h_{m,Sol}} + \frac{\delta}{k_m} + \frac{1}{h_{m,Air}} \right]^{-1}. \quad (2.3)$$

In the above equation, the convective mass transfer coefficients between the membrane and the fluids ($h_{m,Sol}$ and $h_{m,Air}$) are assumed to be constant for any operating conditions. Similarly the water vapor permeability (k_m) of the membrane is assumed to be constant because the k_m is a weak function of temperature and humidity (Larson et al., 2007). Since the thickness of the membrane (δ) is constant, U_m is not a function of the position within the exchanger.

2.2.2.2 Energy balance in the air stream

The energy equation for the air side at any point (x, y) includes energy storage, convection and energy transfer through the membrane and is:

$$\rho_g c_{p_g} d_{Air} \frac{\partial T_{Air}}{\partial t} + \frac{\dot{m}_{Air}}{y_0} c_{p_g} \frac{\partial T_{Air}}{\partial x} + 2U(T_{Air} - T_{Sol}) = 0, \quad (2.4)$$

where T_{Air} is the bulk mean temperature of the air, ρ_g the density of moist air, and c_{p_g} is the thermal capacity of moist air defined as:

$$c_{p_g} = \frac{c_{p\,Air} + c_{p_v} W_{Air}}{1 + W_{Air}}, \quad (2.5)$$

and U is the overall heat transfer coefficient between the air and salt solution and can be expressed as follows:

$$U = \left[\frac{1}{h_{Sol}} + \frac{\delta}{k} + \frac{1}{h_{Air}} \right]^{-1}. \quad (2.6)$$

where h_{Sol} and h_{Air} are the convective heat transfer coefficients between the membrane and the fluids, (k) is the thermal conductivity of membrane and (δ) is the thickness of membrane.

2.2.2.3 Moisture balance in the desiccant stream

At any point (x, y) in the liquid desiccant side within the exchanger, the change of the moisture content (X) with time can be determined by knowing the mass gain/loss to/from the liquid flowing in the y direction and water vapor flux through the membrane:

$$\rho_{Salt} d_{Sol} \frac{\partial X_{Sol}}{\partial t} + \frac{\dot{m}_{Salt}}{x_0} \frac{\partial X_{Sol}}{\partial y} - 2U_m (W_{Air} - W_{Sol}) = 0, \quad (2.7)$$

where $\dot{m}_{Salt}$ is the mass flow rate of dry salt through a single channel, ρ_{Salt} is the amount of salt (kg) per volume (m^3) of salt solution and X_{Sol} is defined as:

$$X_{Sol} = \frac{\text{mass of water}}{\text{mass of salt}}. \quad (2.8)$$

W_{Sol} is obtained from the equation of state [Equation (2.2)], at equilibrium for the salt solution knowing X_{Sol} and T_{Sol} (Appendix A).

2.2.2.4 Energy balance in the desiccant stream

The energy equation for the liquid side at any point (x, y) includes sensible energy storage, convection, the heat of phase change and energy transfer through the membrane. It can be expressed as:

$$\rho_{Sol} c_{p_{Sol}} d_{Sol} \frac{\partial T_{Sol}}{\partial t} + \frac{\dot{m}_{Sol}}{x_0} c_{p_{Sol}} \frac{\partial T_{Sol}}{\partial y} - 2U_m (W_{Air} - W_{Sol}) h_{fc} - 2U(T_{Air} - T_{Sol}) = 0, \quad (2.9)$$

where T_{Sol} is the bulk mean temperature of the salt solution, ρ_{Sol} the bulk mean density of the salt solution, h_{fc} is the net heat of phase change which includes the heat of vaporization of water and the heat of solution and $c_{p_{Sol}}$ is the specific heat capacity of salt solution as a function of temperature and concentration. The analytical expressions presented in Appendix A are used for the salt solution properties.

2.2.2.5 Normalization of equations

The method of deriving the governing dimensionless governing heat and moisture transfer groups for this study from the governing equations follows the method presented by Shah (1981) and Romie (1994). These dimensionless groups are the number of heat transfer units NTU, the number of mass transfer units NTU_m, dimensionless lengths and dimensionless times based on the times required for the resident fluids to be replaced by the incoming fluids. The set of equations are as follows:

Air side:

$$\frac{\partial W_{Air}}{\partial t^*_{Air}} + \frac{\partial W_{Air}}{\partial x^*} + NTU_{m,Air} (W_{Air} - W_{Sol}) = 0, \quad (2.10)$$

$$\frac{\partial T_{Air}}{\partial t^*_{Air}} + \frac{\partial T_{Air}}{\partial x^*} + NTU_{Air} (T_{Air} - T_{Sol}) = 0. \quad (2.11)$$

Liquid Side:

$$\frac{\partial X_{Sol}}{\partial t^*_{Sol}} + \frac{\partial X_{Sol}}{\partial y^*} - NTU_{m,Sol}(W_{Air} - W_{Sol}) = 0, \tag{2.12}$$

$$\frac{\partial T_{Sol}}{\partial t^*_{Sol}} + \frac{\partial T_{Sol}}{\partial y^*} - NTU_{Sol}(T_{Air} - T_{Sol}) - \frac{NTU_{m,Sol}}{c_{p_{Sol}}(1 + X_{Sol})} h_{fc}(W_{Air} - W_{Sol}) = 0. \tag{2.13}$$

where

$$x^* = \frac{x}{x_0}, \tag{2.14}$$

$$y^* = \frac{y}{y_0}, \tag{2.15}$$

$$t^*_{Air} = \frac{tV_{Air}}{x_0}, \tag{2.16}$$

$$t^*_{Sol} = \frac{tV_{Sol}}{y_0}, \tag{2.17}$$

and

$$NTU_{Air} = \frac{2Ux_0y_0}{C_g}, \tag{2.18}$$

where

$$C_g = \dot{m}_{Air}(c_{p_{Air}} + c_{p_v} W_{Air}). \tag{2.19}$$

Also,

$$NTU_{Sol} = \frac{2Ux_0y_0}{C_{Sol}}, \tag{2.20}$$

where the number of heat transfer units for a LAMEE is defined as:

$$NTU = \max\ \{NTU_{Air}, NTU_{Sol}\}. \tag{2.21}$$

Finally,

$$NTU_{m,Air} = \frac{2U_m x_0 y_0}{\dot{m}_{Air}}, \tag{2.22}$$

and

$$NTU_{m,Sol} = \frac{2U_m x_0 y_0}{\dot{m}_{Salt}}. \tag{2.23}$$

where the number mass transfer units for a LAMEE is defined as:

$$NTU_m = \max\ \{NTU_{m,Air}, NTU_{m,Sol}\} \tag{2.24}$$

2.2.2.6 Boundary and initial conditions

The initial temperature of the salt solution and the air are assumed to be equal to the indoor temperature:

$$T_{Air}(x^*, y^*, 0) = T_{Sol}(x^*, y^*, 0) = T_{Indoor}. \tag{2.25}$$

Equation (2.25) indicates that the initial conditions of both exchangers are equal to the temperature representative of the exhaust air conditions. This assumption is due to the fact that the entire system is assumed to be located in a mechanical room that has

conditions similar to the indoor air in the building. Therefore, before the step change in the supply air conditions, the air streams are assumed to be in equilibrium with the indoor condition which has the same temperature as the exhaust side air stream. It should be noted that the initial conditions are set as above in the numerical model and if the initial conditions are different it will be mentioned (e.g. for the experimental validation in Chapter 3).

The inlet temperature of the air on the supply side ($T_{Air,S}$) is assumed to be subjected to a finite step change at time 0:

$$T_{Air,S}(0, y^*, \tau) = T_{Air,in,S}, \tag{2.26}$$

while the inlet temperature of the exhaust air ($T_{Air,E}$) is assumed to be constant throughout the simulation:

$$T_{Air,E}(0, y^*, \tau) = T_{Indoor}. \tag{2.27}$$

A characteristic dimensionless time (τ) for the RAMEE system is defined relative to the transport time for the bulk solution to flow through both exchangers without considering the storage tanks or connecting tubes:

$$\tau = \frac{1}{t^*_{Sol,S}{}^{-1} + t^*_{Sol,E}{}^{-1}}, \tag{2.28}$$

τ indicates the number of complete volume circulations of the salt solution in both exchangers. This dimensionless number is a function of both the liquid desiccant volume flow rate and the length of exchangers in the direction of salt solution flow. This

parameter is used to interpret the transient response of the system at different operating conditions.

The initial humidity ratio of the air is equal to the indoor air humidity ratio (similar to the assumption of the initial air temperature);

$$W_{Air}(x^*, y^*, 0) = W_{Air,Indoor}. \tag{2.29}$$

Similar to the temperature boundary conditions, the air humidity ratio in the supply side is subjected to a finite step change at time 0:

$$W_{Air,S}(0, y^*, \tau) = W_{Air,in,S}, \tag{2.30}$$

while the inlet humidity ratio of the exhaust air remains unchanged as:

$$W_{Air,E}(0, y^*, \tau) = W_{Air,Indoor}. \tag{2.31}$$

AHRI summer and winter test conditions (AHRI, 2005) are used as the air inlet condition of each exchanger (LAMEE) within a run-around system (RAMEE) as shown in Table 2-1. These operating conditions are superimposed on the psychrometric chart in Figure 2-4. The AHRI test conditions are defined to be representative of typical summer and winter operating conditions in many climates. Inlet temperatures below 0° C are not included.

Table 2-1. AHRI Air Conditions used as the Inlet condition of the Supply and Exhaust Exchangers (LAMEEs) in the Run-Around System (RAMEE)

Summer	$T_{Air,in,S}$	308.15 K (35 ºC)
	$W_{Air,in,S}$	17.5 g/kg
	$T_{Air,in,E}$	297.15 K (24 ºC)
	$W_{Air,in,E}$	9.3 g/kg
Winter	$T_{Air,in,S}$	274.85 K (1.7 ºC)
	$W_{Air,in,S}$	3.5 g/kg
	$T_{Air,in,E}$	294.15 K (21 ºC)
	$W_{Air,in,E}$	7.1 g/kg

In practical situations the initial concentration of the salt solution could be selected as an arbitrary single value so that:

$$X_{Sol}(x^*, y^*, 0) = X_{Sol,Initial}. \tag{2.32}$$

The influence of this initial concentration on the system behavior will be discussed in detail later. The difference between the initial concentration and the concentration of the liquid desiccant in equilibrium can be defined as follows:

$$\Delta C_{Salt} = C_{Salt,Initial} - C_{Salt,Steady\,State}. \tag{2.33}$$

However, ΔC_{Salt} is considered to be zero in this study unless otherwise indicated.

2.2.3. Analysis of Mixing Process in the Storage Tanks as Coupling Components in the RAMEE System

In the RAMEE system, the liquid desiccant that leaves an exchanger will mix with salt solution stored in the next reservoir as shown in Figure 2-3. Then, this salt solution will be pumped to the other exchanger to be circulated in the system. Therefore, the preceding storage tank conditions are used as inlet salt solution conditions for the

LAMEEs within the run-around system. The inlet liquid desiccant conditions for the supply exchanger are:

$$T_{Sol,in,ex,S}(x^*,0,\tau) = T_{Sol,st,E}(\tau), \tag{2.34}$$

$$X_{Sol,in,ex,S}(x^*,0,\tau) = X_{Sol,st,E}(\tau). \tag{2.35}$$

As well, for the exhaust exchanger the inlet (boundary) conditions of salt solution are given by the following equations:

$$T_{Sol,in,ex,E}(x^*,0,\tau) = T_{Sol,st,S}(\tau), \tag{2.36}$$

$$X_{Sol,in,ex,E}(x^*,0,\tau) = X_{Sol,st,S}(\tau). \tag{2.37}$$

These equations which reflect the effect of the pumps, piping and storage tanks that couple the two LAMEEs to form a RAMEE.

To determine the conditions of the solution in the storage tanks, the set of governing equations for the storage tanks can be developed using assumption 6 and the constant mass of salt in the system. In order to develop the equations describing the conservation of mass and energy, one exchanger with a storage tank is considered as one control volume and a sub-system as shown in Figure 2-3. The exhaust sub-system, which is not shown, is similar to supply sub-system with a similar exchanger, storage tank and circulating pump.

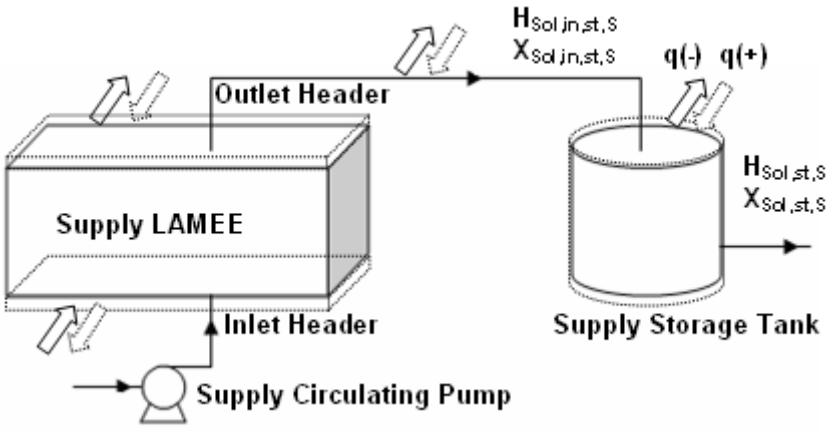

Figure 2-3. Schematic of a storage tank and a LAMEE showing the water mass fractions and enthalpies for the supply sub-system as a control volume.

The principle of conservation of mass for water in the supply storage tank gives:

$$\frac{d}{dt}(M_{Salt,st,S}X_{Sol,st,S}) = \dot{m}_{Salt,in,st,S}X_{Sol,in,st,S} - \dot{m}_{Salt,out,st,S}X_{Sol,st,S}, \tag{2.38}$$

where $M_{Salt,st,S}$ is the mass of salt in the supply storage tank and varies during the transient period. This value can be calculated from the principle of conservation of mass for pure salt in the supply storage tank as follows:

$$\frac{d}{dt}(M_{Salt,st,S}) = \dot{m}_{Salt,in,st,S} - \dot{m}_{Salt,out,st,S}. \tag{2.39}$$

The mass flow rate of salt which enters the supply storage tank is calculated from the volume flow rate of the pump in the supply sub-system and the concentration of the salt solution that exits the supply exchanger:

$$\dot{m}_{Salt,st,in,S} = \frac{\rho_{Sol,out,ex,S}Q_S}{1+X_{Sol,out,ex,S}}, \tag{2.40}$$

where Q_S is the supply circulating pump volume flow rate and $\rho_{Sol,out,ex,S}$ is the density of desiccant fluid as it exits from the supply exchanger. The density of the salt solution is a function of its temperature and concentration. This correlation is given in Appendix A. It should be mentioned that the salt solution in each tank is assumed to be well mixed.

The mass flow rate of the salt leaving the supply storage tank and delivered to the exhaust exchanger is calculated using an equation similar to Equation (2.40):

$$\dot{m}_{Salt,st,out,S} = \frac{\rho_{Sol,st,S} Q_E}{1 + X_{Sol,st,S}}, \tag{2.41}$$

where Q_E is the volume flow rate of the exhaust pump.

In order to calculate the temperature of the desiccant in the storage tank at any time, conservation of energy, including the heat of solution (Stephanopoulos, 1984), is required and is presented in a similar form to Equation (2.38),

$$\begin{aligned} &\frac{d}{dt}\left[M_{Sol,st,S}\left(C_{Salt,st,S}\Delta H_{Sol,st,S}(T_0) + c_{p\,Sol,st,S}(T_{Sol,st,S} - T_0)\right)\right] = \\ &\dot{m}_{Sol,in,st,S}\left[C_{Salt,in,st,S}\Delta H_{Sol,in,st,S}(T_0) + c_{p\,Sol,in,st,S}(T_{Sol,in,st,S} - T_0)\right], \\ &-\dot{m}_{Sol,out,st,S}\left[C_{Salt,st,S}\Delta H_{Sol,st,S}(T_0) + c_{p\,Sol,st,S}(T_{Sol,st,S} - T_0)\right] + q \end{aligned} \tag{2.42}$$

where C_{Salt} is defined as:

$$C_{Salt} = \frac{1}{1 + X_{Sol}}. \tag{2.43}$$

T_0 is the reference temperature and ΔH_{Sol} is the heat of solution per kilogram of salt at temperature T_0 which depends on the salt solution concentration according to the

correlation given in Appendix A. The mass of solution in the storage tank and the mass flow rate of the salt solution used in the conservation of energy equation are respectively equal to:

$$M_{Sol} = M_{Salt}(1 + X_{Sol}), \tag{2.44}$$

$$\dot{m}_{Sol} = \dot{m}_{Salt}(1 + X_{Sol}). \tag{2.45}$$

The detailed development of the governing equations for the storage tanks are given in Appendix C.

In Equation (2.42), q accounts for heat gain to or loss from the salt solution as it flows from the outlet of the supply exchanger to the inlet of the exhaust exchanger as shown schematically in Figure 2-3. Therefore it accounts for heat gain/loss in: (i) the outlet header of the supply exchanger, (ii) the inlet header of the exhaust exchanger, (iii) the supply storage tank, (iv) the piping connecting the outlet of the supply exchanger and the inlet of the exhaust exchanger due to temperature differences between the fluid and the surroundings and (v) the energy that pump adds to the liquid desiccant circuit. In order to introduce the value of heat loss/gain into the system as a dimensionless parameter, the heat loss /gain coefficient σ is defined for supply and exhaust sides of the RAMEE system separately as follows:

$$\sigma = \frac{q_{loss/gain}}{\left| C_{Sol,out,ex} T_{Sol,out,ex} - C_{Sol,in,ex} T_{Sol,in,ex} \right|}, \tag{2.46}$$

where C_{Sol} is the heat capacity rate of salt solution. Heat loss from the system results in a negative value of σ, while heat gain to the system results in a positive coefficient.

The salt solution temperature (T_{Sol}) and water mass fraction (X_{Sol}) within the storage tanks are the properties that couple the two LAMEEs in the run-around system and should be known to investigate the behavior of the system. It is also important to analyze the changes in liquid levels in the storage tanks as the operating conditions change because the volume of water in the system will be low during dry conditions (winter) and high during humid conditions (summer). This analysis of the storage tanks and their maximum volume change is critical to provide design guidance for the selection of the appropriate storage volume of the liquid desiccant in the system for the full range of operating conditions over a typical day, month or year. With storage tanks in the mathematical/numerical model, the question of how the thermal and mass capacitances of the desiccant fluid in the storage tanks are related to the transient response time of the system can be addressed. In order to answer this question a new dimensionless parameter is defined. This parameter is the ratio of the mass of salt in the exchangers to the total mass of salt in the RAMEE system (including, exchanger, headers, piping and storage tanks) and is called the mass ratio (μ) and is expressed as:

$$0 < \mu = \frac{\text{Mass of salt in the exchangers}}{\text{Total mass of salt in the system}} < 1. \qquad (2.47)$$

During a transient simulation, the mass ratio (μ) will change as the concentration of the solution and volume of water in the system change and the value reported will be the value that exists at the initial conditions.

2.3 Overall Heat and Mass Transfer Coefficients

In order to calculate the overall heat and mass transfer coefficients in Equations (2.3) and (2.6), the convection coefficients (h and h_m), the membrane conductivities (k and k_m) and the thickness of membrane (δ) are required. For fully developed laminar flow (Incropera and Dewitt, 2002) with $Re \leq 2300$, the dimensionless heat transfer coefficient (Nu) is independent of Re:

$$Nu = \text{constant} = \frac{hD_h}{k_f}, \tag{2.48}$$

where D_h is the hydraulic diameter of the flow channel. For parallel plates, D_h is the twice the channel spacing. In this study $Nu = 8.24$ is selected (Incropera and Dewitt, 2002), which is the case for fully developed convective heat transfer between infinite rectangular plates with uniform heat flux.

The Chilton-Colburn Analogy (Welty et al., 2001) is used to determine the dimensionless convective mass transfer coefficient (Sh) from Nu and the Lewis number (Le),

$$Sh = NuLe^{-2/3}, \tag{2.49}$$

or the mass transfer coefficient can be calculated as:

$$h_m = \frac{h}{c_p} Le^{-2/3}. \tag{2.50}$$

The heat and mass conductivities (k and k_m) of the semi-permeable membrane depend on the membrane type and are needed to calculate the overall heat and mass transfer

coefficients (U). Polypropylene (PP) which is a polymer that is common in many household applications such as microwave tolerant plastics and indoor/outdoor carpeting is used as the semi-permeable membrane in this study. The thermal and moisture conductivities of the membrane used in this study are $k = 0.3$ W/(m·K) and $k_m = 1.66 \times 10^{-6}$ kg/(m·s) (Larson et al., 2007). The thickness of membrane is 0.5 mm. These values and the other parameters for the liquid-to-air membrane energy exchanger (LAMEE) studied in this research are listed in Table 2-2.

Table 2-2. Selected Design Parameters of the LAMEE

Name	Symbol	Value
Size of exchanger	$x_0 \times y_0 \times z_0$	$0.6 \times 0.3 \times 0.076$ m
Channel thickness, air side	d_A	4.9 mm
Channel thickness, liquid side	d_L	1.7 mm
Number of air channels	n_A	10
Number of liquid channels	n_L	10
Membrane thickness	δ	0.5 mm
Thermal conductivity, membrane	k	0.3 W/(m·K)
Moisture conductivity, membrane	k_m	1.66×10^{-6} kg/(m·s)

2.4 Properties of $MgCl_2$ Solution

Magnesium chloride aqueous salt solution is chosen as the coupling fluid in this study. Empirical property correlations, which are valid for the range $273.15 \le T \le 373.15$ K, are used to calculate the properties of $MgCl_2$ solution. These correlations are given in Appendix A.

To determine the equilibrium humidity ratio of the air adjacent to the solution, the partial pressure of the water vapor, p_v, and the total pressure, P, of an air mixture are used as follows (ASHRAE, 2005):

$$W_{Sol} = 0.62198 \frac{p_v}{P - p_v}. \tag{2.51}$$

In this study, correlations developed by Cisternas and Lam (1991) for the equilibrium water vapor pressure of aqueous solutions are used to calculate the equilibrium water vapor pressure at any temperature and salt solution concentration. These correlations are given in Equations (A.1) to (A.6). The reported average deviation between these correlations and experimental data for $MgCl_2$ salt solution with concentrations less than 27.6% by weight is 0.9% (Cisternas and Lam, 1991). The same correlations are used to extrapolate from 27.6 % salt solution concentration to saturation concentration (35.9%) in this study. Using equation (A.1) in conjunction with Equation (2.51), the equilibrium concentration lines for the $MgCl_2$ can be obtained. Figure 2-4 shows the equilibrium concentration lines superimposed on the psychrometric chart, where C_{Salt} is the salt concentration (kg of salt per kg of solution) at equilibrium:

$$C_{Salt} = \frac{1}{1 + X_{Sol}}. \tag{2.52}$$

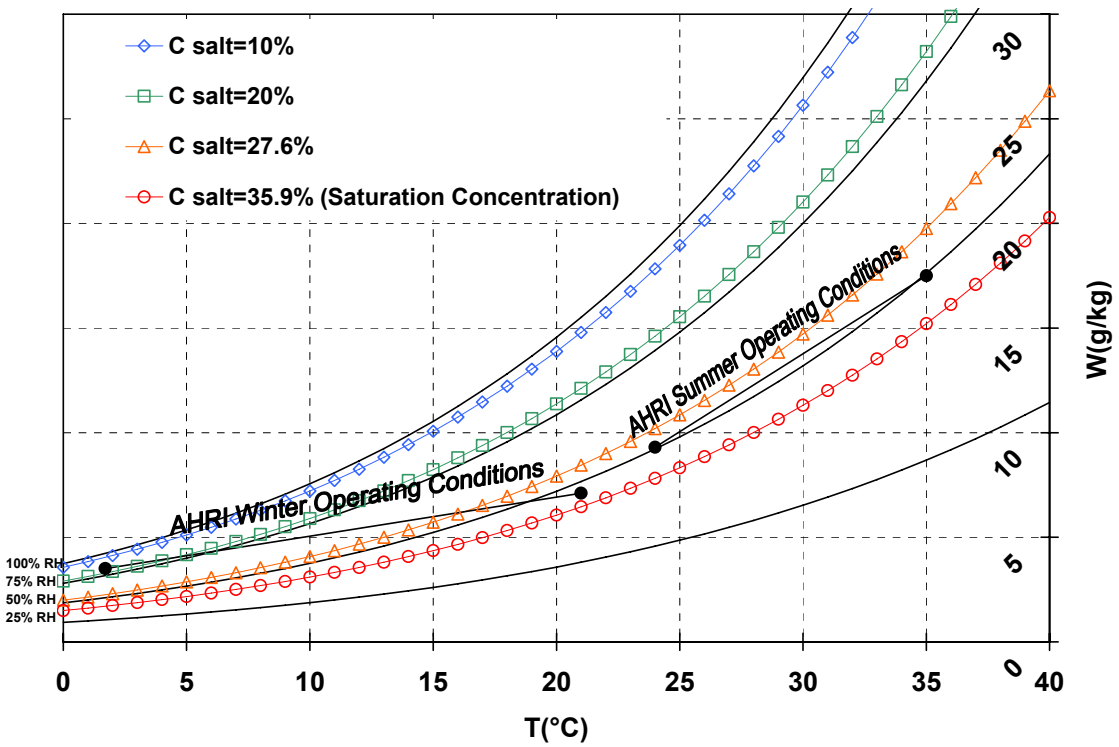

Figure 2-4. Equilibrium constant concentration lines of an $MgCl_2$ solution superimposed on the psychrometric chart.

As it can be seen in Figure 2-4, the equilibrium constant concentration lines of the salt solution nearly follow the same trend as the constant relative humidity. Figure 2-4 also shows the magnesium chloride saturation concentration line as a limit for the salt solution properties calculations. The reader should also be reminded that the correlations used to calculate the equilibrium humidity ratio of magnesium chloride salt solution were developed for $C_{Salt} < 27.6\%$, however it is extrapolated up to saturation condition and shown in Figure 2-4. As illustrated in Figure 2-4 during AHRI winter operating conditions the salt solution will be quite close to saturation conditions when the salt solution is in equilibrium with the indoor air conditions. If saturation conditions exist in a LAMEE, salt crystals could deposit on the membrane surface and alter the heat and moisture transfer characteristics of the semi-permeable membrane (Charles and

Johnson, 2008). As well, solid particles of salt could block the desiccant flow passages and cause pump problems. Therefore, the risk of crystallization of the salt solution must be considered in the numerical model as a constraint or limit because the heat and mass transfer equations used in the simulation are only valid for the case of no salt crystallization. Also, in practical situations, the system should avoid operating conditions where the solution has a concentration close to the saturation concentration in order to avoid the previously mentioned problems. In the current study the crystallization of salt solution is not considered and only conditions where crystallization does not occur are studied.

2.5 Method of Solution

The governing equations for each exchanger are discretised using the implicit finite difference technique for the time derivative and the upwind scheme for the first-order spatial derivative. The discretised equations along with the initial and boundary conditions are solved using the Gauss-Seidel iteration technique. The solution gives two-dimensional temperature and humidity ratio distributions within both the air and salt solution throughout the exchangers as a function of time. Additionally, one may calculate the outlet bulk mean temperatures of the air and liquid desiccant for the LAMEE by using the following equations, respectively,

$$T_{Air,out} = \frac{1}{\dot{m}_{Air} c_{p\,Air} y_0} \int_0^{y_0} \dot{m}_A c_{p\,Air} T_{Air} dy \,, \tag{2.53}$$

$$T_{Sol,out} = \frac{1}{\dot{m}_{Sol} c_{p\,Sol} x_0} \int_0^{x_0} \dot{m}_{Sol} c_{p\,Sol} T_{Sol} dx \,. \tag{2.54}$$

As well, the outlet bulk mean water contents of the air and the salt solution fluid are calculated as follows:

$$W_{Air,out} = \frac{1}{y_0}\int_0^{y_0} W_{Air}\,dy\,, \tag{2.55}$$

$$X_{Sol,out} = \frac{1}{x_0}\int_0^{x_0} X_{Sol}\,dx\,. \tag{2.56}$$

A trial and error method is employed in the well mixed reservoirs to find the time dependent salt solution properties in each storage tank from energy and mass balances equations. The salt solution properties [i.e. temperature (T) and water mass fraction (X_{Sol})] within the storage tanks are the properties that couple the two LAMEEs in the run-around system. The algorithm and numerical code used to simulate the RAMEE system are in Appendix E.

2.6 Effectiveness of the RAMEE System

In order to investigate the effect of various parameters on the heat and moisture transfer rates in the run-around system during the transient period, dimensionless numbers (or effectiveness values) are used. These dimensionless effectiveness values relate the heat and moisture transfer rates at any time relative to the maximum possible heat and moisture transfer rates for the exchangers based on the specific operating conditions. With known air inlet conditions, the sensible effectiveness or dimensionless heat transfer rate at any time (τ) with equal mass flow rates of air for the supply side exchanger is defined as:

$$\varepsilon_{s,S}(\tau) = \frac{T_{Air,in,S} - T_{Air,out,S}}{T_{Air,in,S} - T_{Air,in,E}}, \tag{2.57}$$

and for the exhaust side exchanger is,

$$\varepsilon_{s,E}(\tau) = \frac{T_{Air,out,E} - T_{Air,in,E}}{T_{Air,in,S} - T_{Air,in,E}}. \tag{2.58}$$

Also, the average sensible effectiveness of the RAMEE system can be defined as:

$$\overline{\varepsilon}_{s}(\tau) = \frac{\varepsilon_{s,S}(\tau) + \varepsilon_{s,E}(\tau)}{2}. \tag{2.59}$$

It can be seen in the above equations that the air side properties are used to calculate the effectiveness in this study because the changes in the air properties can be measured more easily and with lower uncertainties than the changes in the salt solution properties. This allows the results from the numerical model to be compared with experimental measurements. Besides, in practical HVAC applications, the air properties and their changes are the most important parameters for the performance of the HVAC system. On the other hand, the liquid desiccant properties [e.g. concentration (C_{Salt})] will often be unknown during a real system operation and therefore the air properties can be used to normalize the heat and moisture transfer rates.

Using the same form of equations as for sensible effectiveness, the latent effectiveness or dimensionless moisture transfer rate for the supply and exhaust side exchangers are respectively:

$$\varepsilon_{l,S}(\tau) = \frac{W_{Air,in,S} - W_{Air,out,S}}{W_{Air,in,S} - W_{Air,in,E}}, \tag{2.60}$$

$$\varepsilon_{l,E}(\tau) = \frac{W_{Air,out,E} - W_{Air,in,E}}{W_{Air,in,S} - W_{Air,in,E}}. \tag{2.61}$$

As well, the average latent effectiveness can be calculated by the following equation:

$$\bar{\varepsilon}_{l}(\tau) = \frac{\varepsilon_{l,S}(\tau) + \varepsilon_{l,E}(\tau)}{2}. \tag{2.62}$$

The total effectiveness or dimensionless energy transfer rate for the supply and exhaust side exchangers of the run-around system with coupled heat and moisture exchange are respectively:

$$\varepsilon_{t,S}(\tau) = \frac{H_{Air,in,S} - H_{Air,out,S}}{H_{Air,in,S} - H_{Air,in,E}}, \tag{2.63}$$

$$\varepsilon_{t,E}(\tau) = \frac{H_{Air,out,E} - H_{Air,in,E}}{H_{Air,in,S} - H_{Air,in,E}}, \tag{2.64}$$

and the average total effectiveness can be calculated by the following equation:

$$\bar{\varepsilon}_{t}(\tau) = \frac{\varepsilon_{t,S}(\tau) + \varepsilon_{t,E}(\tau)}{2}. \tag{2.65}$$

It is important to note that for the case of no heat gain/loss from/to the surroundings, the run-around system energy and mass balances ensure that the dimensionless heat and moisture transfer rates in the supply side exchanger become the same as those in the

exhaust side exchanger and equal to the steady-state effectiveness as the run-around energy recovery system moves toward steady state equilibrium.

2.7. Step Size and Numerical Accuracy

The numerical model must be time accurate because the transient solution is very important to study the dynamic behavior of the RAMEE system. To ensure the numerical solution is time accurate, time is incremented only when a converged solution is reached. The normalized residuals of the governing equations are less than 10^{-12} which is low because upwinding and the tridiagonal matrix algorithm are used. In the numerical solution, the convergence criteria depend on the amount that the dependent variables change in two sequential iterations. For each dependent variable, the convergence criterion which must be satisfied before time is incremented is as follows:

$$\frac{\sum_{i=1}^{m}\left|\psi^{j+1,i,k}-\psi^{j,i,k}\right|}{m(\psi_{max}-\psi_{min})}<1\times10^{-8}. \tag{2.66}$$

where (i) refers to the current node, (k) refers to the current time step and (j) refers to iteration number. Decreasing the convergence limit from 10^{-8} to 10^{-10} increases the solution time by a factor of 1.4 but causes no change to the predicted effectiveness during the transient period. This validates the selected convergence limit in Equation (2.66).

Also, the convergence of the solution has been checked by varying the number of spatial grids and time steps. To establish an acceptable time step and grid size for the numerical solution, the size of the time step, and the number of spatial nodes are varied at AHRI summer operating conditions and results are shown in Figure 2-5 and Figure 2-6

for the transient effectiveness (effectiveness at $\tau = 15$) of the RAMEE system comprised by two LAMEEs with properties mentioned in Table 2-2. For the investigation presented in the following NTU = 5, $C_{Sol}/C_{Air} = 3$, $\mu = 0.15$, $\sigma = 0$ and $\Delta C_{Salt} = 0$. The results in Figure 2-5 are calculated with 100 x 100 nodes and the results in Figure 2-6 are calculated with time steps ($\Delta\tau$) of 1/9. It should be mentioned that the selected number of spatial nodes is always the same in both x (air flow) and y (liquid flow) directions in this study.

To evaluate the sensitivity of step size on the numerically predicted effectiveness of a RAMEE system, the results are presented as changes in effectiveness. Therefore, the change in the transient effectiveness due to using different size of time step and number of spatial nodes are respectively:

$$\Delta\varepsilon = \left|\varepsilon - \varepsilon_{\text{Largest time step}}\right|, \tag{2.67}$$

$$\Delta\varepsilon = \left|\varepsilon - \varepsilon_{\text{Smallest number of nodes}}\right|. \tag{2.68}$$

(a)

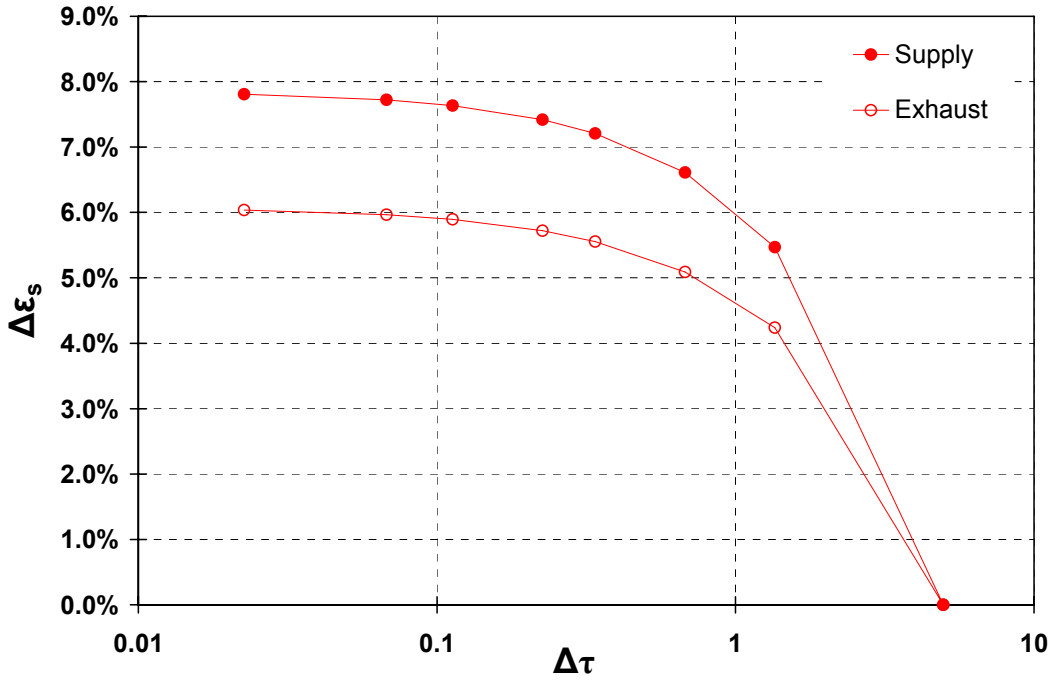
9.0%
8.0%
7.0%
6.0%
5.0%
4.0%
3.0%
2.0%
1.0%
0.0%
Δε_s
0.01
0.1
1
10
Δτ
Supply
Exhaust

(b)

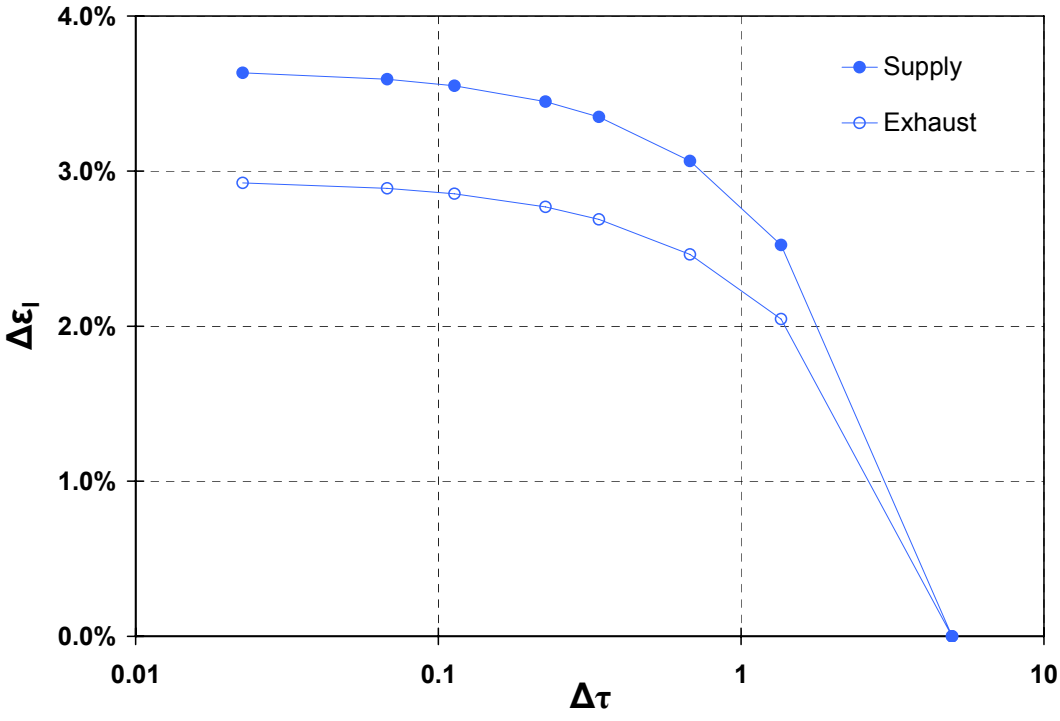
4.0%
3.0%
2.0%
1.0%
0.0%
Δε_l
0.01
0.1
1
10
Δτ
Supply
Exhaust

(c)

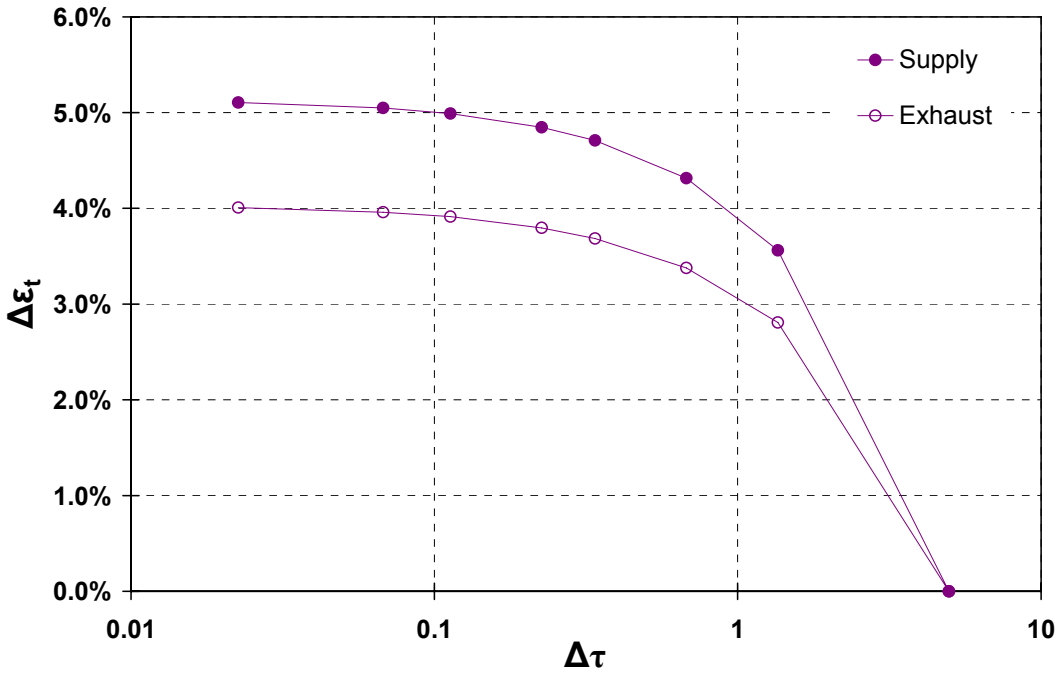

Figure 2-5. Effect of changing time step on the predicted (a) sensible, (b) latent and (c) total transient effectivenesses of the RAMEE system ($|\Delta\varepsilon = \varepsilon - \varepsilon_{\text{Largest time step}}|$).

Figure 2-5 and Figure 2-6 show that decreasing the time step below 1/9 and increasing the number of nodes above 100 x 100 has little effect on the predicted effectiveness values. Thus, $\Delta\tau = 1/9$ and 100 x 100 nodes are employed throughout the rest of this study.

(a)

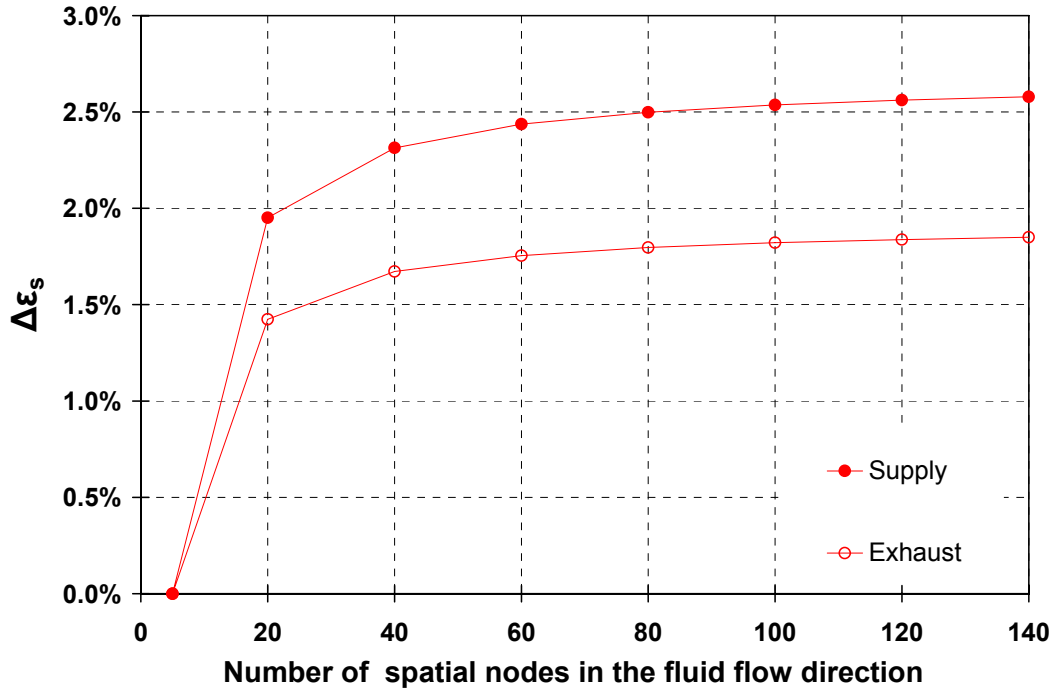
3.0%
2.5%
2.0%
1.5%
1.0%
0.5%
0.0%
$\Delta\varepsilon_s$
0
20
40
60
80
100
120
140
Number of spatial nodes in the fluid flow direction
Supply
Exhaust

(b)

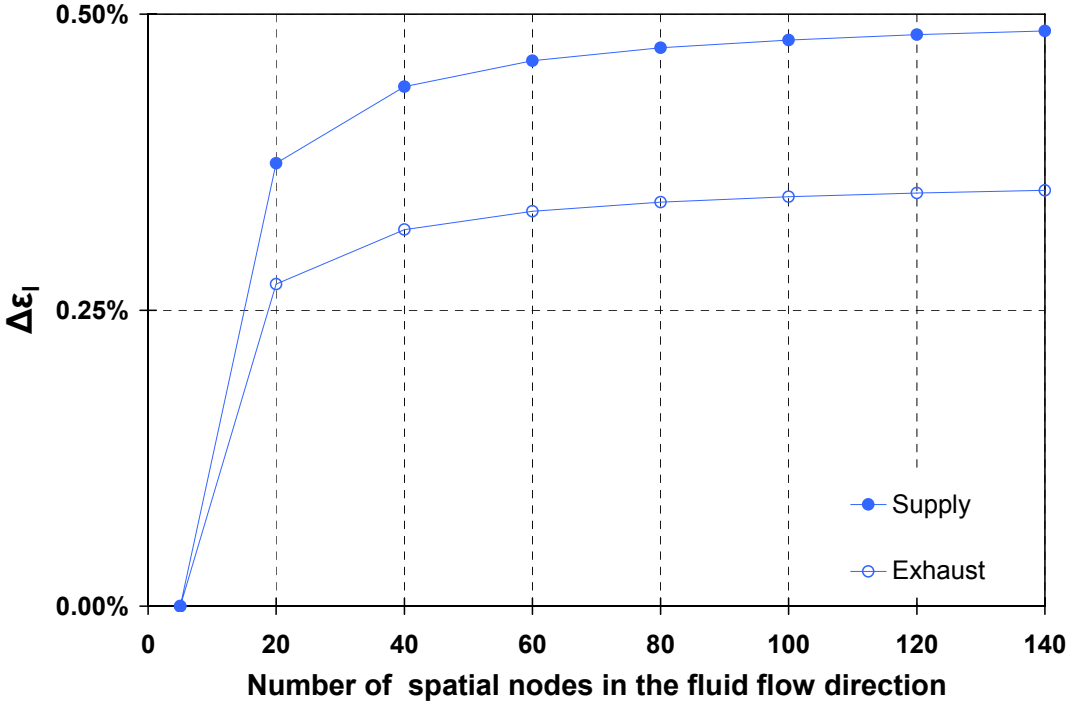
0.50%
0.25%
0.00%
$\Delta\varepsilon_l$
0
20
40
60
80
100
120
140
Number of spatial nodes in the fluid flow direction
Supply
Exhaust

(c)

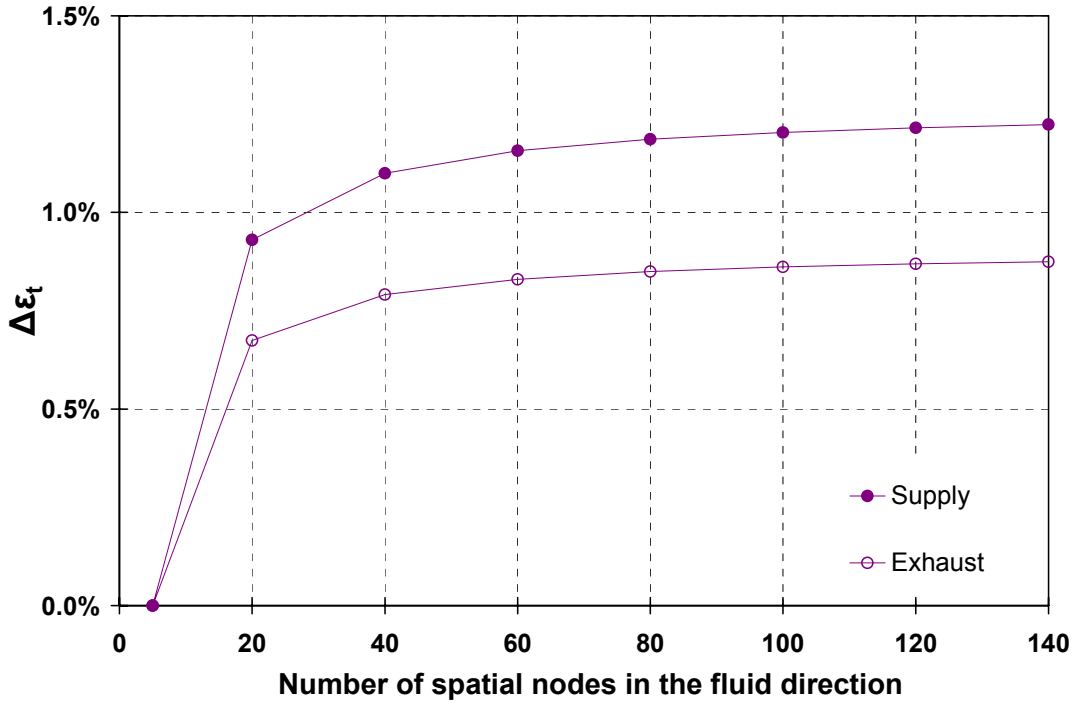

Figure 2-6. Effect of number of spatial nodes on the predicted (a) sensible, (b) latent (c) total transient effectivenesses of the RAMEE system ($\Delta\varepsilon = |\varepsilon - \varepsilon_{\text{Smallest number of nodes}}|$).

The selection of a satisfactory time step and number of nodes is a trade off between the time required to obtain a numerical solution and the accuracy of the simulation results. For instance, increasing the number of spatial grids from 100 x 100 to 140 x 140 and decreasing the time step from 1/9 to 1/45, changes the predicted effectiveness values of the RAMEE system during transient time by less than 0.2%, but increases the solution time by a factor of 2.6.

2.8 Quasi-steady State

The RAMEE system is subjected to a step variation in the supply air inlet temperature and humidity ratio. Then, the temperature and water mass fraction of the fluid streams in the exchangers as well as the salt solution in the storage tanks will continuously change

until the system attains quasi-steady state. That is when the conditions of the fluids at any point in the RAMEE system are no longer changing with time. However, it should be mentioned that even at quasi-steady state, the condition of liquid desiccant changes as liquid travels through the RAMEE system between the supply and exhaust LAMEEs. The temperature and water mass fraction of fluids at any intermediate time steps can be obtained with a help of the current numerical model.

In order to investigate the transient behaviour of the system the performance of the RAMEE system is studied for a sufficient time duration that quasi-steady state is obtained for each operating condition. In this study, the number of circulations needed to reach quasi-steady state is given the symbol η; in other words when $\tau \geq \eta$, the RAMEE system is operating in a quasi-steady state condition. Two different sets of criteria are adopted to define quasi steady state conditions for different initial salt solution concentrations.

The first definition is based on energy and mass balances of the air streams and is applied for the case of $\Delta C_{Salt} = 0$ in Equation (2.33). For this initial condition, quasi-steady state is defined as the time when all the moisture and energy that is lost by one air stream is taken up by the other air stream. This exists, for balanced air flow rates, when:

$$\left| \frac{(W_{Air,in,S} - W_{Air,out,S}) - (W_{Air,out,E} - W_{Air,in,E})}{(W_{Air,in,S} - W_{Air,in,E})} \right| \leq 1 \times 10^{-2}, \qquad (2.69)$$

and,

$$\left|\frac{(H_{Air,in,S} - H_{Air,out,S}) - (H_{Air,out,E} - H_{Air,in,E})}{(H_{Air,in,S} - H_{Air,in,E})}\right| \leq 1 \times 10^{-2} . \qquad (2.70)$$

If the quasi-steady convergence criteria are set to 5×10^{-3}, the quasi steady effectiveness values (i.e. sensible, latent and total effectivenesses) change by less than 0.3% from those predicted with convergence criteria of 1×10^{-2}, indicating that the convergence limits in Equations (2.69) and (2.70) are satisfactory.

Knowing the steady state concentration of the salt solution is very crucial to interpret the transient behaviour of the RAMEE system (See Chapter 4). Therefore, a steady state version of the current numerical model was also developed to calculate the steady state properties of the air and salt solution in the exchangers. The principle, equations and method to develop the steady state model are similar to Fan (2005) and are not presented in this thesis. In the transient model, when the system reaches its equilibrium condition the average quasi-steady state effectiveness values should be the same as those predicted by the steady state model. Figure 2-7 shows a comparison between the transient model results and the simulated data from the steady state numerical model. The maximum difference for sensible, latent and total effectivenesses are 0.7%, 0.1% and 0.2%, respectively, which occurs at lower heat capacity rate ratio (e.g. $C_{Sol}/C_{Air} = 1$) values.

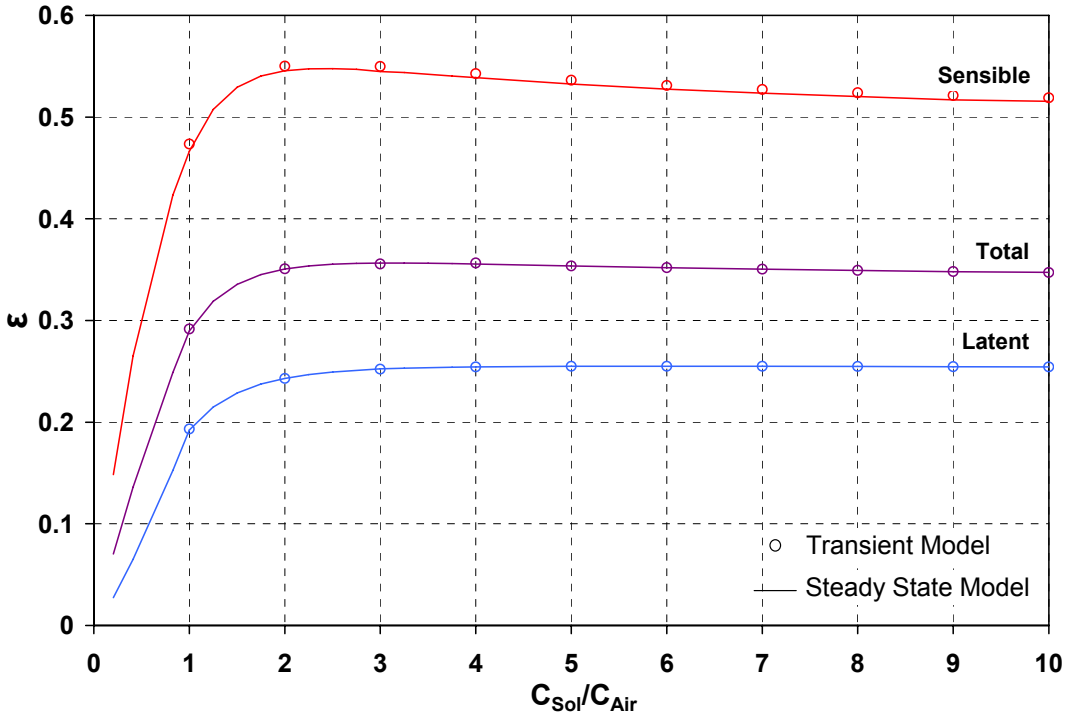

Figure 2-7. Comparison of effectivnesses simulated by the steady state model and the average effectivenesses at quasi-steady state condition simulated by the transient model for AHRI summer operating conditions (NTU = 5).

In presence of heat loss/gain from/to the RAMEE system Equation (2.70) is modified to account for the impact of those losses or gains on the energy balance of the system:

$$\left|\frac{(H_{Air,in,S}-H_{Air,out,S})-(H_{Air,out,E}-H_{Air,in,E})+\sigma_S(H_{Air,in,S}-H_{Air,out,S})+\sigma_E(H_{Air,out,E}-H_{Air,in,E})}{(H_{Air,in,S}-H_{Air,in,E})}\right| \le 1\times10^{-2} \quad (2.71)$$

When the initial salt solution concentration is different from the steady state value (i.e. $\Delta C_{Salt} \neq 0$), the time required to satisfy the energy and mass balances is very large. This is observed from both simulation (See Chapter 4) and experimental results (See Chapter 3) as will be discussed in detail later. Due to the very slow transient response of the RAMEE system for the case of $\Delta C_{Salt} \neq 0$, substantial computational resources are

required to reach quasi-steady state as defined by the energy and mass balances. As a result, a second quasi-steady state convergence criterion is proposed as follows:

$$\left|\frac{\partial \varepsilon}{\partial \tau}\right| \leq 5 \times 10^{-6} . \tag{2.72}$$

This criterion illustrates that quasi-steady state is achieved where the rate of change in the effectiveness values of the RAMEE system is less than a certain value during the transient period. As shown in Figure 2-8, simulation results reveal that decreasing this value from the selected value of 5×10^{-6} to 1×10^{-6} changes the predicted individual effectiveness values (e.g. supply latent effectiveness) by less than 1.7%, while the average sensible and latent effectiveness values change by less than 0.05%. Due to aforementioned decrease the in the convergence criterion value (i.e. from 5×10^{-6} to 1×10^{-6}), the number of circulations of the liquid desiccant and, as a consequence, the numerical solution time, are nearly doubled.

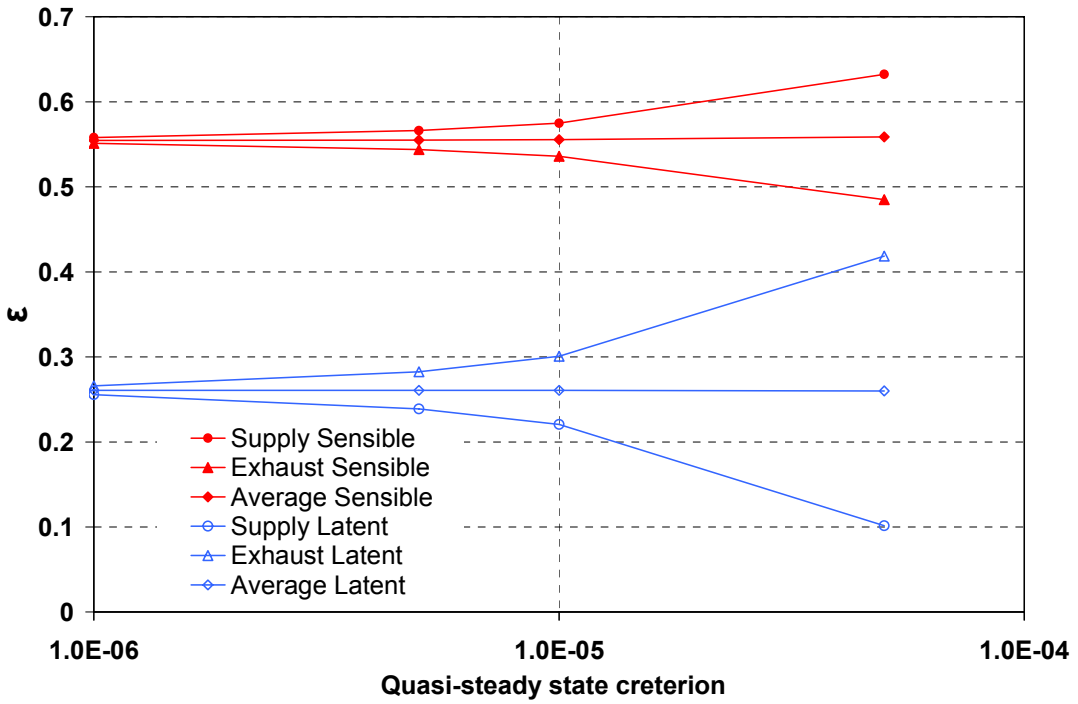

Figure 2-8. The RAMEE system effectivenesses versus quasi-steady state criterion for the case where $\Delta C_{Salt} \neq 0$.

Figure 2-8 indicates that the average effectivenesses reach their quasi-steady state values much more quickly than the individual effectiveness and can be predicted by proposed quasi-steady convergence criterion satisfactorily. Using equation (2.72) saves significant computation time, especially when $\Delta C_{Salt} \neq 0$. It should be reminded that ΔC_{Salt} is considered to be zero in this study unless otherwise indicated. Therefore the energy and mass balance criteria [Equations (2.69) and (2.70)] will be used unless otherwise noted.

2.9 Sensitivity Studies

The purpose of this section is to investigate the effect of some parameters and certain assumptions on the predicted transient effectiveness values of the RAMEE system. This study provides insight into the accuracy of the numerical results due to the uncertainty in

the input properties and assumptions. The parameters investigated in this chapter are the thermal resistance and moisture diffusion resistance of the semi-permeable membrane and the assumptions of negligible edge channel effects and entry length. The parameters and the properties of the two LAMEEs coupled to form a RAMEE and used in this section are listed in Table 2-2. Since the purpose of this section is to emphasize the sensitivity of various assumptions and property data on the numerically predicted effectiveness of a RAMEE system, all the results are presented as changes in effectiveness by considering the uncertainty of property data:

$$\Delta\varepsilon = \varepsilon(\psi \pm \varphi_{\psi}) - \varepsilon(\psi)\,, \tag{2.73}$$

where φ is the uncertainty of an arbitrary input value (ψ).

As well, the change in the predicted effectiveness by including a certain assumption is defined as:

$$\Delta\varepsilon = \varepsilon_{\text{Including the effect}} - \varepsilon_{\text{Neglecting the effect}}\,. \tag{2.74}$$

The simulation in this section are performed for AHRI summer operating conditions and the base parameters are NTU = 5 (NTU_m = 1.8), C_{Sol}/C_{Air} = 3 ($\dot{m}_{Salt}/\dot{m}_{Air}$ = 0.4), μ = 0.15, σ = 0 and ΔC_{Salt} = 0.

2.9.1 Thermal Resistance of Semi-permeable Membrane

In the development of the numerical model, the number of heat transfer units for each exchanger is defined as,

$$NTU = \frac{2Ux_0 y_0}{C_{min}}, \tag{2.75}$$

U is the overall heat transfer coefficient between the air and salt solution and is calculated as:

$$U = \left[\frac{1}{h_{Sol}} + \frac{\delta}{k} + \frac{1}{h_{Air}} \right]^{-1}. \tag{2.76}$$

In Equation (2.76), (δ/k) is the thermal resistance of the membrane where k = 0.3 W/(m·K) and δ = 0.5 mm are adopted in this study. It is known that a decrease in the resistance of membrane enhances the heat transfer between two fluid flows and improves the effectiveness values. The effect of changing the thermal resistance of membrane (δ/k) on the sensible effectiveness of the RAMEE system during transient period is presented in Figure 2-9. As illustrated in Figure 2-9, the numerical model reveals an increase in the effectiveness values ($\Delta\varepsilon > 0$) for a decrease in thermal resistance of membrane and a decrease in both supply and exhaust side effectivnesses ($\Delta\varepsilon < 0$) for an increase in thermal resistance of membrane as expected.

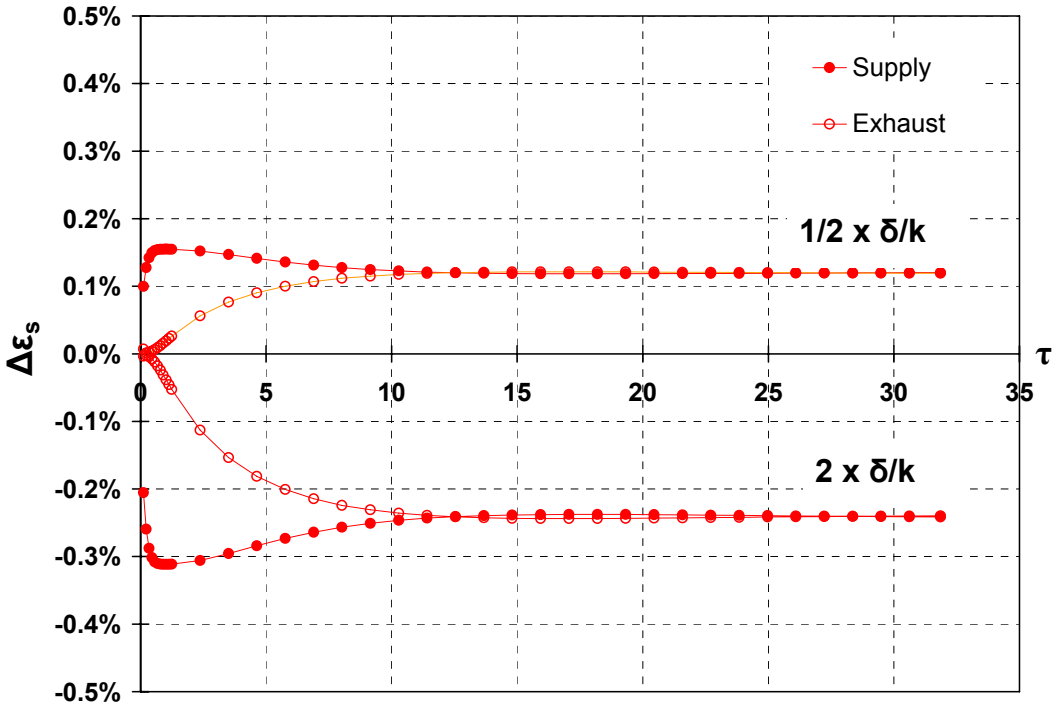

Figure 2-9. Change in transient sensible effectiveness of the RAMEE system due to membrane thermal resistance (δ/k) variations $\Delta\varepsilon = \varepsilon - \varepsilon(\delta/k)$.

The thermal conductivity of the semi-permeable membrane (k) is approximated in this thesis and was not measured in previous studies. Therefore, the high uncertainty value equal to +100% and -50% of the reported value for thermal resistance of membrane is considered to account for the fact that the thermal conductivity value is unknown. Figure 2-9 shows that increasing the thermal resistance of membrane by a factor of 2 results in a maximum 0.32% reduction in the predicted sensible effectiveness during the transit period. This shows that an increase in the thermal resistance of the membrane has small impact on the total resistance of heat transfer through the membrane and reducing the heat transfer rate between airstreams and salt solution. Also, decreasing the thermal resistance of the membrane in half results in a trivial change in the total heat transfer resistance and as a consequence the transient effectiveness values change slightly as

shown in Figure 2-9. It is observed that changing the thermal resistance of membrane by a factor of 0.5 or 2 changes the latent effectiveness only less than ±0.03% and is not presented graphically.

2.9.2 Moisture Diffusion Resistance of Semi-permeable Membrane

In the development of the numerical model, the number of mass transfer units for each exchanger is defined as,

$$NTU_m = \frac{2U_m x_0 y_0}{\dot{m}_{min}}, \tag{2.77}$$

U_m is the overall mass transfer coefficient between the air and salt solution and calculated as:

$$U_m = \left[\frac{1}{h_{m,Sol}} + \frac{\delta}{k_m} + \frac{1}{h_{m,Air}} \right]^{-1}. \tag{2.78}$$

In the above equation (δ/k_m) is the moisture diffusion resistance of the membrane where $k_m = 1.66 \times 10^{-6}$ kg/(m·s) and $\delta = 0.5$ mm are adopted in this study. The uncertainty associated with the moisture diffusion resistance value is comprised of both thickness and water vapor permeability of membrane uncertainties. This uncertainty value was determined to be ±22% of the measured value (Larson et al., 2007). The effect of considering the change of moisture diffusion resistance (δ/k_m) within its uncertainty range on the latent effectiveness of the RAMEE system during the transient period is presented in Figure 2-10. Figure 2-10 depicts an increase in the latent effectiveness ($\Delta\varepsilon > 0$) values using membrane with lower moisture diffusion resistance and a decrease

in the latent effectiveness ($\Delta\varepsilon < 0$) for an increase in moisture diffusion resistance value. This indicates that the numerical solution is enable to predict the expected trends.

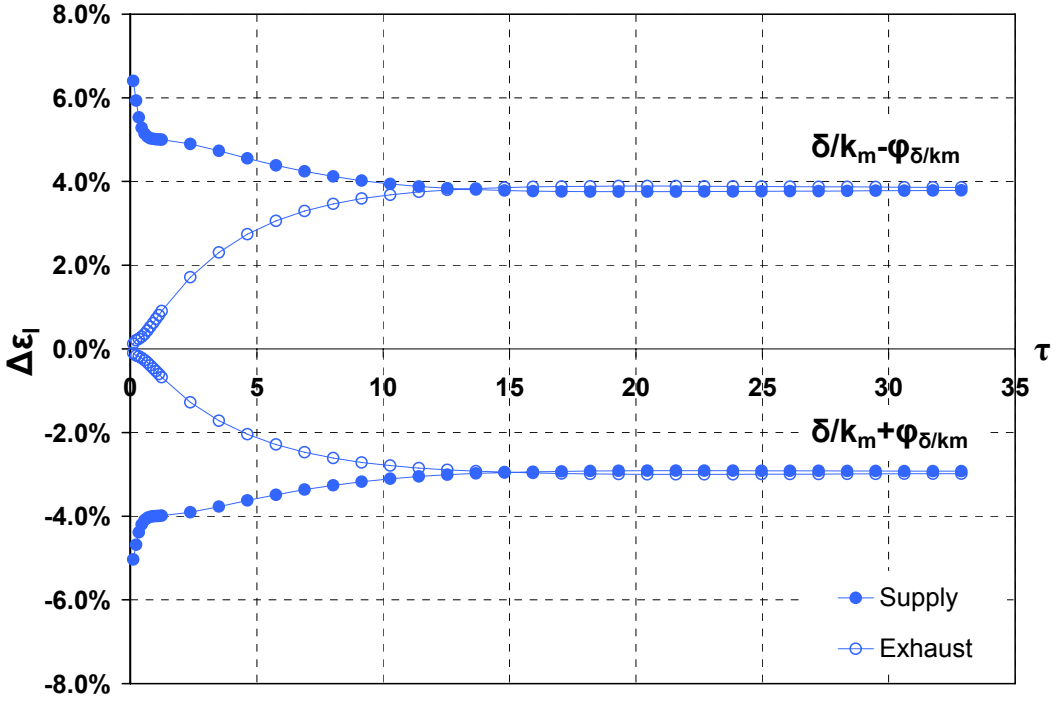

Figure 2-10. Change in transient latent effectiveness of the RAMEE system due to moisture diffusion resistance (δ/k_m) variations within its uncertainty range $\Delta\varepsilon = \varepsilon(\delta/k_m \pm \varphi_{\delta/k_m}) - \varepsilon(\delta/k_m)$.

As illustrated in Figure 2-10, varying the moisture diffusion resistance within its uncertainty limits results in up to a ±6.5% and ±3.9% variation in the predicted transient and quasi-steady state latent effectiveness values, respectively. These significant changes in the effectiveness of the system imply that the moisture diffusion resistance as a property data is the most important/sensitive parameter when comparing the numerical model prediction with the behavior of the system during laboratory test conditions. Therefore, the uncertainty caused by varying the moisture diffusion resistance within its uncertainty limits should be considered as a source of the total uncertainty for

numerically predicted effectiveness values. Changing the moisture diffusion resistance within its uncertainty limits changes the predicted transient and quasi-steady state sensible effectiveness by less than ± 1.3% and ±0.06%, respectively and is not presented graphically.

2.9.3. The Effect of Edge Channels

In a liquid-to-air membrane energy exchanger (LAMEE), all flow channels adjacent to each channel are assumed to be identical, implying that only one air channel and one liquid channel needs to be modeled (See Appendix B). As it can be seen in Figure 2-11, the liquid flow channels in the middle of the LAMEE will be surrounded by two air channels and the air channels in the middle of the LAMEE will be surrounded by two liquid channels. The governing equations for the LAMEE in this study are presented considering these middle channels heat and mass transfer surface area. However, the channels on the very edge of the LAMEE will only have one channel with which they can exchange heat and moisture (i.e. it will be similar to having half the NTU) as shown in Figure 2-11. Therefore, the outlet conditions in these edge channels will be different than the channels in the middle of the LAMEE.

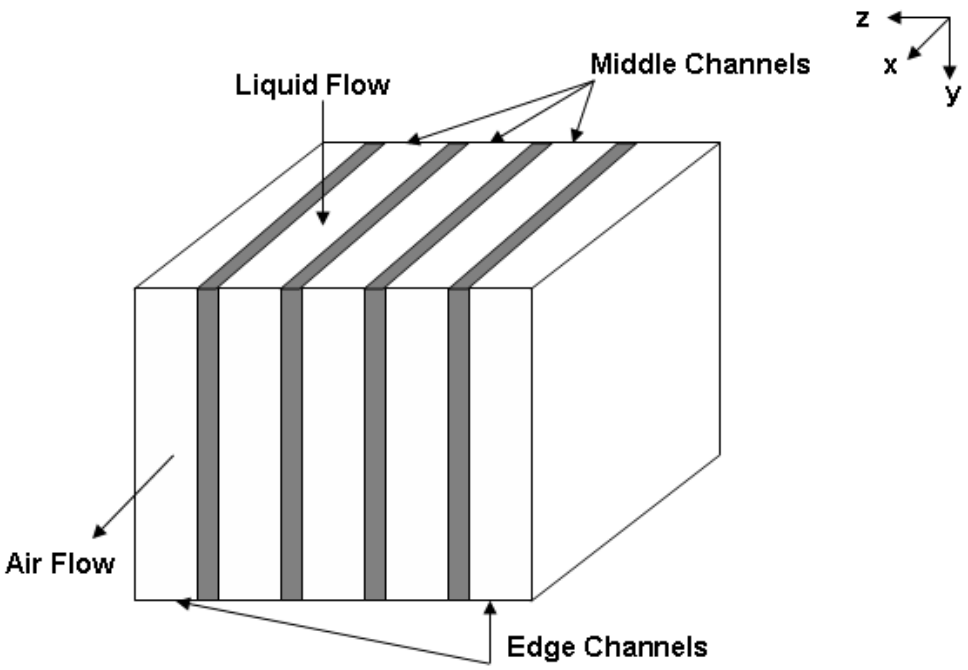

Figure 2-11. Schematic of the LAMEE showing middle and edge channels.

The following method is used to estimate the effect of edge channels on the performance of the RAMEE system:

1. The outlet conditions of the middle channels are determined using the current model and the complete NTU and $NTU_{m.}$

2. The outlet conditions of the edge channel are estimated using the current model and the half of NTU and $NTU_{m.}$

3. All the streams are adiabatically mixed to calculate the bulk outlet conditions and then these bulk mean properties are used to calculate the effectivnesses.

The effect of edge channels with lower heat and mass transfer area on the performance of the system will be more significant when the total number of panels (i.e. a pair of

liquid and air channels shown in Figure 2-2) decreases. As shown in Figure 2-12, the numerical model predicts a similar impact on the RAMEE system effectivenesses by using LAMMEs with different number of panels for the same operating conditions.

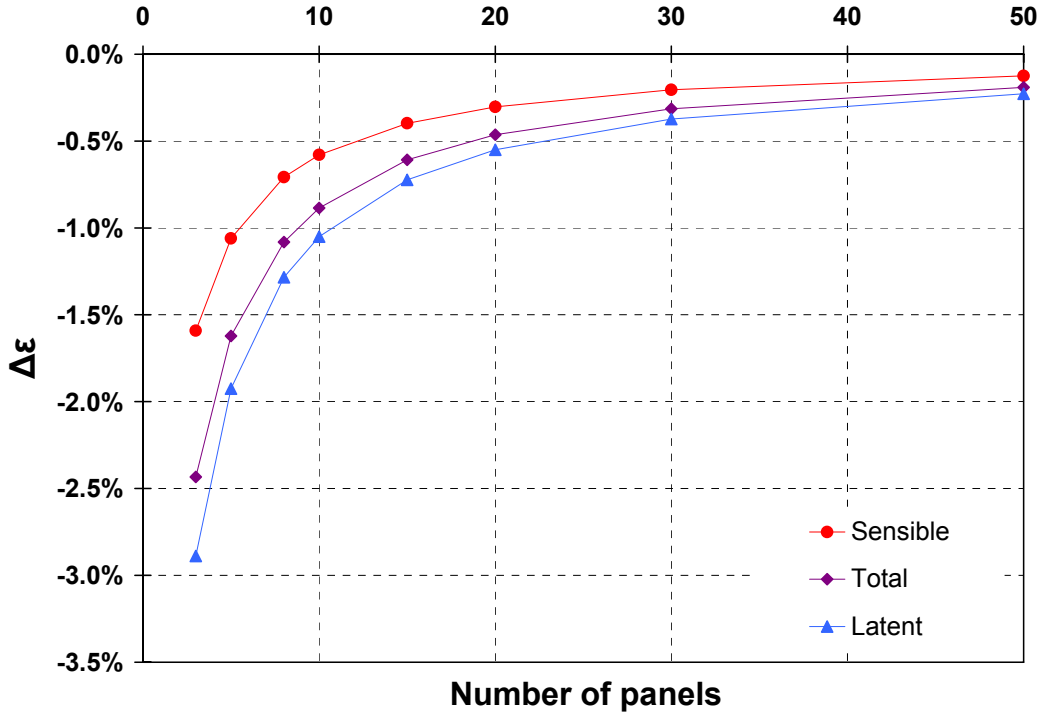

Figure 2-12. Effect of edge channels on the RAMEE system effectivnesses at quasi-steady state condition versus different number of panels in LAMMEs (NTU = 5, C_{Sol}/C_{Air} = 3, AHRI summer operating conditions, $\Delta\varepsilon = (\varepsilon_{Including\ effect\ of\ edge\ channels} - \varepsilon_{Neglecting\ effect\ of\ edge\ chaneels})$

As illustrated in Figure 2-12, the average sensible, latent and total effectivnesses of the system at quasi-steady state using LAMEEs with 10 panels change -0.6%, -1.1% and -0.9%, respectively, when the effect of edge channels is included in the numerical model.

2.9.4. Entrance Length

In the developed model the increased heat and mass transfer in the hydrodynamic and thermal entry length region for the air and liquid entering the exchangers is neglected. In this section the influence of including the entry length on the predicted effectiveness is

investigated. For the case of including the thermal entry length for parallel plates with constant and equal wall heat fluxes, (Shah and London, 1987) suggested the following equations to calculate the Nusselt numbers for laminar flow:

$$\mathrm{Nu} = \begin{cases} 2.236(x^+)^{-1/3} & \text{for } x^+ \le 0.001 \\ 2.236(x^+)^{-1/3} + 0.9 & \text{for } 0.001 < x^+ < 0.01, \\ 8.235 + \dfrac{0.0364}{x^+} & \text{for } x^+ \ge 0.01 \end{cases} \tag{2.79}$$

where x^+ is defined as:

$$x^+ = \frac{2x / D_h}{\mathrm{Re}\,\mathrm{Pr}}. \tag{2.80}$$

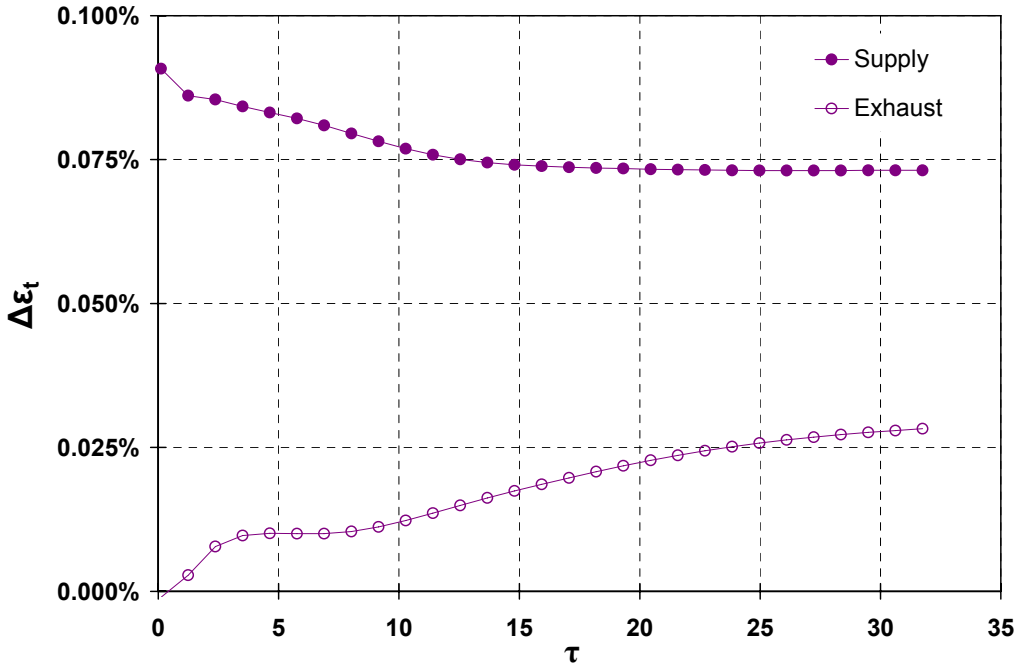

Figure 2-13. Effect of including the enhanced heat and mass transfer coefficients in the entry region on the total effectiveness of the RAMEE system during the transient period $\Delta\varepsilon = (\varepsilon_{\text{Including entry length}} - \varepsilon_{\text{Neglecting entry length}})$.

Neglecting the entry length will result in an under prediction of the effectiveness because the convective heat and mass transfer coefficients are higher in the entry region. As illustrated in Figure 2-13, with the above equations incorporated in the numerical model to include the entrance effect slightly higher effectiveness values ($\Delta\varepsilon>0$) are obtained. Figure 2-13 demonstrates that the difference between the total effectiveness values including the thermal entry effects and neglecting the thermal entry length effects during a transient period as well as for a quasi-steady state condition are less than 0.1% and can be neglected.

2.10 Summary

In this chapter, a mathematical/numerical model that predicts the transient behavior of the RAMEE system has been developed. All the assumptions are explained in detail and justified. The model is two-dimensional, transient and includes the effect of the salt solution storage as well as heat loss/gain from /to the liquid desiccant loop. This model of the RAMEE system can been used to predict the sensible, latent and total transient effectivenesses as well as the time required to reach quasi steady state for different LAMEE designs and operating conditions. The uncertainty in the numerically predicted transient effectiveness including only the numerical accuracy (i.e. grid size, time step and convergence criteria) is less than 0.2%.

The simulations presented in this chapter show that the thermal resistance of membrane is moderately important. Changing the thermal resistance value by a factor of 2 can lead to up to a 0.32% decrease in the predicted sensible effectiveness for the investigated operating condition.

The moisture diffusion resistance of membrane is very important in the range of the selected value. At the investigated operating conditions, varying the moisture diffusion resistance within its measured uncertainty bounds lead to deviations up to ±6.5 % in the predicted transient latent effectiveness.

The impact of outside edge channels of the LAMEEs on the system effectiveness is presented in this chapter. The average sensible, latent and total effectivenesses of the system at quasi-steady state using LAMEEs with 10 panels change -0.6%, -1.1% and -0.9%, respectively, due to this effect. It was also shown that an increase in the total number of panels diminishes the effectiveness reduction caused by these channels.

The entry region in the exchangers of the RAMEE system is found to affect the predicted performance slightly. For the test conditions in this chapter, neglecting the entry region under predicts the transient and steady state effectivenesses by less that 0.1%.

CHAPTER 3
ANALYTICAL AND EXPERIMENTAL VALIDATION

3.1 Introduction

The purpose of this chapter is to validate the numerical model presented in Chapter 2. The numerical results for the case of only heat transfer for a single heat exchanger is compared to an available analytical solution. For the simultaneous heat and moisture transfer in a run-around membrane energy exchanger (RAMEE) a comparison between numerical results and experimental measurements obtained from laboratory testing of the RAMEE for both sensible and latent effectiveness is performed at summer and winter operating conditions.

3.2 Verification and Numerical Results for a Single Heat Exchanger

The numerical model developed as outlined in Chapter 2, is for the case of both heat and moisture transfer, however its accuracy is verified in this section with the case of only heat transfer in a single exchanger because this is the only available analytical solution. Romie (1994) simplified the solution of transient response for the cross flow heat exchangers for the case of negligible thermal capacitance of the wall compared to the thermal capacitance of the fluids in the exchanger which is consistent with assumption 5 in Chapter 2. In Romie's study, the fluid capacitances rates, (C_a and C_b), and the overall heat transfer coefficient (U) were assumed to be constant, which is consistent with the assumption used in the model developed in this thesis when there is no moisture transfer. In addition, there was no heat transfer from the external surface of

the exchanger ($\sigma = 0$ in this study). The fluids were unmixed and the analysis was based on ideal plug flow (assumption 3 in Chapter 2).

A direct transfer cross-flow heat exchanger with zero wall capacitance is shown schematically in Figure 3-1. In this figure x is the distance from the fluid "a" entrance and the flow length is x_0; also, y is distance from the fluid "b" entrance and the flow length is y_0.

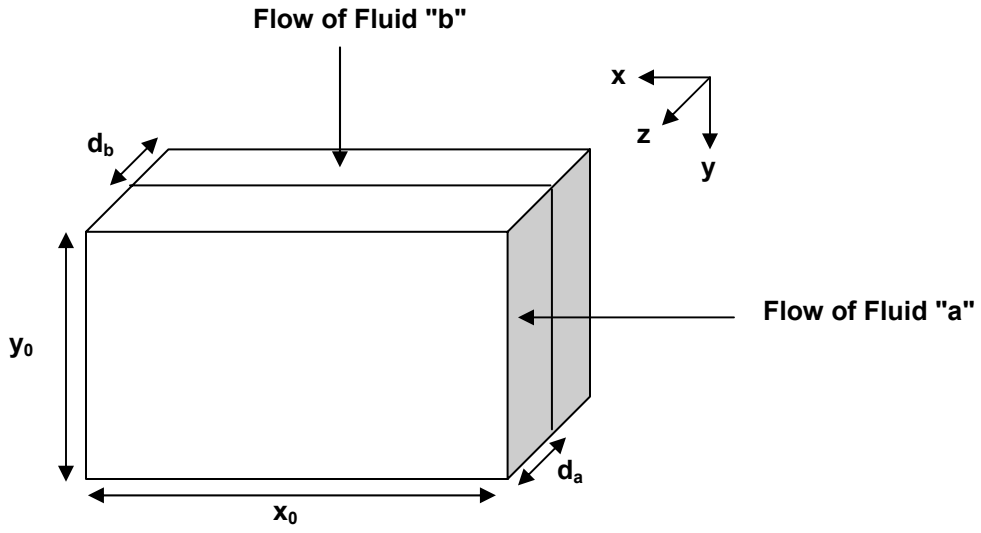

Figure 3-1. Schematic of a cross flow heat exchanger with zero wall capacitance.

Conversation of energy for the two fluid streams can be expressed as follows (Romie, 1994):

$$\rho_a c_{p_a} A_{c,a} \frac{\partial T_a}{\partial t} + \rho_a c_{p_a} V_a A_{c,a} \frac{\partial T_a}{\partial x} + U y_0 (T_a - T_b) = 0 , \tag{3.1}$$

$$\rho_b c_{p_b} A_{c,b} \frac{\partial T_b}{\partial t} + \rho_b c_{p_b} V_b A_{c,b} \frac{\partial T_b}{\partial y} - U x_0 (T_a - T_b) = 0 . \tag{3.2}$$

Where all the dependent properties are the bulk mean values and

$$A_{c,a} = y_0 d_a , \tag{3.3}$$

and

$$A_{c,b} = x_0 d_b . \tag{3.4}$$

To rewrite Equations (3.1) and (3.2) in dimensionless form , dimensionless times for each stream are presented based on the times required for fluid "a" and "b" in the exchanger to be replaced by the incoming fluids flow (similar to definition of dimensionless times for the (LAMEE) in Chapter 2). For a single cross flow exchanger, the time to reach a new steady-state condition due to a step change in one or two incoming fluid temperatures can be expressed by dimensionless times when the exchanger wall capacitance is negligible as follow:

$$\tau^* = \frac{1}{t_a^{*-1} + t_b^{*-1}}, \tag{3.5}$$

where

$$t_a^* = \frac{tV_a}{x_0}, \tag{3.6}$$

$$t_b^* = \frac{tV_b}{y_0}. \tag{3.7}$$

Also dimensionless lengths can be defined as follows:

$$x^* = \frac{x}{x_0} , \tag{3.8}$$

$$y^* = \frac{y}{y_0} . \tag{3.9}$$

Romie (1994) obtained the dimensionless fluid temperatures following a step change of fluid "a" temperature at time 0 where dimensionless temperature is defined as:

$$\theta(\tau^*) = \frac{T - T_{b,in}}{T_{a,in} - T_{b,in}}, \tag{3.10}$$

By substituting Equations (3.5) to (3.10) into Equations (3.1) and (3.2), the dimensionless governing equations are formed (Romie, 1994):

$$\alpha \frac{\partial \theta_a}{\partial \tau^*} + \frac{\partial \theta_a}{\partial x^*} + NTU_a(\theta_a - \theta_b) = 0, \tag{3.11}$$

$$(1-\alpha)\frac{\partial \theta_b}{\partial \tau^*} + \frac{\partial \theta_b}{\partial y^*} - \frac{C_a}{C_b} NTU_a(\theta_a - \theta_b) = 0. \tag{3.12}$$

where

$$\alpha = \frac{t_b^*}{t_a^* + t_b^*}, \tag{3.13}$$

and

$$NTU_a = \frac{U x_0 y_0}{C_a}. \tag{3.14}$$

In order to express the analytical solution for the differential equations, Romie (1994) used the Anzelius - Schuman functions, $G_0(\psi, \omega)$ and $F_0(\psi, \omega)$, and their extension. These functions are presented in Appendix D. The transient response was obtained by the threefold Laplace transform. The temperature fields were obtained by inversion of the resulting Laplace equations and the results are as follows:

$$\theta_a(x^*, y^*, \tau^*) = U^1(\tau^* - x^*\alpha)F_0(x^*NTU_a, y'\frac{C_a}{C_b}NTU_a), \tag{3.15}$$

$$\theta_b(x^*, y^*, \tau^*) = U^1(\tau^* - x^*\alpha)G_0(x^*NTU_a, y'\frac{C_a}{C_b}NTU_a), \tag{3.16}$$

where

$$y' = \min(y^*, \frac{(\tau^* - x^*\alpha)}{(1-\alpha)}). \tag{3.17}$$

As the bulk mean outlet temperatures, $\theta_{a,out}(\tau^*)$ and $\theta_{b,out}(\tau^*)$, are of most interest for heat exchanger analysis, Romie (1994) presented the bulk mean temperatures, which are calculated as follows:

$$\theta_{a,out}(\tau^*) = U^1(\tau^* - \alpha)\int_0^1 F_0(NTU_a, y'\frac{C_a}{C_b}NTU_a)dy^*, \tag{3.18}$$

where $y' = \min(y^*, \frac{(\tau^* - x^*\alpha)}{(1-\alpha)})$, $(x^* = 1)$ and

$$\theta_{b,out}(\tau^*) = \int_0^{x'} G_0(x^*NTU_a, y'\frac{C_a}{C_b}NTU_a)dx^*, \tag{3.19}$$

where $x' = \min(1, \frac{\tau^*}{\alpha})$ and $y' = \min(y^*, \frac{(\tau^* - x^*\alpha)}{(1-\alpha)})$, $(y^* = 1)$.

This analytical solution can be used to validate the numerical model presented in this thesis for the case of only heat transfer. Using a grid of 100 x 100 nodes, the numerical

solution is very close to the analytical solution for the bulk outlet temperatures shown in Figure 3-2. The comparison is made for $NTU_a = 2$, $C_a/C_b = 0.75$ and $\alpha = 1/2$.

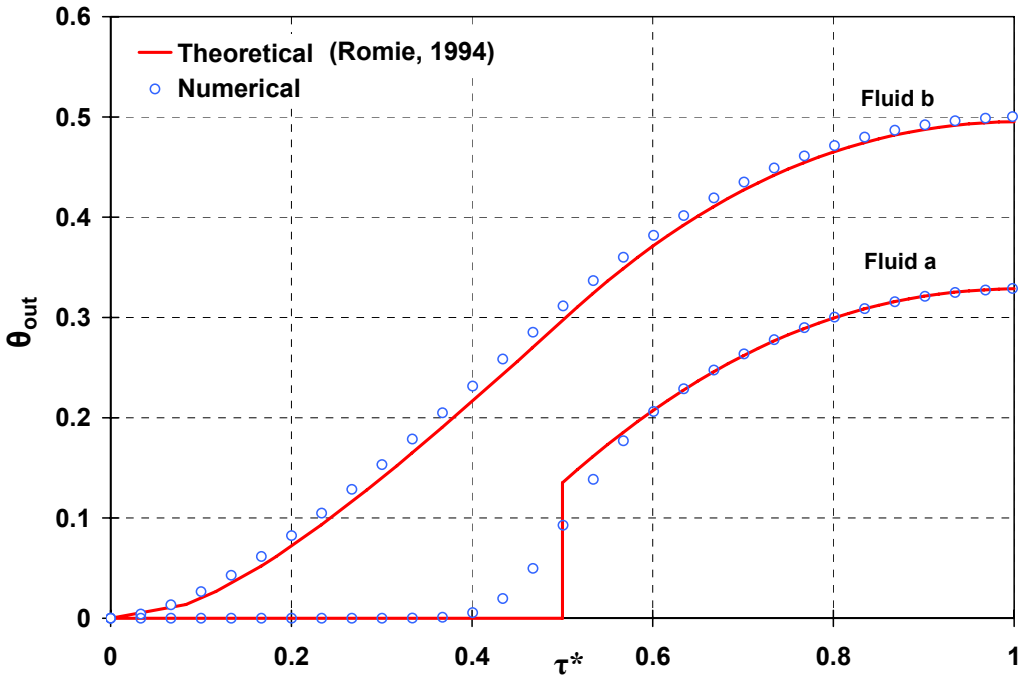

Figure 3-2. Comparison between the bulk outlet temperature of a cross-flow heat exchanger calculated with the numerical model in this thesis and the analytical solution of Romie (1994) following a step change in fluid "a" temperature at time 0. ($NTU_a = 2$, $C_a/C_b = 0.75$ and $\alpha = 1/2$).

From Figure 3-2, it can be seen that numerical solution is in agreement with the analytical solution except for the temperature of fluid "a" over an interval near the time $\tau^* = \alpha = 0.5$. In the analytical solution, the fluid "a" exhibits a step response, when $\tau^* = \alpha$ and therefore $t = x_0/ V_a$. This abrupt step change is due to the assumption that the outlet temperature of fluid "a" can not change until the fluid flow that enters at time zero with a step change in its temperature passes through the exchanger (i.e. at $t = x_0/ V_a$). On the other hand, the outlet temperature of fluid "a" changes smoothly in the numerical model results. The reason for the observed behavior is a phenomenon called false diffusion

(Patankar, 1980). In this problem, it is expected that due to neglecting the axial dispersion in the direction of fluid flows, the outlet temperature of fluid "a" does not change until the perturbation in its inlet temperature is advected to the exit cross section of the channel. However, a backward scheme in the numerical solution causes an earlier change in the outlet temperature of fluid "a" due to numerical solution diffusion. It should be noted that the numerical results may be more physically realistic than the analytical results near this time because a small amount of diffusion would occur in reality.

As shown in Figure 3-2, the numerical diffusion causes a faster initial response at the outlet of fluid "a" temperature. This change in the initial response does not have influence on that the prediction of the transient response time of the exchanger ($\tau^* = 1$) and the quasi-steady state effectiveness values which are the main interest in this study. Moreover, this discrepancy occurs early in the transient response after a perturbation in fluid "a" temperature within a single heat exchanger which has a much lower transient response time compared to the RAMEE system containing a coupling fluid with a high thermal and mass transfer capacitance (See Chapter 4).

The numerical solution for fluid "a" agrees with the analytical solution within the error of ±1 % outside the range of $0.4 < \tau^* < 0.6$, also the maximum discrepancy between the simulated bulk outlet temperature of fluid "b" and its theoretical value is 4% during the transient period. At quasi-steady state condition ($\tau^* = 1$), the discrepancy between numerical and analytical value of the dimensionless temperature of fluid "a" and fluid "b" is 0.07% and 1%, respectively.

3.3 Experimental Validation

In order to validate the numerical model, the data from the numerical model are compared with data from a laboratory experiment on a RAMEE system comprising two LAMEEs and two storage tanks.

3.3.1 RAMEE Prototype

A RAMEE prototype was built and tested by Erb (2007). The RAMEE consisted of two exchangers each with 10 desiccant flow channels, separated from the airstream by a Propore^{TM} membrane. The exchanger characteristics were identical to the characteristics in Table 2-2. The exchangers were cross-flow in design, and a liquid $MgCl_2$ desiccant was pumped from the bottom of the exchanger to the top to provide pressurization and better flow distribution.

3.3.2 Transient Experimental Test Setup

Testing the RAMEE system requires an experimental facility (Erb, 2007) shown schematically in Figure 3-3. The Run-Around Membrane Energy Exchanger Testing Apparatus (RAMEETA) provides two airstreams, each with well controlled temperature, humidity and flow rate. One airstream was designed to simulate outdoor air entering a building and was supplied from an environmental chamber. Constant airflow was provided by two vacuum pumps which were located both upstream and downstream of the supply exchanger, which provided equal pressures on either side. The exhaust airstream mass flow rate was identical to the supply airstream, except that the inlet air was taken from a large laboratory room which provided nearly constant conditions during the test. The airstream temperatures were measured on each side of both exchangers using both T-type thermocouples and resistance temperature detectors (RTD's).

Humidity was measured on each side of both exchangers using a capacitive humidity sensor. The temperature and humidity sensors were all calibrated and the uncertainties were calculated according to ANSI/ASME PTS 19.1-1998. The mass flow rate of air was measured on both sides of each exchanger using an orifice plate and a differential pressure transducer. The orifice plates and piping were designed following ISO Standard 5167-1. $MgCl_2$ solution was supplied to each exchanger using a 0.092 kW ($1/8^{th}$ hp) magnetic drive pump, and the flow rate was measured using a rotometer. To allow for fluctuations in the desiccant volume due to changes in concentration, a storage tank was placed in the desiccant line after the outlet of each exchanger as shown in Figure 3-3. These storage tanks and lines were insulated to reduce the heat gains/losses between the solution and the surroundings. The entire data acquisition was handled with the use of LabVIEW software, and data was collected at 10 second intervals.

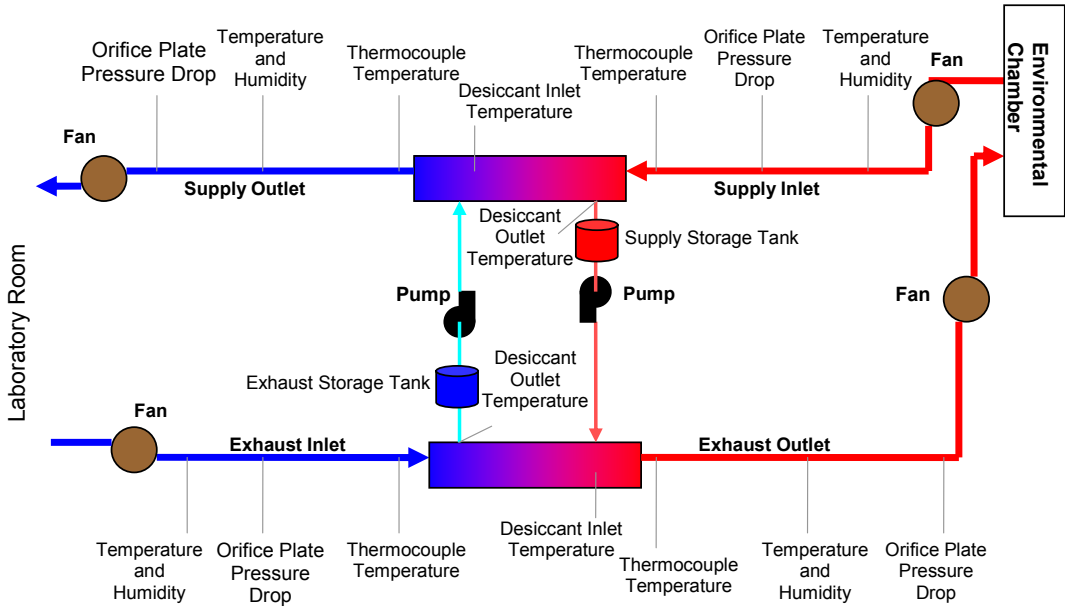

Figure 3-3. Schematic of the Run-Around Membrane Energy Exchanger Testing Apparatus (Erb, 2007).

3.3.3 Comparison of Experimental and Numerical Data

The results from the numerical model are compared to the experimental measurements for both summer and winter operating conditions. This comparison requires the physical size and dimension of the exchangers, headers, storage tanks and piping as well as the heat loss/gain from/to the RAMEE system during the laboratory testing. The external heat gains/losses (σ) were estimated assuming steady state heat transfer from the RAMEE system based on the measured temperatures of the solution and the surroundings, and the size, material and insulation of the experiment components (e.g. storage tanks, pipes and LAMEE headers). The value of σ depends on the test conditions and was estimated to be -0.1 and 0.45 for the supply side of the system and -0.1 and 0.85 for the system exhaust side during the summer and winter test conditions, respectively. This means that the solution looses heat to the surroundings during the summer test conditions and gains heat from the surroundings during the winter test conditions. It needs to be mentioned that the test conditions (i.e. temperature and humidity ratio) are close to, but not exactly, AHRI test conditions (Table 3-1) due to restrictions in conditioning the air to precise values. However, the initial and boundary conditions are taken from the experimental measurements.

Table 3-1. Air and Desiccant Conditions Used in the RAMEE Experimental Comparison

Summer	$T_{Air,in,S}$	305.75 K (32.6ºC)
	$W_{Air,in,S}$	18.3 g/kg
	$T_{Air,in,E}$	298.15 K (25 ºC)
	$W_{Air,in,E}$	9.06 g/kg
	$T_{Sol,Initial,Supply}$	300.35 K (27.2 ºC)
	$T_{Sol,Initial,Exhaust}$	298.55 (25.4 ºC)
Winter	$T_{Air,in,S}$	278.85 K (5.7 ºC)
	$W_{Air,in,S}$	0.616 g/kg
	$T_{Air,in,E}$	296.45 K (23.3 ºC)
	$W_{Air,in,E}$	6.05 g/kg
	$T_{Sol,Initial,Supply}$	293.25 K (20.1 ºC)
	$T_{Sol,Initial,Exhaust}$	295.05 K (21.9.ºC)

The initial salt solution concentration ($C_{Salt,Initial}$) is reported to be (~34%) by weight in the laboratory testing. Knowing inlet air conditions in the supply and the exhaust side of the system, the steady state concentration of liquid desiccant can be calculated from the steady state model for the RAMEE system described in Chapter 2. Therefore, the value of ΔC_{Salt} is obtained to be 8% and -1% during the summer and winter test conditions respectively.

Figures 3-4 and 3-5 show a numerical/experimental comparison of the transient effectiveness for heat and moisture transfer during summer and winter testing respectively. The numerical uncertainties in Figures 3-4 and 3-5 are determined considering the uncertainty of moisture diffusion resistance (δ/k_m) of the membrane and heat loss/gain ratio (σ). The reason for taking the uncertainty of moisture diffusive resistance into account for the comparison of the numerical model data and experimental measurements is the indication of sensitivity studies presented in Chapter 2. It was shown that the moisture diffusion resistance of the membrane has the greatest influence

on the predicted effectiveness of the RAMEE system relative to other simplifying assumptions and property data. The uncertainty of heat loss/gain ratio should be included in the comparison because the exact physical properties (e.g, wall thickness, thermal conductivity, diameter, length) of pipes, headers and reservoirs used to estimate the heat loss/gain from/to the liquid desiccant loop is unknown. The uncertainty of heat loss/gain ratio (φ_σ) is considered to be ±0.05.

The total uncertainty in predicted effectiveness will be a function of both the uncertainty of moisture diffusion resistance and the uncertainty of heat loss/gain ratio. Following ANSI/ASME PTS 19.1-1998, the uncertainty in the predicted transient effectiveness can be estimated as,

$$\varphi_\varepsilon = \sqrt{(\varphi_{\delta/k_m})^2 + (\varphi_\sigma)^2} \tag{3.20}$$

As shown in Figures 3-4 and 3-5 the effectiveness values from the numerical model are in good agreement with experimental data. The simulated effectivenesses show the same trends as the measured data. The sensible effectivenesses cross over in both simulated and experimental data at summer operating conditions as shown in Figure 3-4. As illustrated in Figure 3-5 for winter operating conditions, a divergence trend for supply side and exhaust side effectivenesses and higher differences between these values compared to summer operating conditions were observed during laboratory testing of the RAMEE system. A similar trend is evident in the simulation data.

In Figures 3-4 and 3-5 for most of the transient times the agreement between simulated and experimental results is within the uncertainty limits. In addition, the model

predicts very well the quasi-steady state effectiveness values and the simulated effectivenesses are well within the 95% uncertainty limits of the experiment data. The differences between the numerical and experimental data are mainly attributed to flow distribution problem within liquid channels in the experiment. In the exchangers designed by Erb (2007), the entrances of the liquid channels do not have uniform thicknesses to distribute the liquid desiccant within the liquid channels evenly. As well, the thickness of the liquid channels are not exactly the same in all the panels due to manufacturing variations. Additionally, the membrane deflections in the pressurized RAMEE system cause changes in the hydraulic diameter of the fluid channels. These problems in the design and construction of the exchangers are not addressed in this study.

As illustrated in Figures 3-4 and 3-5, a discrepancy between the simulation and the experiment is observed at initial times. This is due to the fact that it takes time to fill the exchangers with the salt solution in the experiment and also the exact initial conditions are difficult to determine.

(a)

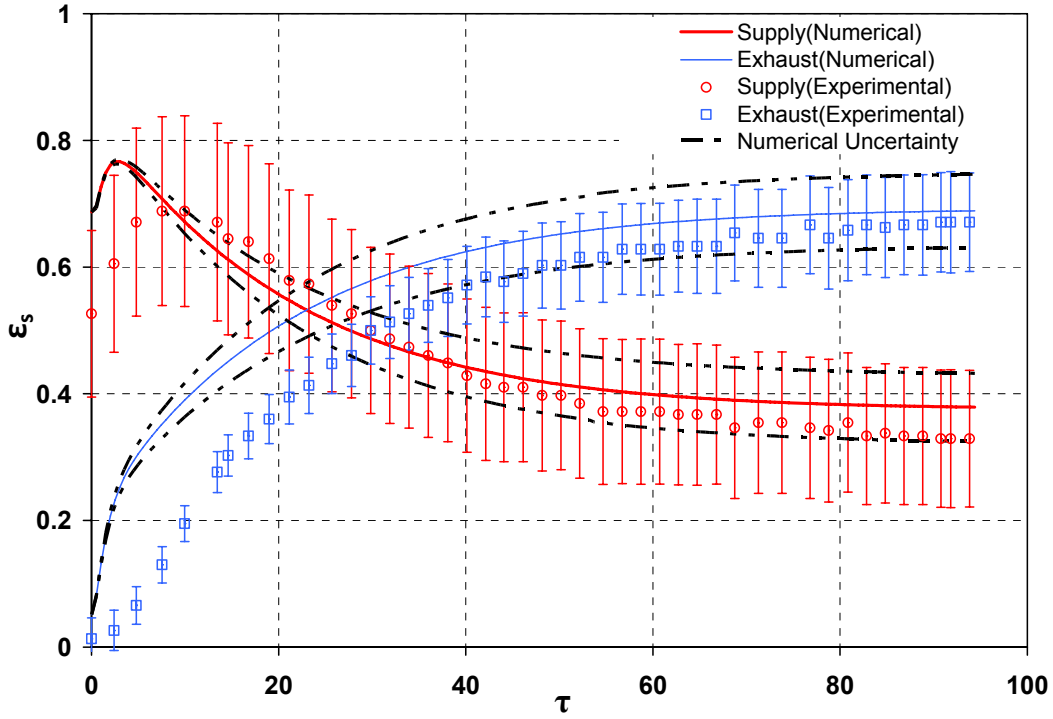
Supply(Numerical)
Exhaust(Numerical)
Supply(Experimental)
Exhaust(Experimental)
Numerical Uncertainty
ε_s
τ
0
0.2
0.4
0.6
0.8
1
0
20
40
60
80
100

(b)

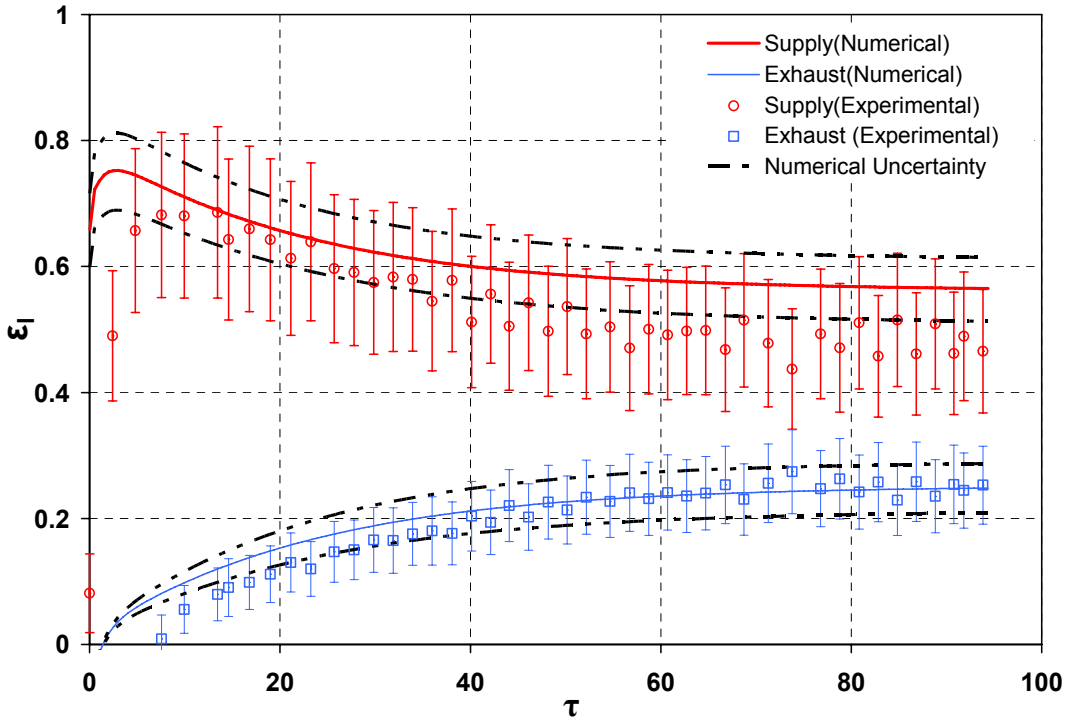
Supply(Numerical)
Exhaust(Numerical)
Supply(Experimental)
Exhaust (Experimental)
Numerical Uncertainty
ε_l
τ
0
0.2
0.4
0.6
0.8
1
0
20
40
60
80
100

(c)

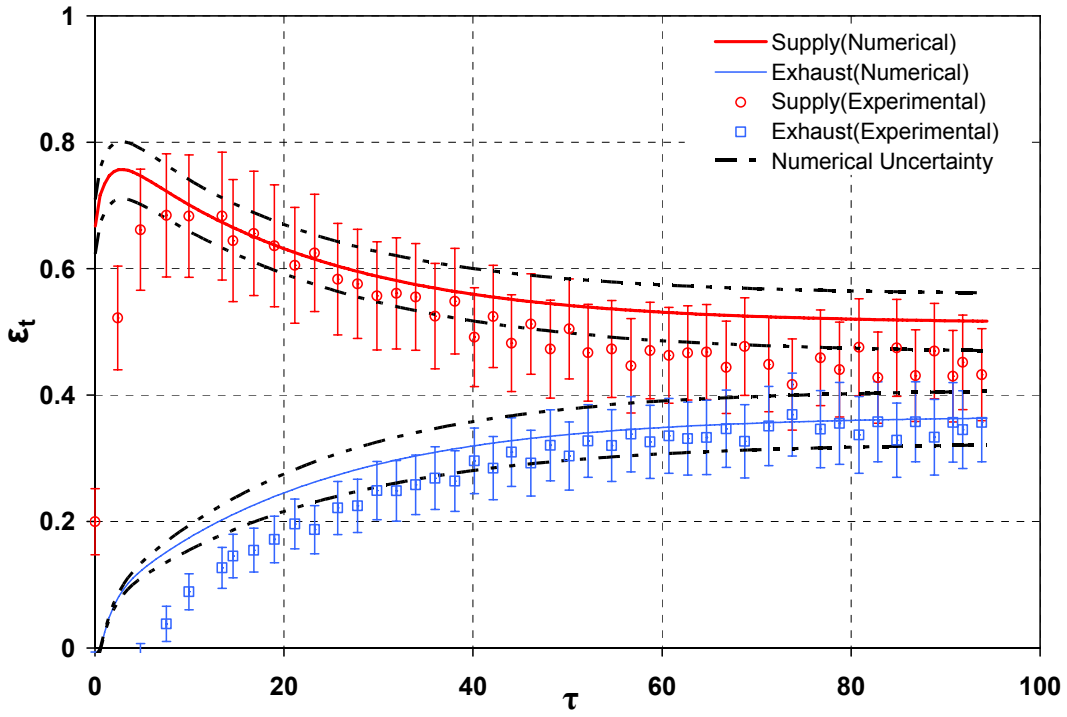

Figure 3-4. Comparison of transient (a) sensible, (b) latent and (c) total effectivenesses calculated from the numerical model with experimental data for a RAMEE system (Summer operating conditions, $NTU_S = NTU_E = 11.5$, $C_{Sol}/C_{Air} = 15$, $\mu = 0.15$, $\sigma_S = -0.1$, $\sigma_E = -0.1$, $\Delta C_{Salt} = 8\%$).[Error bars indicate the 95% uncertainty in measured data.]

During winter test conditions, heat gain from the environment has a significant influence on the transient behavior of the RAMEE system. As shown in Figure 3-5, this phenomenon results in a large difference between the sensible effectiveness of the supply and exhaust exchangers due to excessive addition of heat to the liquid desiccant from the surroundings. This results in high effectiveness values in the supply side while the exhaust side has much lower effectiveness values. As illustrated in Figure 3-5, the aforementioned behavior also can be predicted by the numerical model, and the simulated values show good agreement with the measured values within numerical and experimental uncertainty bounds where the heat loss/gain and salt starting concentration are included.

(a)

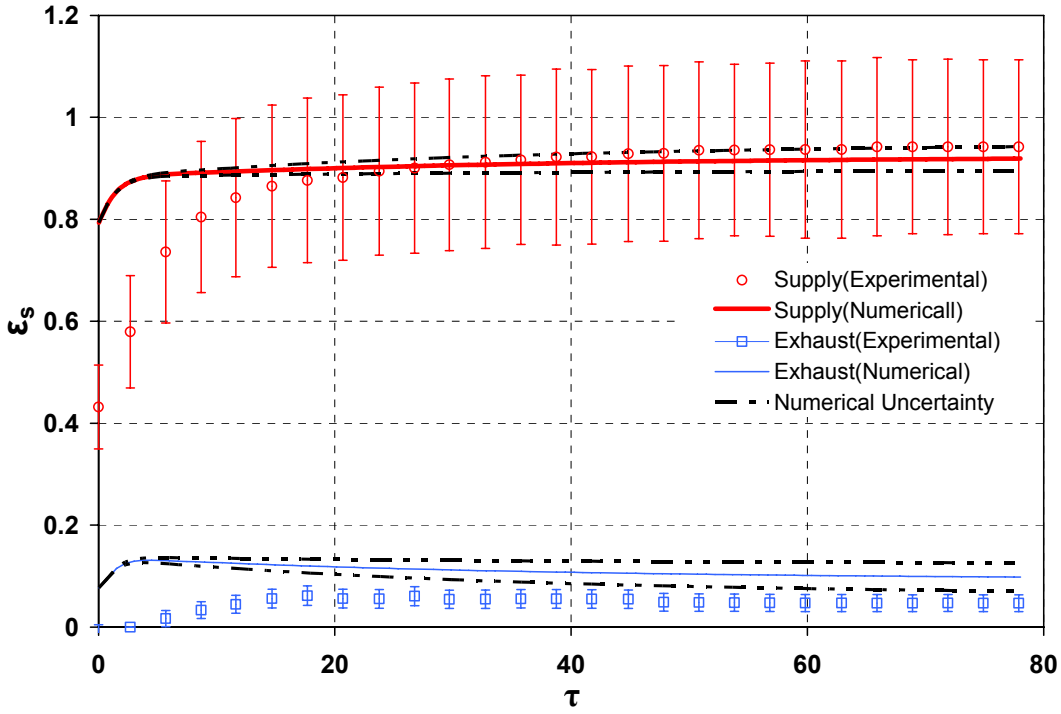
1.2
1
0.8
0.6
0.4
0.2
0
ε_s
0
20
40
60
80
τ
Supply(Experimental)
Supply(Numericall)
Exhaust(Experimental)
Exhaust(Numerical)
Numerical Uncertainty

(b)

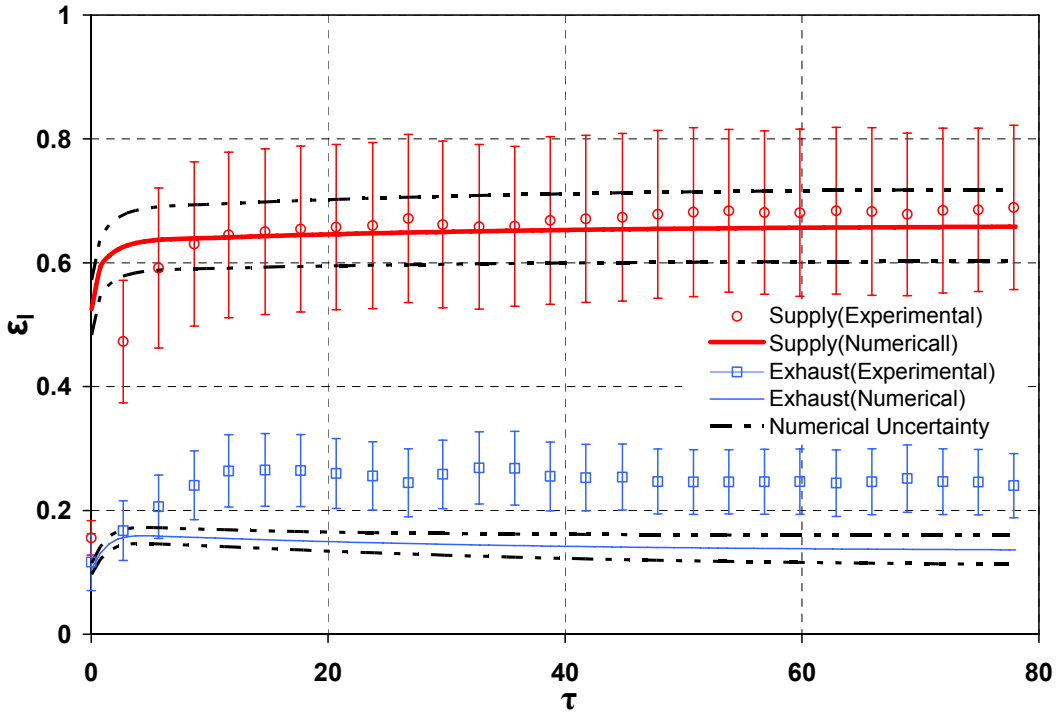
1
0.8
0.6
0.4
0.2
0
ε_l
0
20
40
60
80
τ
Supply(Experimental)
Supply(Numericall)
Exhaust(Experimental)
Exhaust(Numerical)
Numerical Uncertainty

(c)

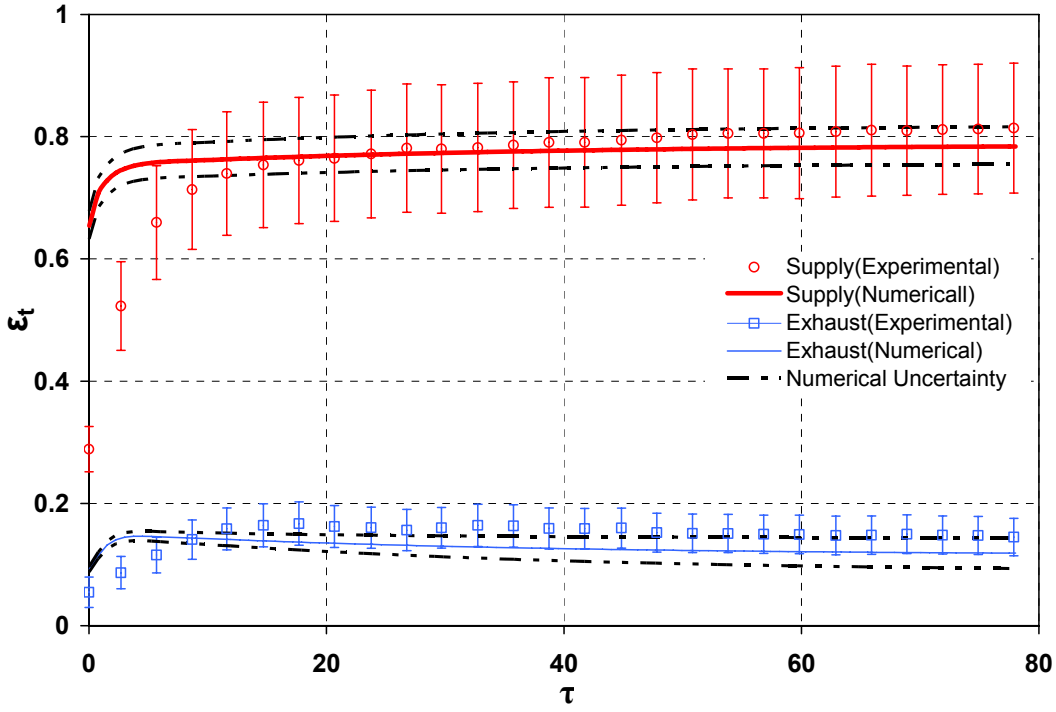

Figure 3-5. Comparison of transient (a) sensible, (b) latent and (c) total effectivenesses calculated from numerical model with experimental data for RAMEE system (Winter operating conditions, $NTU_S = NTU_E = 11.3$, $C_{Sol}/C_{Air} = 22$, $\mu = 0.15$, $\sigma_S = 0.45$, $\sigma_E = 0.85$, $\Delta C_{Salt} = -1\%$).[Error bars indicate the 95% uncertainty in measured data.]

To have a better assessment of the comparison between the numerical and experimental data, the root mean square error (RMSE) for the prediction of simulation model can be calculated as follow:

$$RMSE = \sqrt{\frac{\sum_{1}^{N}(\varepsilon_{Simulation} - \varepsilon_{Experimental})^2}{N}} \tag{3.21}$$

where N is the number of data points in the transient solution used to compare the results. During summer and winter testing conditions, the value of RMSE for various effectiveness values are presented in Table 3-2. One may use these data to evaluate accuracy of a numerical model considering the influence of more parameters

(e.g. non-uniform flow in the exchangers, possible crystallization of the salt solution on the membrane, etc.) on the RAMEE system performance when it is compared to the current model.

Table 3-2. The root mean square error of effectiveness values from the experimental comparison of the RAMEE system at summer and winter operating condition

	Supply sensible	Exhaust sensible	Supply latent	Exhaust latent	Supply total	Exhaust total
Summer testing	0.044	0.097	0.088	0.035	0.073	0.052
Winter testing	0.069	0.065	0.037	0.1	0.051	0.03

In addition to the RMSE, the average absolute difference can be used to quantify the comparison between numerical and experimental data. This value is defined as:

$$\text{Average Absolute Difference} = \frac{\left|\varepsilon_{\text{Simulation}} - \varepsilon_{\text{Experimental}}\right|}{N} \tag{3.22}$$

This average absolute difference for various effectiveness values is presented in Table 3-3. The maximum average absolute difference between the measured and simulated effectivenesses is 7.5% (i.e. exhaust sensible) and 10.3% (i.e. exhaust latent) for summer and winter operating conditions, respectively. Theses errors indicate that the prediction of numerical model is quite good and the validated model can be utilized to investigate the characteristics of the RAMEE system with various parameters and operating conditions.

Table 3-3. The average absolute difference of effectiveness values from the experimental comparison of the RAMEE system at summer and winter operating conditions

	Supply sensible	Exhaust sensible	Supply latent	Exhaust latent	Supply total	Exhaust total
Summer testing	0.035	0.075	0.074	0.024	0.059	0.039
Winter testing	0.037	0.062	0.025	0.103	0.03	0.029

3.4 Summary

In this Chapter the model developed in Chapter 2 for the case of only heat transfer for a single heat exchanger is compared to an available analytical solution and good agreement is obtained. It is shown that the discrepancy between the numerical model results and theoretical solution for the dimensionless bulk outlet temperature of fluids is less than 4% during the transient period. Also, the model is validated with the case of simultaneous heat and moisture during the laboratory testing of a RAMEE system. The results for both sensible and latent effectiveness showed good agreement at different operating conditions. It is shown that the agreement is often within experimental and numerical uncertainties. However, there are some discrepancies between the transient simulation and laboratory testing of the RAMEE system due to experimental flow distribution problems within the exchangers during the laboratory testing. Further investigation should be conducted to include flow mal-distribution in the numerical model to improve this comparison. The maximum average absolute difference between the simulated and experimental data for the transient effectiveness is obtained to be 10.3% which implies good accuracy of the numerical model for the RAMEE system with complex design characteristic and testing facilities.

CHAPTER 4
SENSITIVITY STUDY FOR A RANGE OF INITIAL CONDITIONS

4.1 Introduction

The purpose of this chapter is to employ a parametric study with several dimensionless variables to investigate the transient performance of the RAMEE system consisting of two cross flow heat and moisture exchangers with the parameters and properties of the LAMEE described in Table 2-2. Results are presented for different values of NTU, C_{Sol}/C_{Air}, and μ for balanced air flow rates for a sufficient time duration so that quasi-steady state operating conditions can be deduced. As well, a finite heat loss/gain ratio is included in the RAMEE system to study the effect of external heat loss or gain on the performance of the run-around heat and moisture recovery system. Finally, an investigation of the initial salt solution concentration and its impact on the transient response of the RAMEE system is presented.

4.2 Effects of Number of Heat Transfer Units (NTU)

The effectiveness values change with time after a step change in the inlet conditions. The time it takes to reach a new quasi-steady state is strongly influenced by the operating conditions. Figure 4-2 shows the dynamic behavior of the supply and exhaust exchangers at different operating conditions as a function of the number of the liquid desiccant circulations in the system, τ, which is a dimensionless characteristic time. Excluding the reservoirs and piping, the time for one circulation is the time required for the bulk mean properties of the salt solution to flow through both the supply and exhaust exchangers or

the time for the salt solution in both exchangers to be replaced by the incoming fluid. From Figure 4-1 (a) and (b) (AHRI summer conditions) and Figure 4-2 (a) and (b) (AHRI winter conditions), it is noted that approximately the same number of liquid desiccant circulations are required to reach quasi-steady state for both sensible and latent effectiveness. Figure 4-1 and Figure 4-2 show that, at quasi-steady state conditions, the effectiveness values for the supply and exhaust exchangers are the same due to mass and energy balances in the RAMEE system. As shown in these figures, the NTU for the supply exchanger is approximately equal to NTU for the exhaust exchanger. This is due to the fact that exchangers in the supply and exhaust side are identical and the fluid flow rates are equal. In the rest of this chapter, the value of NTU is considered equal for both supply and exhaust exchanger and therefore, a unique value is reported. Nevertheless, due to the different properties of the air and salt solution in each exchanger this NTU value will slightly deviate (less than 0.1%) from the reported value. The similar explanation is valid for number of mass transfer units (NTU_m).

(a)

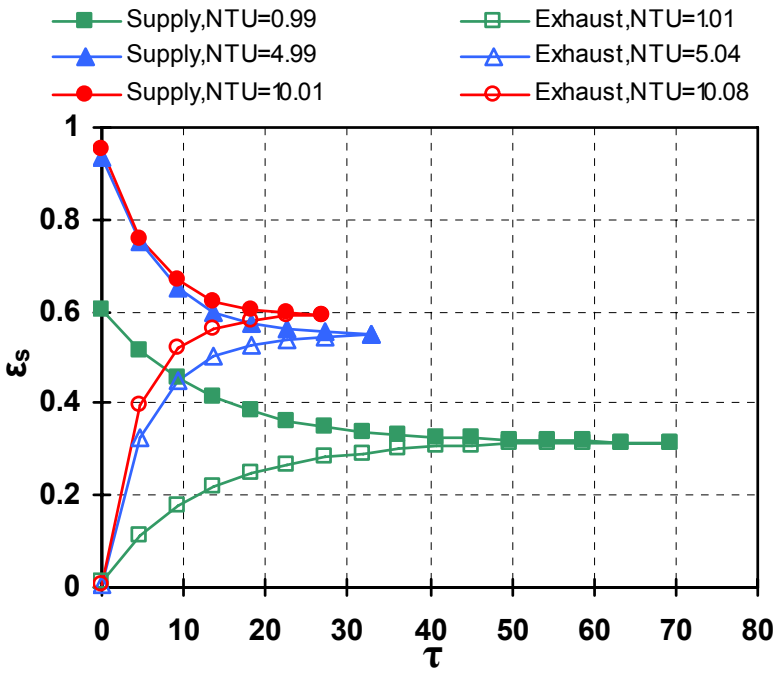

(b)

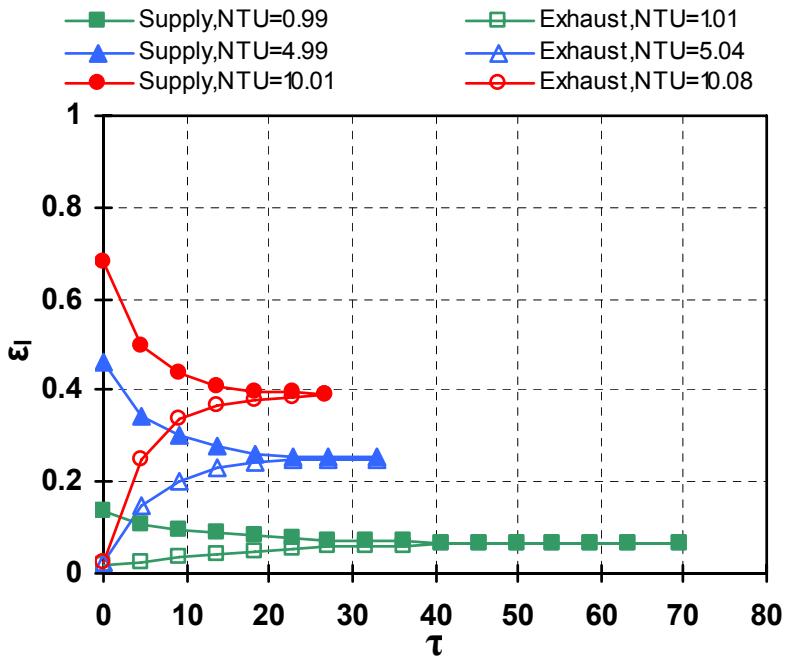

Figure 4-1. Effectiveness of the RAMEE system for (a) sensible and (b) latent heat transfer during AHRI summer test conditions versus the number of liquid desiccant circulation cycles at different NTU values(C_{Sol}/C_{Air} = 3, μ = 0.15, σ = 0, ΔC_{Salt} = 0).

(a)

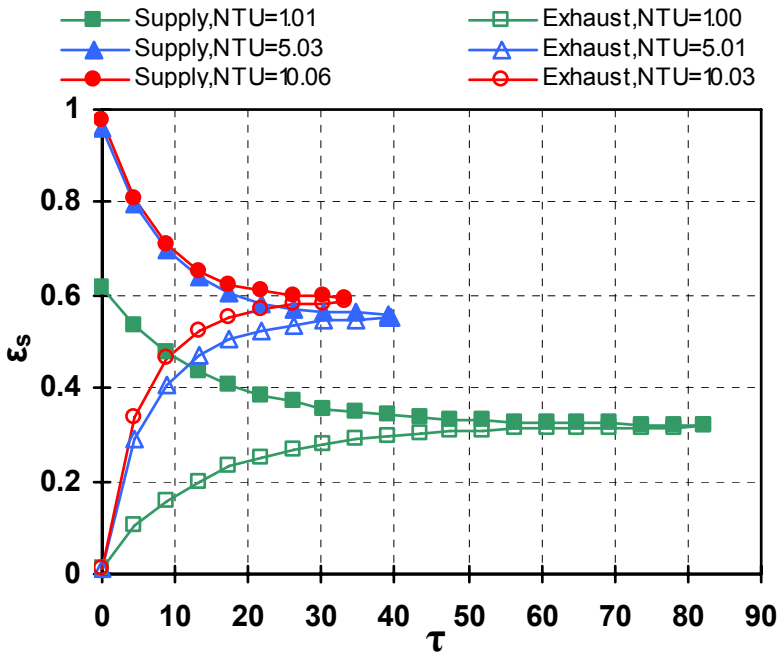

(b)

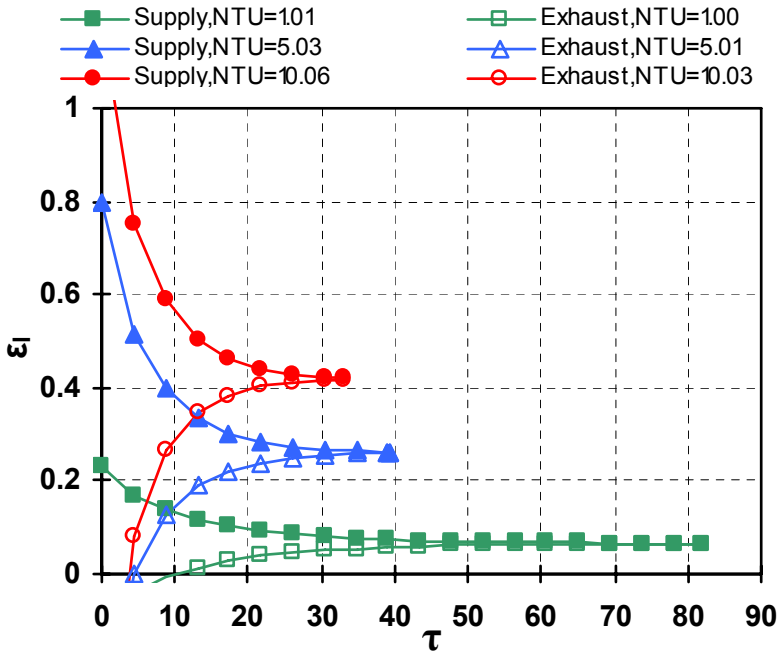

Figure 4-2. Effectiveness of the RAMEE system for (a) sensible and (b) latent heat transfer during AHRI winter test conditions versus the number of liquid desiccant circulation cycles at different NTU values($C_{Sol}/C_{Air} = 3$, $\mu = 0.15$, $\sigma = 0$, $\Delta C_{Salt} = 0$).

For the RAMEE system consisting of two identical exchangers with parameters and properties used in the experimental comparison section (See Table 2-2), the real time (min.) equivalent to one circulation depends on both NTU and C_{Sol}/C_{Air}. This real time (τ') is defined as the dimensional value of one circulation. Figure 4-3 shows that doubling number of heat transfer units (NTU), doubles the τ' and doubling heat capacity ratio (C_{Sol}/C_{Air}), halves τ'. One may use this figure to convert the number of desiccant circulations to real time (min.) by knowing the operating condition of the RAMEE system. As illustrated in Figure 4-3, the real time equivalent to one circulation is equal to 7.4 min. where NTU = 5 and C_{Sol}/C_{Air}= 3 for AHRI summer operating condition. This value in conjunction with number of circulations shown in Figure 4-2 (a) and (b) indicates that it will take 242 min (or 4.03 hours) for the aforementioned system with NTU = 5, C_{Sol}/C_{Air} = 3, μ = 0.15, σ = 0, ΔC_{Salt} = 0 to reach quasi-steady state condition at AHRI summer operating conditions.

(a)

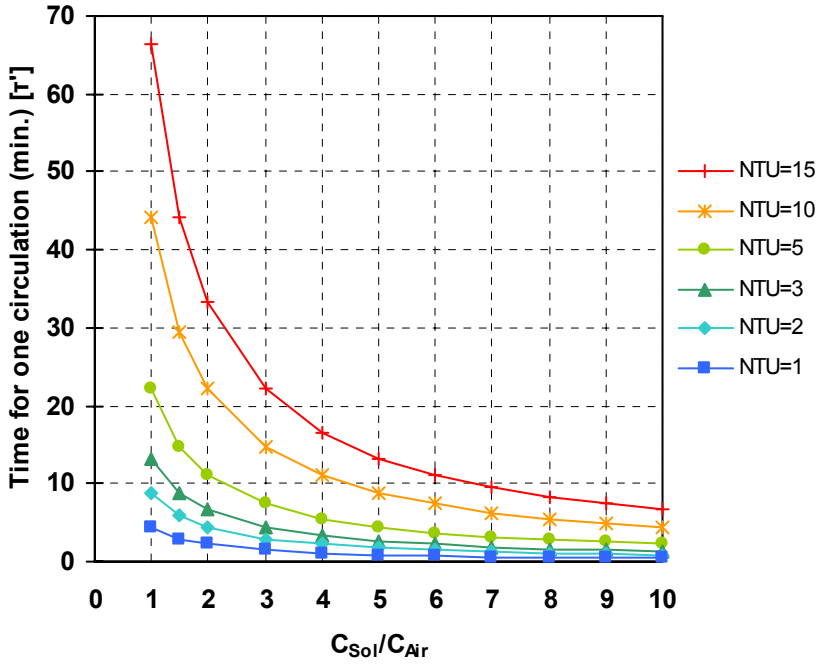

(b)

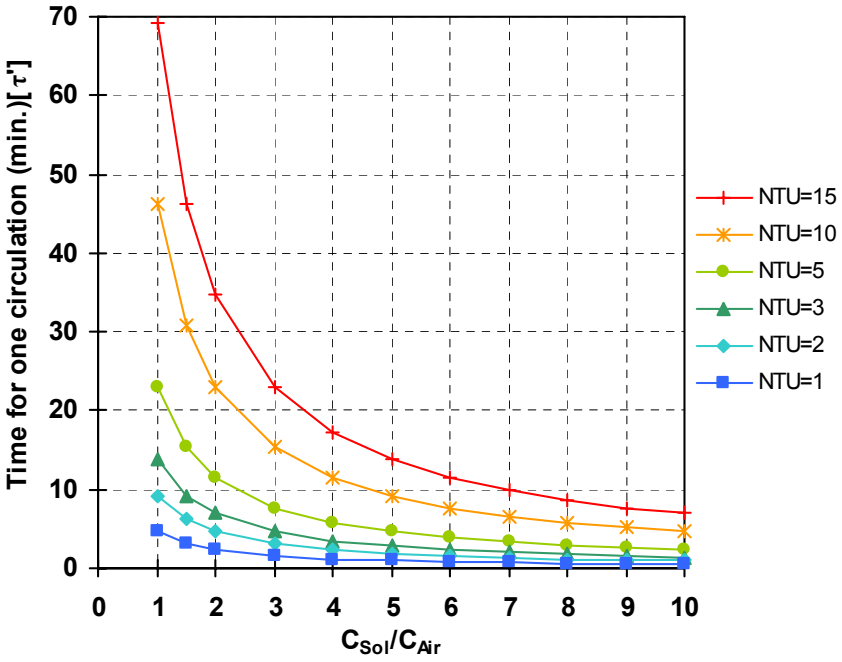

Figure 4-3. The real time required for one circulation versus C_{Sol}/C_{Air} with NTU as a parameter for the RAMEE system with two identical exchangers with parameters and properties in Table 2-2 for (a) AHRI summer and (b) AHRI winter operating conditions.

The effect of the number of heat transfer units (NTU) on the transient response of the system at AHRI operating conditions (AHRI 2005) is more evident in Figure 4-4. It should be reminded that NTU increases when the heat exchanger dimensions increase or the mass flow rate of air decreases (the mass flow rate of air is modified in this thesis since the geometry of the LAMEEs are fixed). At low air mass flow rates, more time is required for the air within the channels to be replaced by incoming air. This causes the air and the liquid desiccant within the exchangers to have more time to be in contact with each other. As a result the RAMEE system requires a fewer number of desiccant circulations (η) to reach equilibrium. Therefore, an increase in NTU reduces the number of liquid desiccant circulations required for quasi-steady state to be reached. Figure 4-4 shows that when NTU changes from 5 to 10, the number of circulations required to reach quasi-steady state decreases from 33 to 27 which is a 19% reduction for the AHRI summer operating conditions. Figure 4-4 demonstrates that η decreases by more than 52% in both AHRI summer and winter operating conditions when NTU is increased from 1 to 5.

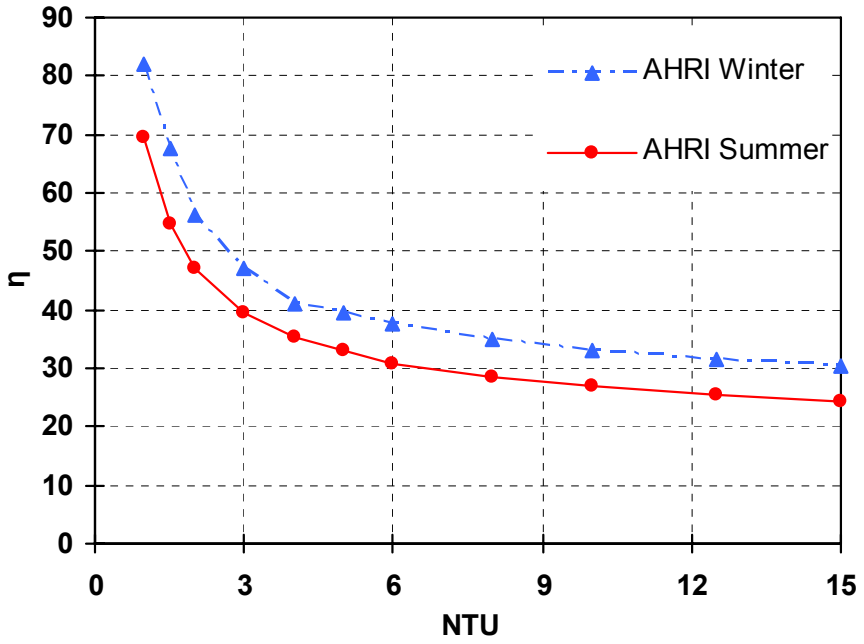

Figure 4-4. Change in the number of liquid desiccant circulations to reach quasi-steady state for the RAMEE system due to different NTU values at AHRI operating conditions ($C_{Sol}/C_{Air} = 3$, $\mu = 0.15$, $\sigma = 0$, and $\Delta C_{Salt} = 0$).

On the other hand, the actual time or real time required to reach equilibrium (η') will increase with NTU as shown in Figure 4-5. This occurs because the higher the NTU the more slowly the run-around fluid is pumped for a given geometry of each exchanger in order to keep the same heat capacity ratio (C_{Sol}/C_{Air}) as shown in Figure 4-3 and the slower the RAMEE system will reach steady state condition. As illustrated in Figure 4-3, τ' is proportional to NTU (doubling NTU, doubles τ'), however doubling NTU in Figure 4-4 does not half η. Therefore, it can be expected that the real time required to reach quasi-steady state (η') will increase as NTU increases as shown in Figure 4-5. It is shown that η' increases from 242.5 min. (4.04 hours) to 395 min. (6.58 hours) when NTU changes from 5 to 10 for the AHRI summer operating conditions

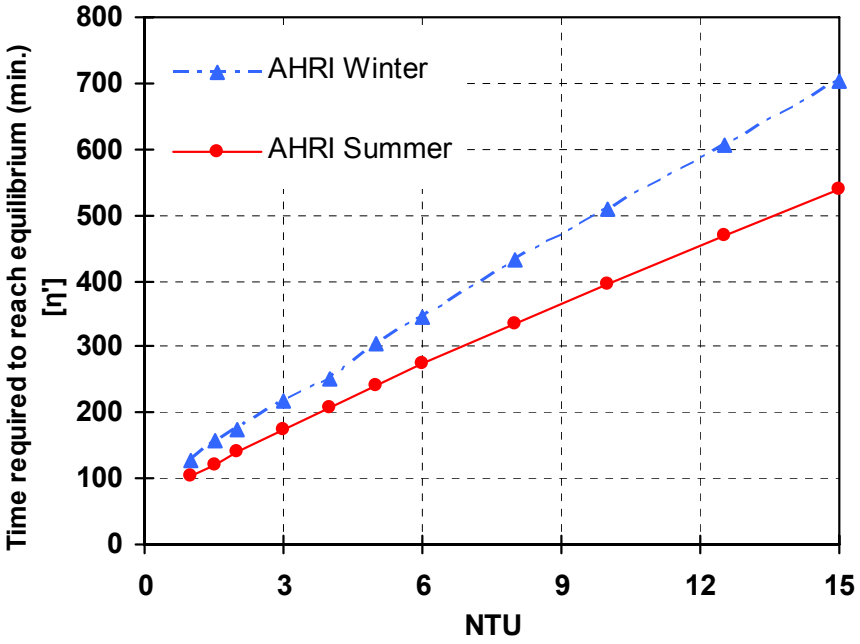

Figure 4-5. The real time (min.) required to reach equilibrium versus NTU for the RAMEE system with two identical LAMEEs with parameters and properties in Table 2-2 at AHRI operating conditions ($C_{Sol}/C_{Air} = 3$, $\mu = 0.15$, $\sigma = 0$, and $\Delta C_{Salt} = 0$).

4.3. Effects of Heat Capacity Rate Ratio (C_{Sol}/C_{Air})

The run-around system allows the pumping rate of the liquid salt solution to be selected arbitrary, independent of the inlet air conditions. The effectiveness values (Fan et al., 2006) as well as the time required to reach steady state will vary with different salt solution mass flow rates in the RAMEE system. The higher desiccant pump flow rates result in an increase in the heat capacity ratio of the exchanger when NTU is kept constant for a fixed geometry. As seen in Figure 4-6, the number of liquid desiccant circulations required to reach quasi-steady state decreases as C_{Sol}/C_{Air} decreases because the dwell time of the salt solution in the exchanger channels increases as C_{Sol}/C_{Air} decreases. This provides more time for the air and desiccant liquid to exchange heat and moisture during one pass of the liquid. Figure 4-6 displays the number of times the salt solution must pass through both exchangers before quasi-steady state is achieved. At

AHRI summer operating conditions, η is reduced by up to 81% when C_{Sol}/C_{Air} changes from 10 to 1 at NTU = 5.

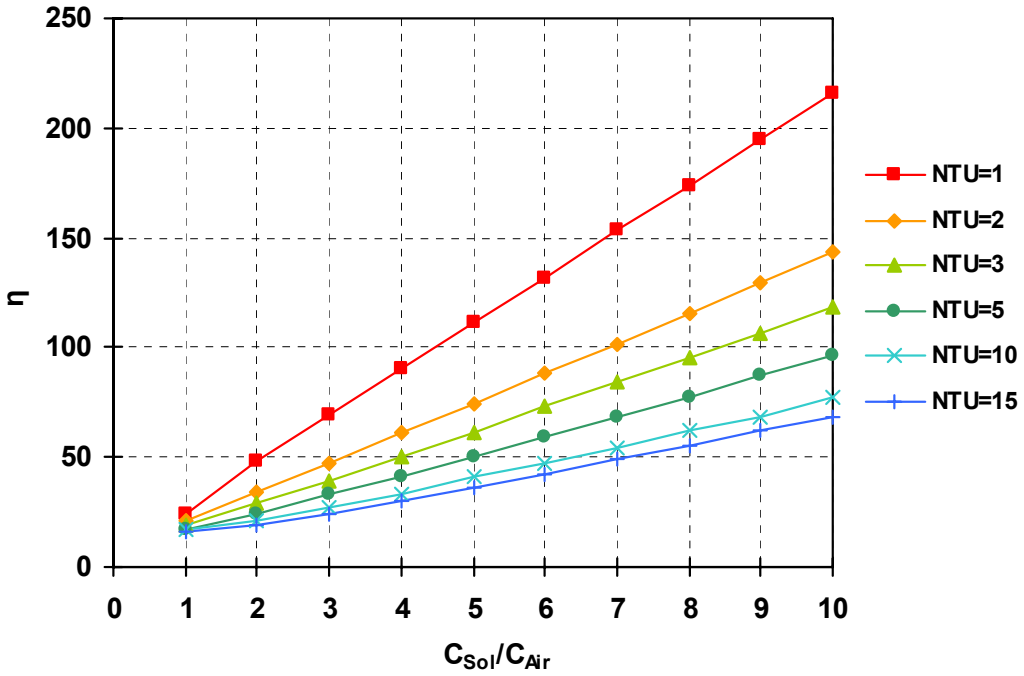

Figure 4-6. Change in the number of liquid desiccant circulations to reach quasi-steady state conditions for the RAMEE system for different C_{Sol}/C_{Air} values with NTU as a parameter for AHRI summer operating conditions ($\mu = 0.15$, $\sigma = 0$, and $\Delta C_{Salt} = 0$).

In practical applications, the real time required to reach quasi-steady state (η') is of interest and the HVAC engineer would need to know how η' changes as the solution pumping rate changes. Figure 4-7 shows that the transient response of the system decreases (in real time) as C_{Sol} increases. Although the number of circulations required for the salt solution to flow through both the supply and exhaust exchangers decreases from 96 to 17 for AHRI summer operating conditions when the C_{Sol}/C_{Air} value changes from 10 to 1, Figure 4-7 shows that the response time will increase from 212.7 min. (or 3.54 hours) to 387.5 min. (or 6.46 hours) in real time for the RAMEE system with two identical LAMEEs with parameters and properties in Table 2-2. This is expected because

τ' increases by a factor of 10 when C_{Sol} decreases by a factor of 10 as shown in Figure 4-3, while η only decreases by a factor of 5.6. Therefore, η' will nearly double.

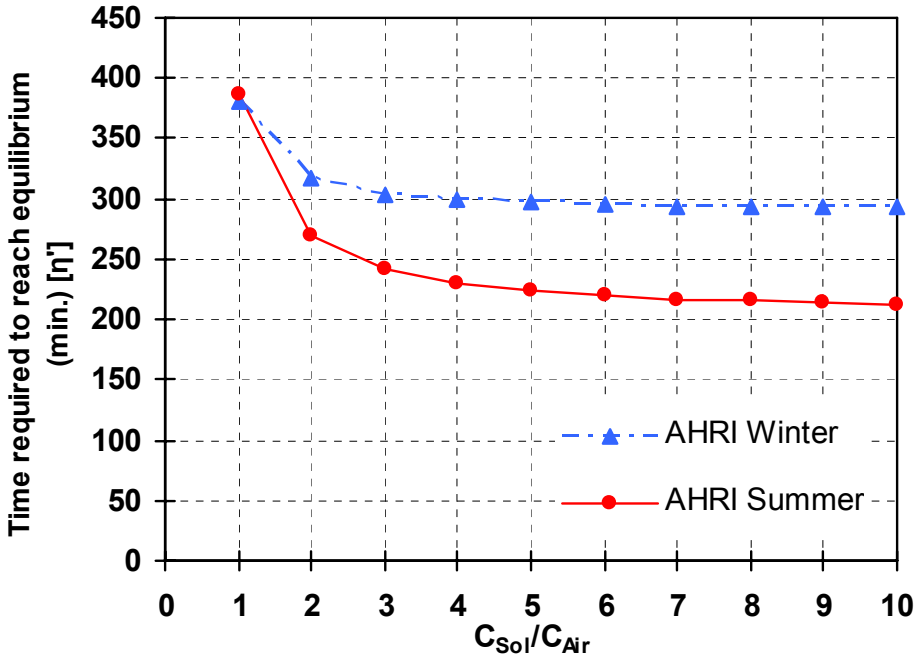

Figure 4-7. The real time (min.) required to reach equilibrium versus C_{Sol}/C_{Air} for the RAMEE system with two identical LAMEEs with parameters and properties in Table 2-2 at AHRI operating conditions (NTU=5, μ = 0.15, σ = 0, and ΔC_{Salt} = 0).

The change in the airstream inlet conditions affects the dynamic response of the RAMEE system. A comparison between the AHRI summer and winter results is presented in Figure 4-8. Figure 4-8 shows that the RAMEE system reveals a similar behavior in both AHRI summer and winter conditions with an increase in the mass flow rate of the liquid desiccant in the exchangers where the other parameters are the same. However, there is a difference in the dimensionless time it takes the system to reach steady state. This response time variation between different operating conditions is believed to be caused by a higher change in the temperature that the liquid desiccant will undergo to reach quasi-steady state at AHRI winter operating conditions. The numerical

model shows that at NTU = 5 and $C_{Sol}/C_{Air} = 3$ the average change in the liquid desiccant temperature is 9.6ºC for AHRI winter operating conditions, while this change will be 6.7ºC at AHRI summer operating conditions for the identical exchangers at the same NTU and C_{Sol}/C_{Air} values.

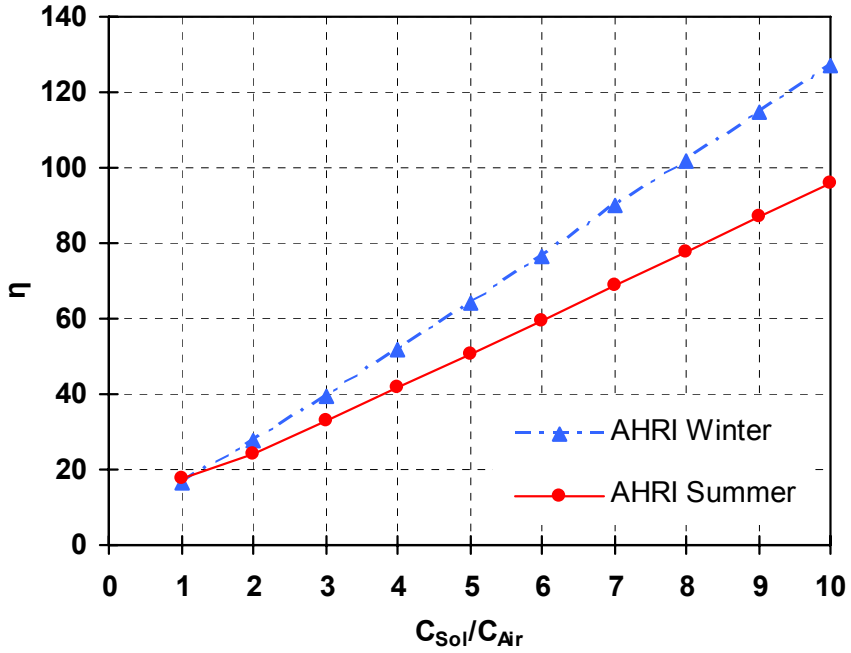

Figure 4-8. Change in the number of liquid desiccant circulations to reach quasi-steady state conditions for the RAMEE system for different C_{Sol}/C_{Air} values at different operating conditions (NTU = 5, $\mu = 0.15$, $\sigma = 0$, and $\Delta C_{Salt} = 0$).

The various heat capacity ratio values, C_{Sol}/C_{Air}, not only change the transient response of the RAMEE system, but also the quasi-steady state effectiveness values. Figure 4-9 reveals that the RAMEE system at AHRI summer operating conditions has a higher total effectiveness at approximately $C_{Sol}/C_{Air} = 3$ which is in agreement with the previous finding (Fan et al., 2006). It should be mentioned that the numerical model results in this section are presented at NTU = 5 which may not clearly show the occurrence of the effectiveness peak at $C_{Sol}/C_{Air} = 3$; however, this peak is be more

evident as NTU increases (See Figure 1-6). It is also shown that the maximum effectiveness of a run-around heat and moisture recovery system depends on the operating conditions so that the peak value occurs at a different C_{Sol}/C_{Air} value for AHRI winter operating conditions. This is due to the fact that the ratio between the sensible and latent energy transfers changes as the system operating condition changes. Simonson and Besant (1999a; 1999b) developed an operating condition factor as follow:

$$H^* \approx 2500\frac{\Delta W}{\Delta T} = 2500\frac{W_{Air,in,S} - W_{Air,in,E}}{T_{Air,in,S} - T_{Air,in,E}} \tag{4.1}$$

The operating condition factor (H^*) represents the ratio of latent to sensible energy differences between the inlets of air streams. During the AHRI summer operating conditions the value of operating condition factor ($H^* = 1.86$) is greater than the value for AHRI winter test conditions ($H^* = 0.47$). Therefore more latent energy needs to be transported by the salt solution in the summer and the heat capacity rate of the salt solution (C_{Sol}) needs to be greater to transport this energy.

(a)

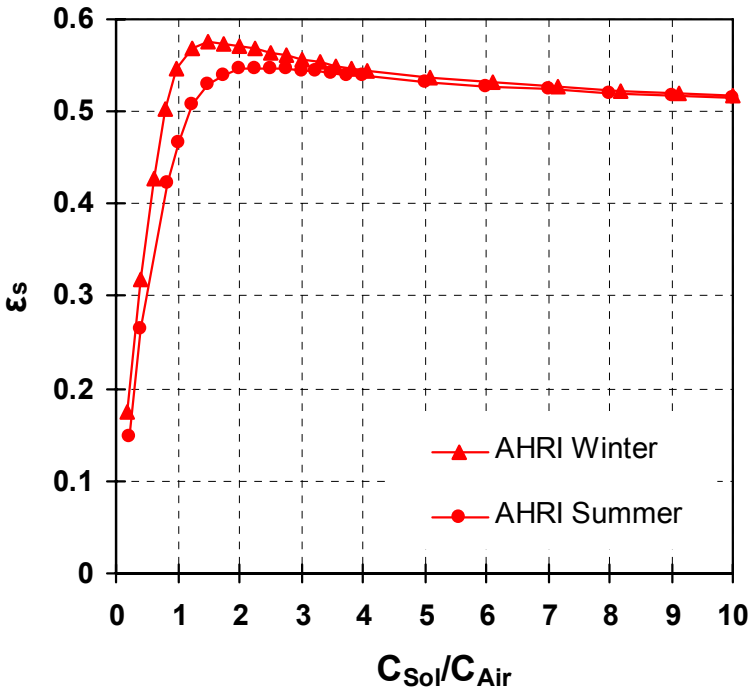
0.6
0.5
0.4
0.3
0.2
0.1
0
εs
AHRI Winter
AHRI Summer
0
1
2
3
4
5
6
7
8
9
10
CSol/CAir

(b)

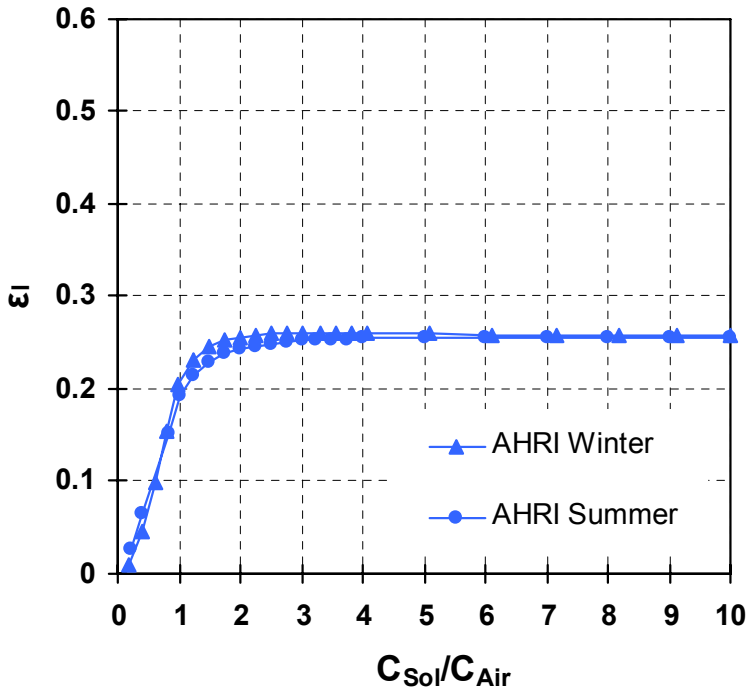
0.6
0.5
0.4
0.3
0.2
0.1
0
εl
AHRI Winter
AHRI Summer
0
1
2
3
4
5
6
7
8
9
10
CSol/CAir

(c)

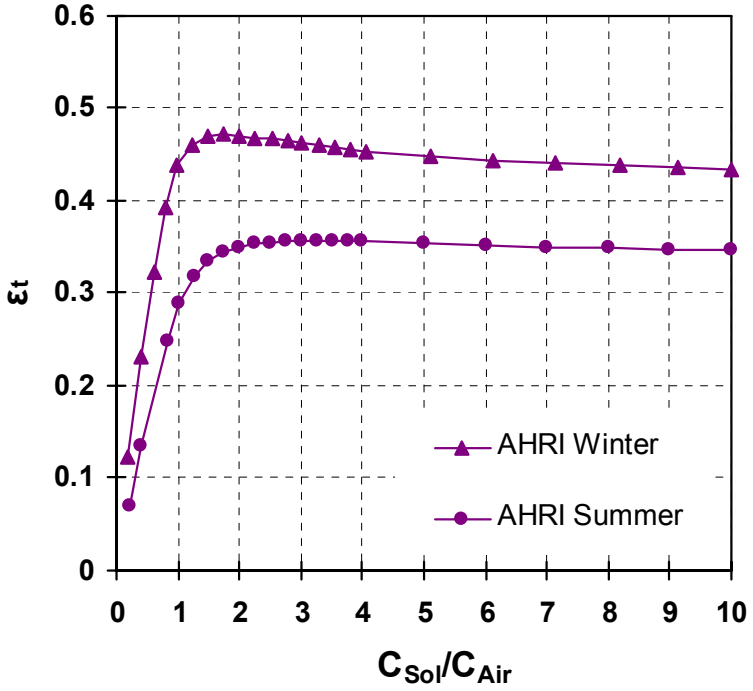

Figure 4-9. Variation of the (a) sensible, (b) latent and (c) total effectivenesess of the RAMEE system as a function of C_{Sol}/C_{Air} for AHRI summer and winter operating conditions (NTU = 5).

The quasi-steady state performance of the RAMME system can be analyzed with changes in another two parameters associated with mass transfer in the system. These parameters, which appear in the governing equations, are number of mass transfer units (NTU_m) and mass flow rate of pure salt in the coupling fluid to dry air ($\dot{m}_{Salt}/\dot{m}_{Air}$). Figure 4-10 depicts the effectiveness of the RAMEE system at $NTU_m = 5$ with various mass flow rate of pure salt to mass flow rate of dry air ratios ($\dot{m}_{Salt}/\dot{m}_{Air}$). As illustrated in Figure 4-10 (c), the maximum total effectiveness of the system occurs approximately at $\dot{m}_{Salt}/\dot{m}_{Air} = 1$ for AHRI summer operating conditions. The same behavior for the RAMEE system at steady state condition was observed in another numerical study (Fan et al., 2006). This indicates that in the practical operation of the run-around system at its

best energy transfer rate, the pumping rate of the coupling fluid should be adjusted to a value in order that the mass flow rate of the pure salt in the fluid is approximately the same as the mass flow rate of dry air. Nevertheless, this maximum value will occur at lower $\dot{m}_{Salt}/\dot{m}_{Air}$ value for AHRI winter operating condition as shown Figure 4-10 (c).

(a)

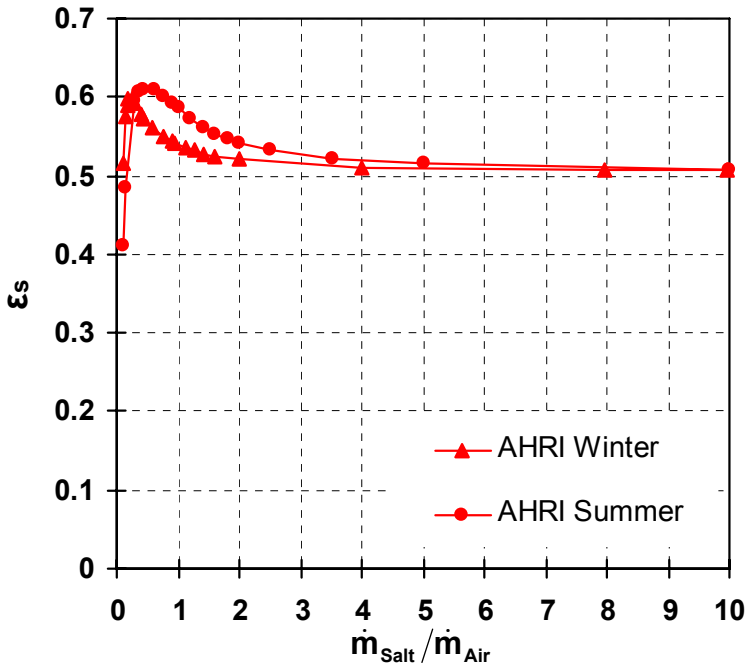

(b)

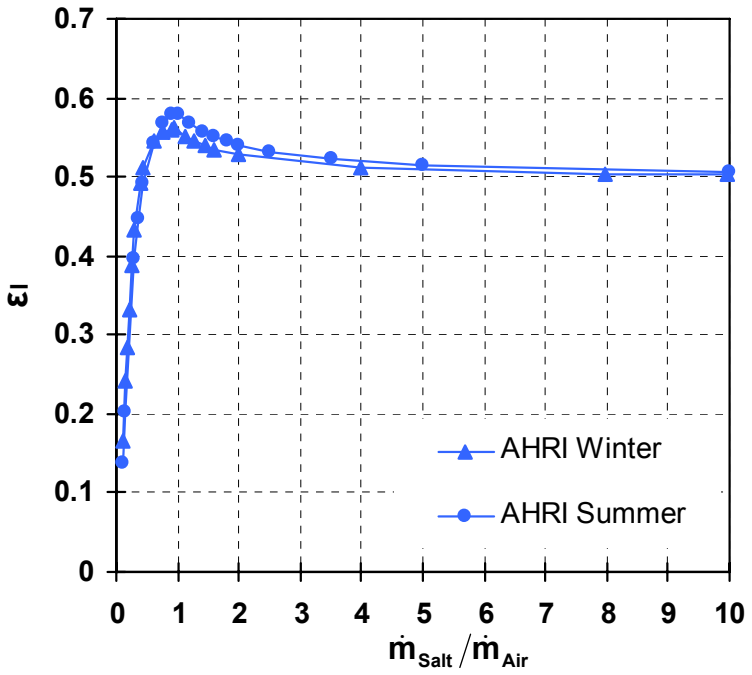

(c)

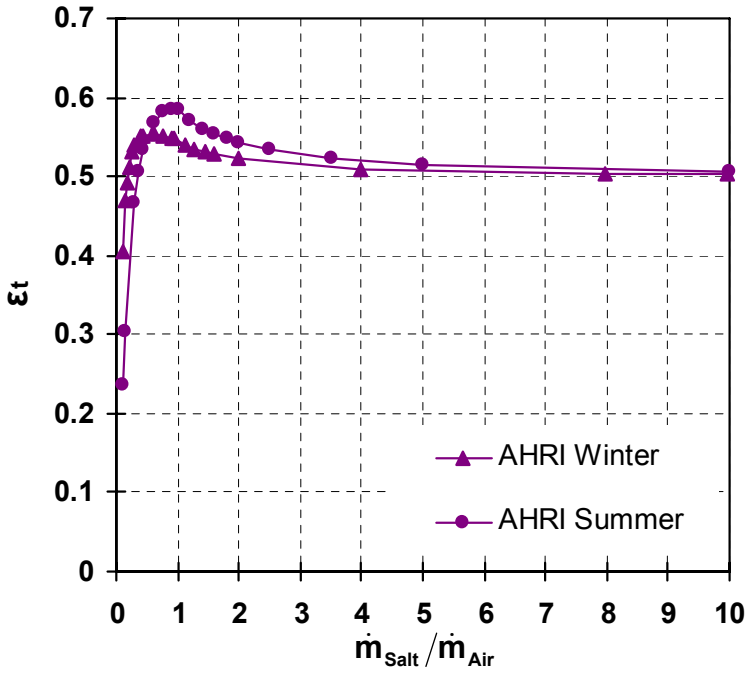

Figure 4-10. Variation of the (a) sensible, (b) latent and (c) total effectivenesess of the RAMEE system as a function of $\dot{m}_{Salt}/\dot{m}_{Air}$ for AHRI summer and winter operating conditions (NTU_m = 5).

4.4 Effect of Storage Volume of Salt Solution on the Transient Response (μ)

One of the aims of the present work is to study the effect of salt solution storage volume on the transient response of the RAMEE system. As shown in Figure 4-11, the size of the reservoirs has a substantial impact on the rate at which the RAMEE system moves toward equilibrium. The presence of a large liquid volume in the reservoirs increases the mass of desiccant that must undergo a transient change in temperature and concentration. This increases the time it takes the system to reach steady state. Large time delays may be problematic for the operation of the HVAC system in some climates where the temperature and humidity change frequently and by large amounts. In this study, a large liquid volume in each storage tank corresponds to a small value of μ, where μ is the initial fraction of the mass of salt in the exchangers to the mass of salt in the entire system including exchangers, storage tanks and piping. Figure 4-11 presents the effect of the initial mass fractions on the time required to reach quasi-steady state (η) for both AHRI summer and winter operating conditions. Figure 4-11 demonstrates that an increase in μ from 0.15 (used in the experimental comparison) to 0.5, which corresponds to a 5.5 times reduction in the size of storage tanks, results in a 75% faster response time for both AHRI operating conditions. The transient response could be reduced by a further 33% if μ is increased from 0.5 to 0.75, i.e., if the volume of the storage tank is reduced to two thirds.

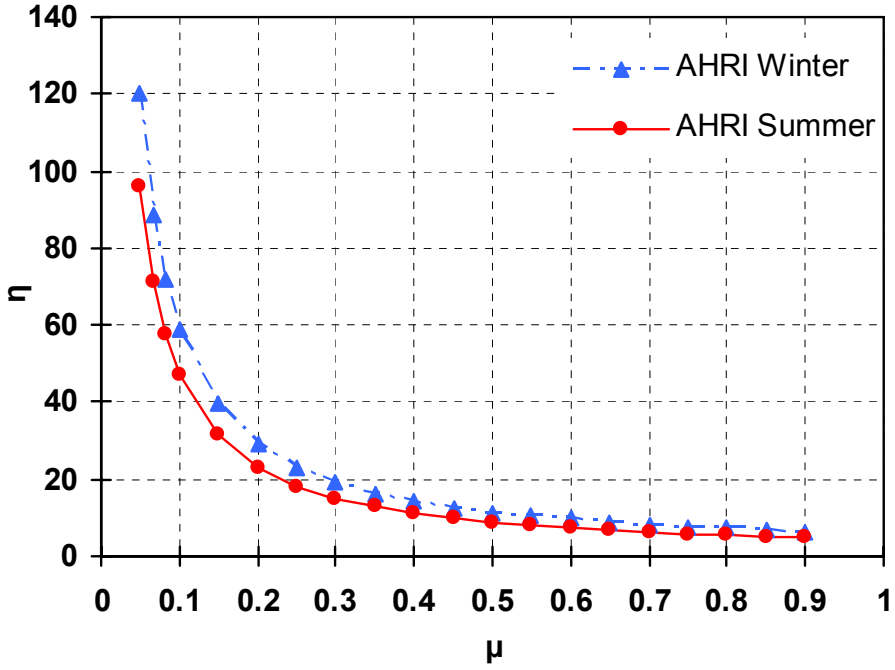

Figure 4-11. Change in the number of liquid desiccant circulations to reach quasi-steady state condition for the RAMEE system due to different size of storage tanks for AHRI operating conditions (NTU = 5, $C_{Sol}/C_{Air} = 3$, $\sigma = 0$, $\Delta C_{Salt} = 0$).

It is worth noting that even though a higher μ values result in a faster system response, there will be a minimum allowable storage volume for a range of ambient weather conditions. This minimum storage volume depends on several parameters which cannot be selected arbitrarily. The operating condition of the system, including inlet air conditions, has a significant impact on the appropriate size of the storage volume. In practice, the operating condition may change on a daily or even an hourly basis. This suggests that the appropriate liquid desiccant storage volume must be chosen to cover a range of humidity conditions from dry to humid during which the desiccant volume will change significantly. To determine this range of desiccant volumes, the appropriate desiccant type and concentrations must first be determined. It should be mentioned that

the storage volume of the piping is included in μ and therefore μ will decrease as the distance between the supply and exhaust exchangers increases.

4.5 Effect of Heat loss or Gain (σ)

As presented in Chapter 2, both heat losses from the salt solution (shown with a (-) value for σ) and heat gains to the liquid desiccant (shown with a (+) value for σ) have a significant effect on both the supply and exhaust sensible and latent effectiveness values of a practical RAMEE system. In this section, the effect of heat loss/gain during summer and winter operating conditions will be studied for a wide range of heat losses/gains and compared to the case where the system is perfectly insulated.

Figure 4-12 demonstrates that in the presence of heat loss, the transient response of the system at AHRI summer operating conditions is similar to the case where $\sigma = 0$; however, the quasi-steady effectiveness values on both sides of the RAMEE system change as σ changes. The effect is similar for AHRI winter operating conditions and is not shown graphically.

(a)

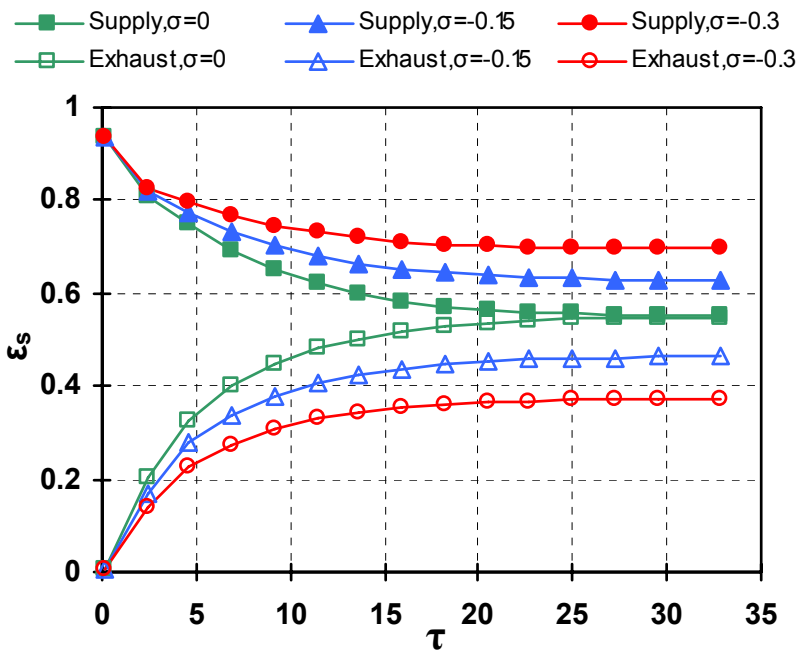

(b)

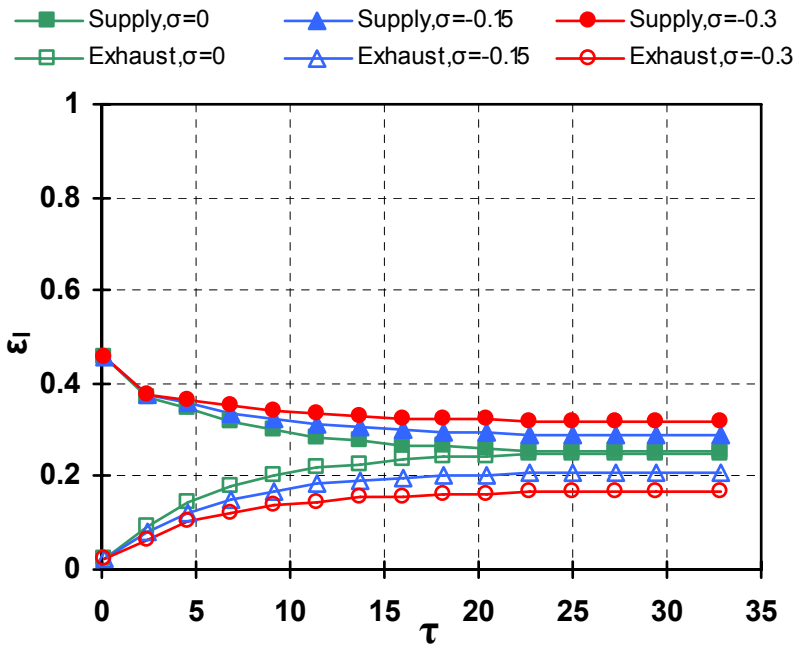

Figure 4-12. Transient (a) sensible and (b) latent effectivnesses of the RAMEE system due to heat loss for AHRI summer operating conditions (NTU = 5, C_{Sol}/C_{Air} = 3, μ = 0.15, and ΔC_{Salt} = 0).

During summer operating conditions, the temperature of the liquid desiccant is higher than its surrounding temperature if the RAMEE system is housed in a mechanical room which is conditioned close to room temperature. This may result in a heat loss ($\sigma < 0$) from the RAMEE system to the surroundings. Figure 4-12 shows that the supply side effectiveness increases as the heat loss increases. In the presence of heat loss from the salt solution, the liquid desiccant temperature will drop and provide higher potential to exchange heat between the warm supply air and the salt solution flow. As shown in Figure 4-13, the temperature difference between the supply airstream and the salt solution inlet flow ($T_{Air,in,S} - T_{Sol,in,S}$) is higher when there is a heat loss ($\sigma_S = -0.3$) from the system compared to the case of no heat loss ($\sigma_S = 0$). As well, the lower desiccant temperature at a certain concentration ($C_{Salt} = 31.5\%$ corresponds to $\Delta C_{Salt} = 0$ for AHRI summer operating conditions) causes a decrease in the equilibrium humidity ratio of the solution as depicted in psychrometric chart in Figure 4-13. As it can be seen in Figure 4-13, the difference between the humidity ratio of the supply airstream and the equilibrium humidity ratio of salt solution ($W_{Air,in,S} - W_{Sol,in,S}$) increases due to heat loss from the liquid desiccant. Hence, the moisture transfer will enhance in the supply side due to the higher moisture content differences between the humid air and the liquid desiccant. This results in an increase in the latent effectiveness of the supply side.

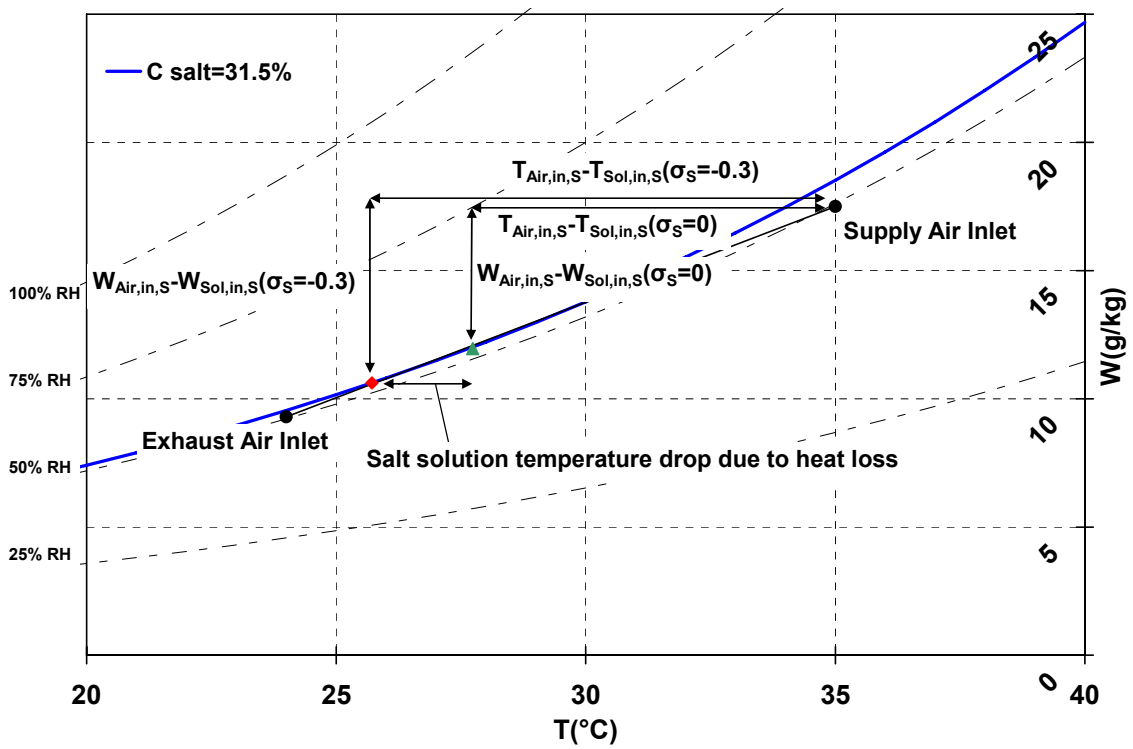

Figure 4-13. Change in the heat and moisture transfer potential in the supply exchanger of the RAMEE system due to heat loss effect for AHRI summer operating conditions(NTU = 5, C_{Sol}/C_{Air} = 3, μ = 0.15, and ΔC_{Salt} = 0, σ_S = σ_E = -0.3).

Figure 4-14 reveals changes in the effectiveness values on each side of the RAMEE system in the presence of heat loss/gain. From Figure 4-14 (a) it can be seen that during summer operation an increase in the sensible effectiveness of up to 15% occurs and an increase of up to 7% occurs in the latent effectiveness for the supply exchanger when σ_S = σ_E = -0.3 compared to the case where σ_S = σ_E = 0. In contrast, for the exhaust side, heat and moisture transfer potential will reduce and result in reduced effectiveness values due to a lower liquid desiccant temperature in the exhaust side of the run-around system. As seen in Figure 4-14 (a), a significant reduction of up to 18% occurs in the sensible effectiveness of the exhaust side where σ_S = σ_E = -0.3. Also, the simulation result shows that the latent effectiveness decreases by up to 8% for the same heat loss value.

(a)

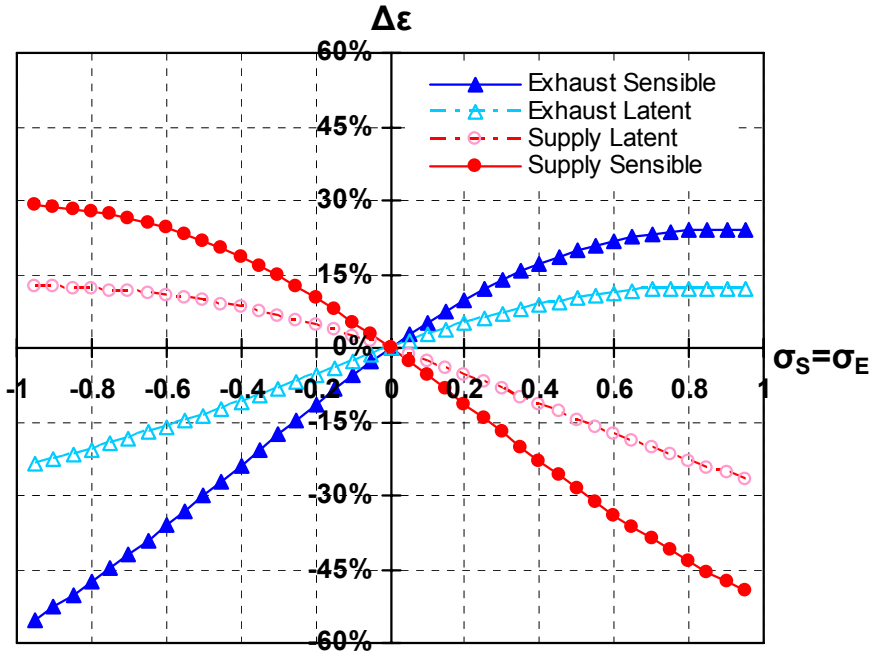

(b)

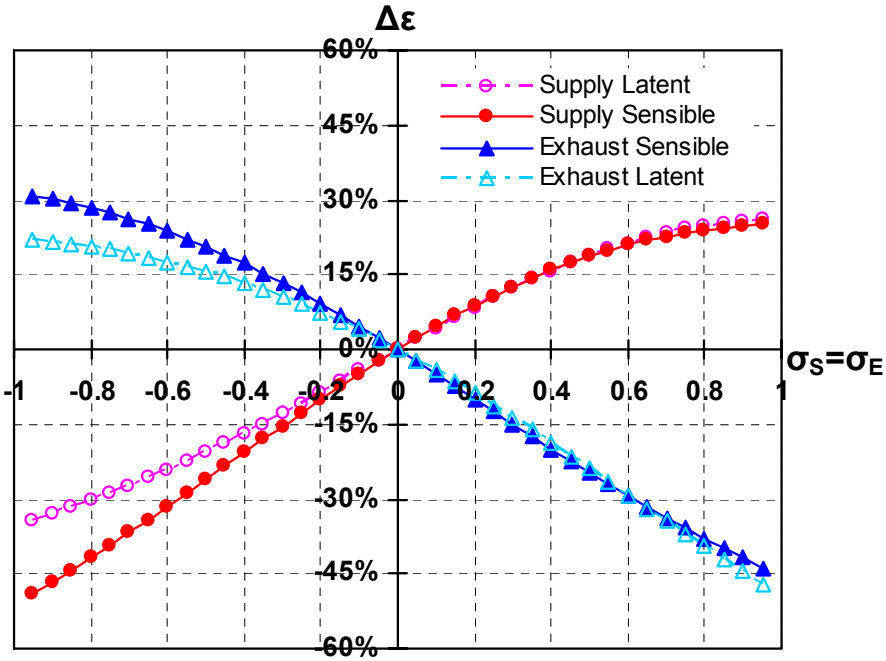

Figure 4-14. Change in sensible and latent effectivnesses of the RAMEE system due to heat loss/gain for (a) AHRI summer and (b) AHRI winter operating conditions (NTU = 5, $C_{Sol}/C_{Air} = 3$, $\mu = 0.15$, $\Delta C_{Salt} = 0$).

It is worth mentioning that the average effectiveness is not influenced as much as the individual effectiveness due to heat loss/gain effect. During summer operation, a -1.6% change occurs in the average sensible effectiveness, and the average latent effectiveness change only -0.9% when $\sigma_S = \sigma_E = -0.3$ compared to the case where $\sigma_S = \sigma_E = 0$.

The effect of the heat loss/gain on the average effectiveness of the system at AHRI operating conditions is more evident in Figure 4-15. Figure 4-15 depicts the change in the average sensible and latent effectiveness values where the heat loss/gain ratio (σ) is the same in both supply and exhaust side of the system. As shown in Figure 4-15, both average sensible and latent effectiveness values decrease as heat loss/gain ratio increases. As illustrated in Figure 4-14, the same value of heat loss/gain ratio for both sides of the system causes either the supply or exhaust side effectiveness to increase, while the other decreases. Therefore, reduction of the average effectiveness due to heat loss/gain implies that the decrease in effectiveness on one side is always greater than the increase in effectiveness on the other side. This is very important when the average effectiveness of the system is estimated from data measured in the laboratory testing of the RAMEE system. The measured average value for sensible and latent effectivnesses will represent the effectiveness that would be obtained when there is heat gain/loss in the system (non-ideal system).

(a)

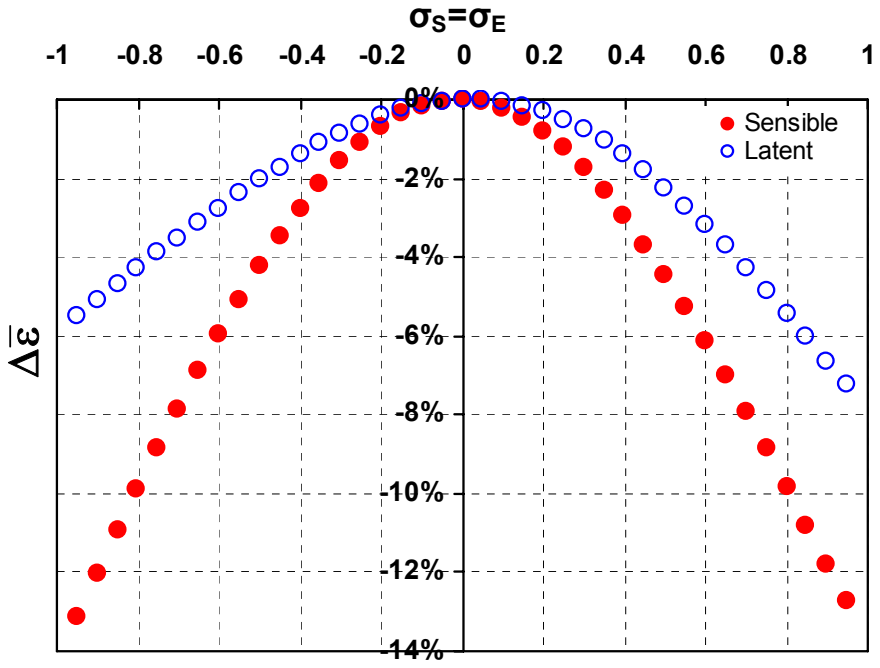

(b)

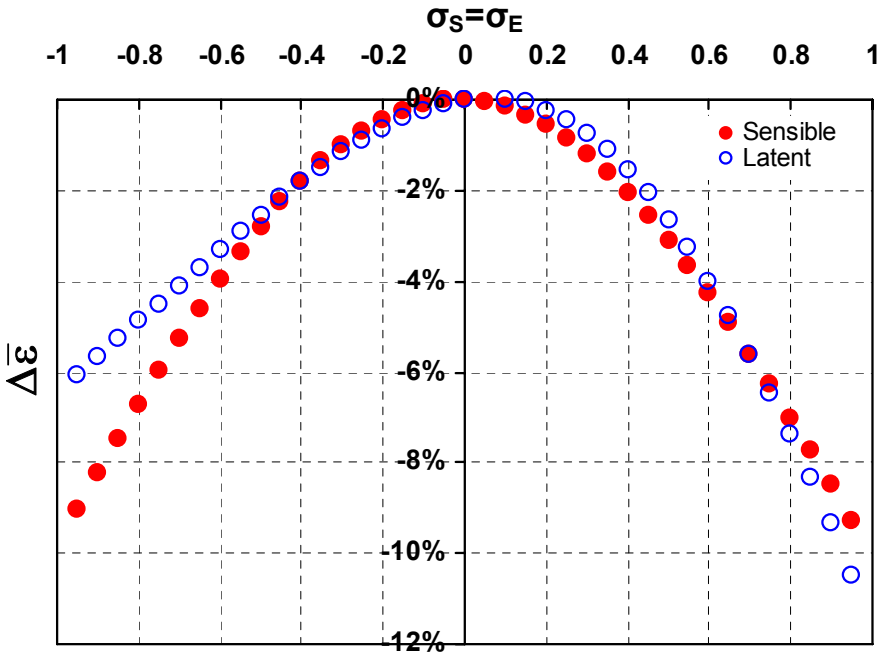

Figure 4-15. Change in the average sensible and latent effectivnesses of the RAMEE system due to heat loss/gain for (a) AHRI summer and (b) AHRI winter operating conditions (NTU = 5, $C_{Sol}/C_{Air} = 3$, $\mu = 0.15$, $\Delta C_{Salt} = 0$).

4.6. Effect of Initial Salt Solution Concentration (ΔC_{Salt})

In practical situations, the RAMEE system may operate with an initial liquid desiccant concentration that can be different than the quasi-steady concentration value. If the initial concentration is different than the quasi steady concentration value, the moisture transfer rate in each LAMEE will be different until the liquid desiccant reaches its equilibrium concentration. For example, if the concentration is initially too high during summer operating conditions, more moisture will be transferred from the supply air to the desiccant in the supply exchanger than will be rejected in the exhaust exchanger. Over time, the concentration of the liquid desiccant will decrease until the moisture accumulated in the supply exchanger equals the moisture rejected in the exhaust exchanger. The RAMEE system may require a long time to reach this quasi-steady state. To study this effect one of the most likely cases is considered.

As the conditions of the inlet air change over each day, the conditions of the desiccant salt solution also change in order to approach equilibrium. When the salt solution is exposed to indoor conditions during the system shut-down, it may reach an equilibrium concentration at the indoor temperature and humidity ratio. As illustrated in Figure 4-16, this condition indicates $\Delta C_{Salt} = 0.5\%$ at AHRI summer condition and $\Delta C_{Salt} = 7.6\%$ at the AHRI winter condition. The steady state concentration values are obtained from the steady state version of the model described in chapter 2.

(a)

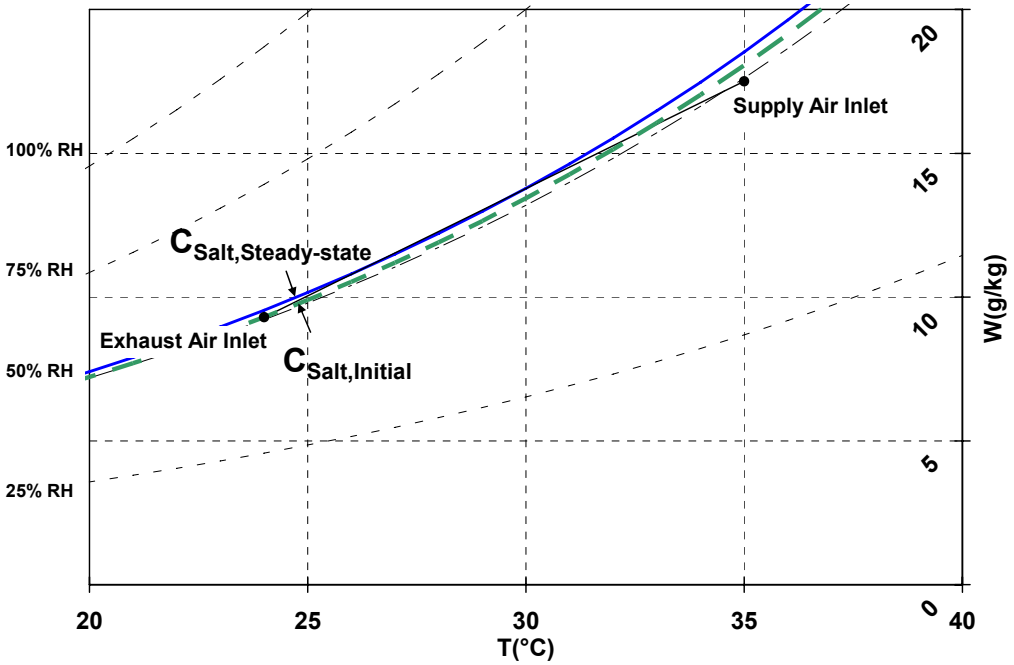

(b)

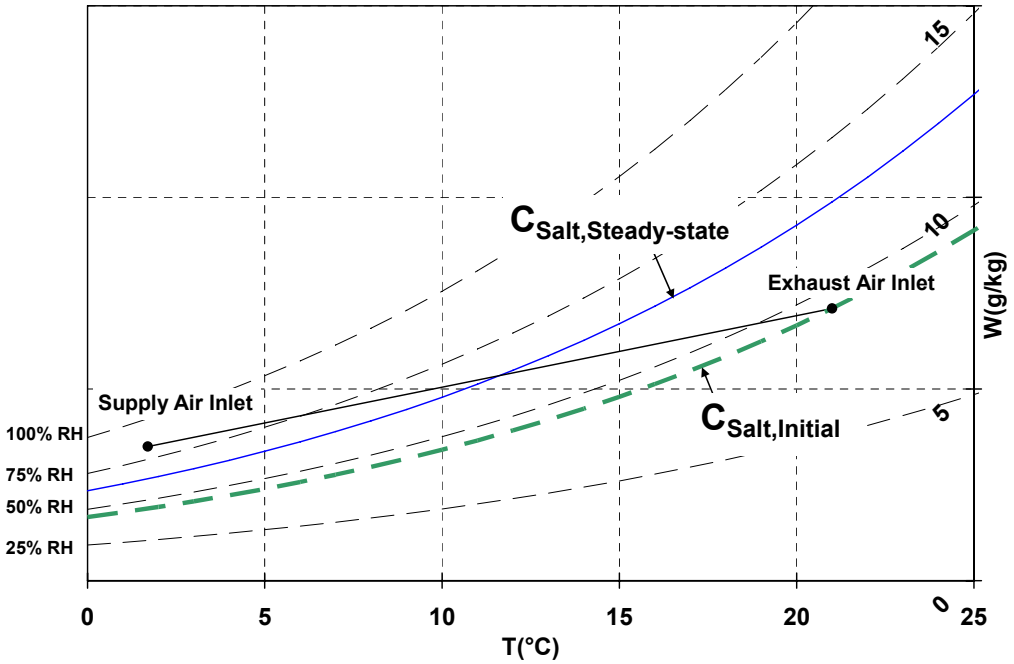

Figure 4-16. The difference between initial salt solution concentration ($C_{Salt,\ Initial}$) and steady state value ($C_{Salt,\ Steady\text{-}state}$) for AHRI (a) summer and (b) winter operating conditions superimposed in the pscychrometric chart.

Figures 4-17 and 4-18 show the changes in the RAMEE effectiveness values with this initial equilibrium concentration for the AHRI summer and winter operating conditions, respectively. The transient effectiveness values are simulated and compared with the case of $\Delta C_{Salt} = 0$. As seen in Figure 4-17, the change in the initial concentration of the liquid desiccant has a trivial influence on the system effectiveness at the AHRI summer conditions. This is caused by the fact that the salt solution concentration remains nearly constant during the AHRI summer operating conditions. The small difference between initial salt solution concentration and its steady state value results in negligible changes in the effectiveness values. Theses changes are considerably smaller than the uncertainties associated with determining the effectiveness of the run-around system.

(a)

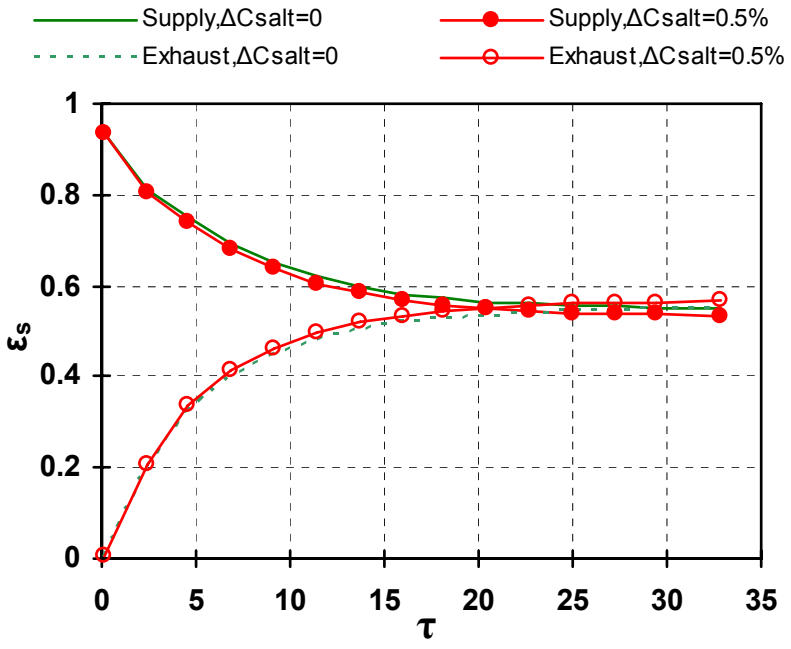

(b)

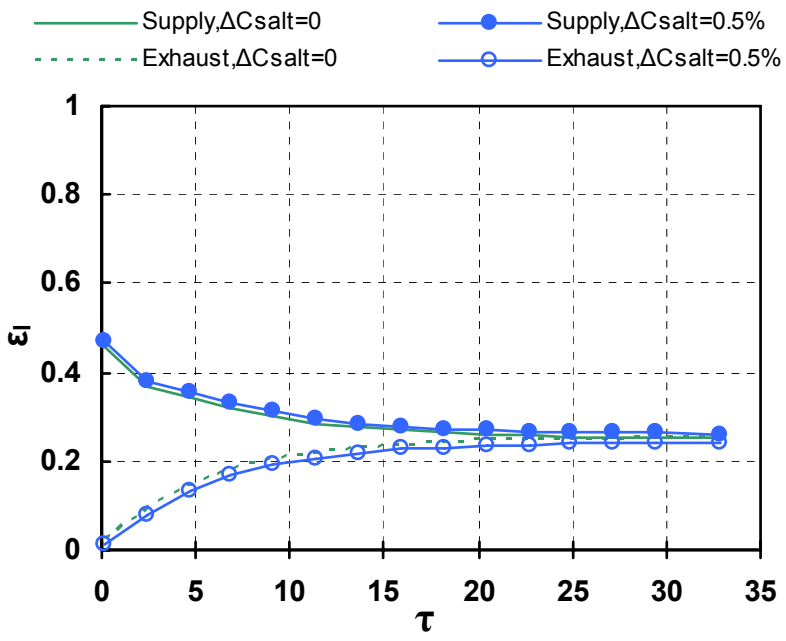

Figure 4-17. System (a) sensible and (b) latent effectivenesses versus dimensionless time for AHRI summer conditions with $\Delta C_{Salt} = 0.5\%$ (NTU = 5, $C_{Sol}/C_{Air} = 3$, $\mu = 0.15$, $\sigma = 0$).

In contrast to Figure 4-17, Figure 4-18 shows a substantial impact on the transient effectiveness values as a result of using the liquid desiccant concentration associated with the indoor (exhaust) condition as an initial value at AHRI winter operating conditions. From this figure, it is clear that the RAMEE system and liquid desiccant have not reached quasi-steady state during the period of simulation ($\tau = 40$) with its new selected initial concentration ($\Delta C_{Salt} = 7.6\%$). At the same number of liquid desiccant circulations ($\tau = 40$), Figure 4-18 (a) demonstrates an 8% increase in the sensible effectiveness of the supply exchanger while the exhaust exchanger sensible effectiveness is reduced by 7%. As seen in Figure 4-18 (b) the latent effectiveness of the supply side crosses over the exhaust latent effectiveness curve at $\tau = 4.6$. At the end of the simulation, the supply latent effectiveness is reduced by up to 16% compared to the case with $\Delta C_{Salt} = 0$ at

$\tau = 40$. This reduction in water vapor transfer or latent effectiveness may be a disadvantage at this operating condition but it should be noted that the supply air will be humidified during the entire transient period, which may be a very desirable result even if it is small. Contrary trends for the latent effectiveness of the exhaust exchanger are obtained, as an increase of up to 16% is found compared to the predicted value where $\Delta C_{Salt} = 0$. Again this implies more water vapor is added to the liquid salt solution in the exhaust exchanger than is removed in the supply exchanger. This phenomenon is expected, since the liquid desiccant moves toward its equilibrium concentration which is 7.6% lower than its initial concentration.

(a)

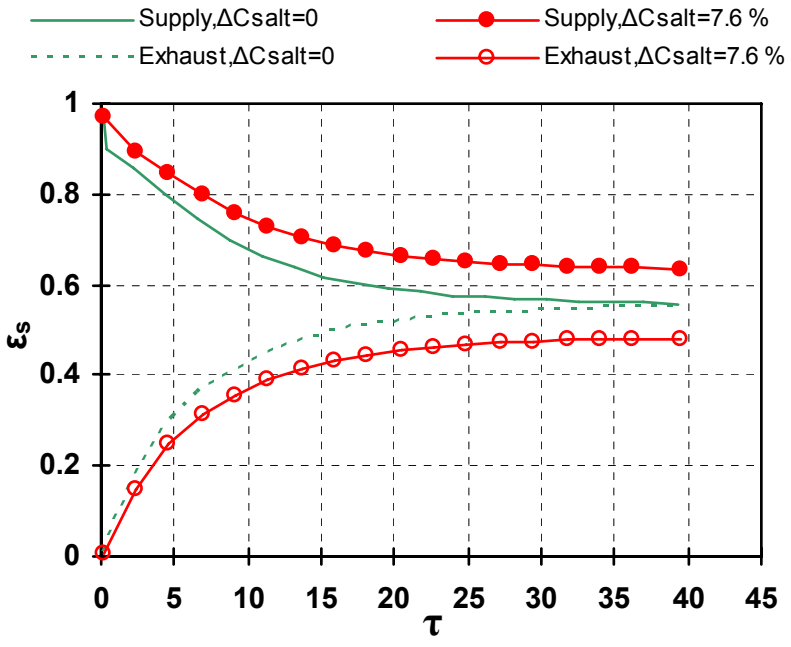

(b)

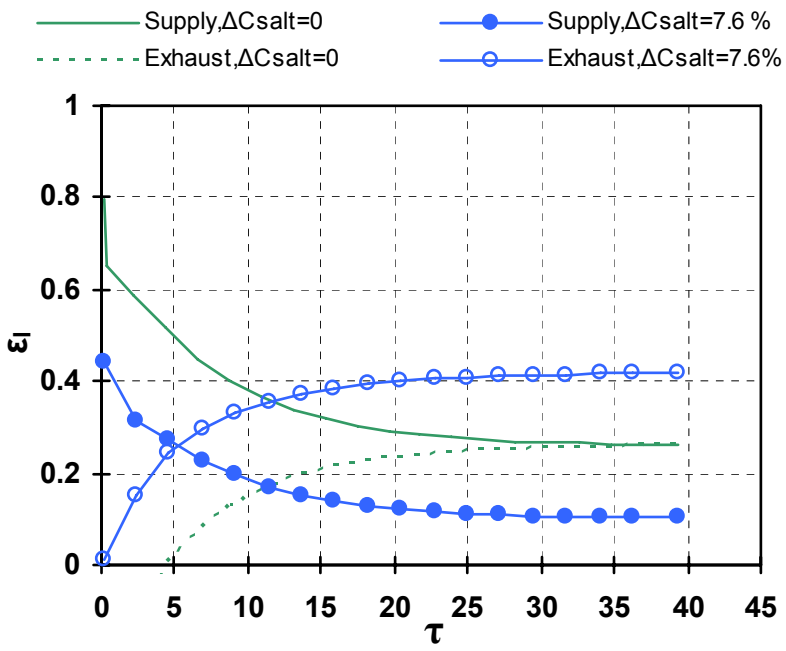

Figure 4-18. System effectiveness versus dimensionless time for AHRI winter condition with $\Delta C_{Salt} = 7.6\%$ (a) sensible and (b) latent transient effectivnesses of the RAMEE system (NTU = 5, $C_{Sol}/C_{Air} = 3$, $\mu = 0.15$, $\sigma = 0$, $0 < \tau < 40$).

The reason for these observed behaviors in Figure 4-18 is mainly attributed to the concentration of the salt solution in the system, which results in different equilibrium humidity ratio values. In order to investigate this effect, Figure 4-19 shows the transient conditions of the liquid desiccant at the inlet of each exchanger on the psychrometric chart for the cases where $\Delta C_{Salt} = 0$ and $\Delta C_{Salt} = 7.6\%$ at AHRI winter operating conditions. In this graph each point represents the condition of liquid desiccant as a function of dimensionless time where each point is an equal time apart ($\Delta\tau = 2.6$). As illustrated in Figure 4-19, the initial condition of the salt solution will vary based on the difference between the initial salt solution concentration and its quasi-steady value (ΔC_{Salt}). Figure 4-19 depicts that during the investigated transient time ($0<\tau<40$), the concentration of salt solution remains approximately constant while its temperature

changes. This indicates that when $\Delta C_{Salt} \neq 0$, the transient times for heat transfer are much smaller than the transient times for moisture transfer.

During the winter operating condition where $\Delta C_{Salt} = 7.6\%$, the higher concentration results in a lower humidity ratio for air in equilibrium with the liquid desiccant as shown in Figure 4-19. As illustrated in Figure 4-18 (b), this reduction when $\Delta C_{Salt} = 7.6\%$ results in a higher moisture transfer rate on the exhaust side exchanger compared to the moisture transfer rate where $\Delta C_{Salt} = 0$ at $\tau = 40$. It is due the fact that the driving potential for moisture transfer is higher (i.e. more water is transferred from the humid exhaust air to the desiccant during the transient period) as shown Figure 4-19 (b). Similarly, the moisture transfer rate in the supply side decreases because the driving potential for moisture transfer is lower due to the high salt concentration compared to the case where $\Delta C_{Salt} = 0$ as depicted in Figure 4-19 (a). Consequently, the latent effectiveness values are higher on the exhaust side and lower on the supply side at $\tau = 40$ as compared to the quasi-steady state conditions as shown in Figure 4-18 (b) when $\Delta C_{Salt} = 0$.

(a)

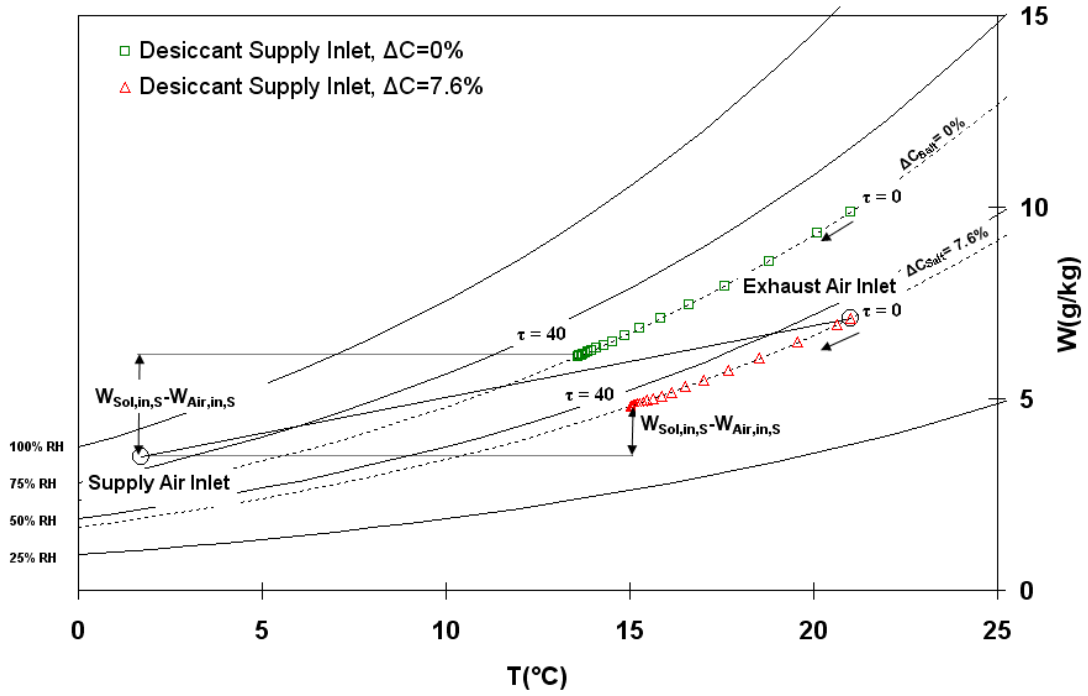

(b)

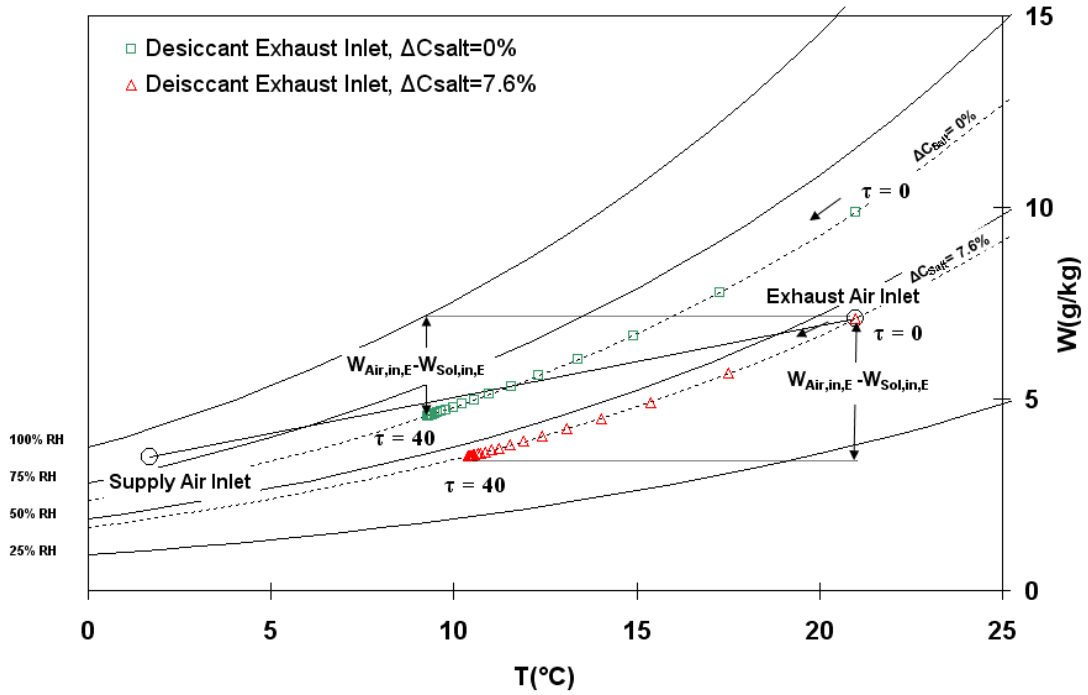

Figure 4-19. Transient condition ($0 < \tau < 40$) of salt solution at the inlet of (a) supply (b) exhaust exchangers superimposed on the psychrometric chart for AHRI winter operating conditions (NTU = 5, $C_{Sol}/C_{Air} = 3$, $\mu = 0.15$, $\sigma = 0$)

Figure 4-18 (a) shows that the sensible effectiveness is higher on the supply side when $\Delta C_{Salt} = 7.6\%$ than when $\Delta C_{Salt} = 0$. These higher sensible effectiveness values are due to the lower moisture transfer rate from the liquid desiccant to the air in the supply side when $\Delta C_{Salt} = 7.6\%$ than when $\Delta C_{Salt} = 0$. The lower moisture transfer rate reduces the cooling of the liquid by the evaporation phase change and thus the liquid desiccant temperature is higher when $\Delta C_{Salt} = 7.6\%$. This increases the temperature difference between the two fluids in the supply side for the case of $\Delta C_{Salt} = 7.6\%$ which causes more heat to transfer from the liquid desiccant to the air. This results in an increase in the sensible effectiveness on the supply side when $\Delta C_{Salt} = 7.6\%$ compared to when $\Delta C_{Salt} = 0$. The lower sensible effectiveness on the exhaust side will mean that there will be smaller decrease in air temperature on the exhaust side compared to $\Delta C_{Salt} = 0$. These results reveal the complex nature of the RAMEE system which means that many parameters and operating conditions must be considered if one is to understand the reason for a change in the system effectiveness for the supply and exhaust side exchangers.

Figure 4-18 shows that when $\Delta C_{Salt} \neq 0$, the supply and exhaust effectivenesses change very slowly for $\tau > 30$. The simulations were continued for longer time periods as shown in Figure 4-20 and the results show that the liquid desiccant concentration continues to change very gradually with increasing time. However, this change is very slow and the system requires a significant number of desiccant circulations to satisfy both conservation of energy and mass criteria for the air streams.

(a)

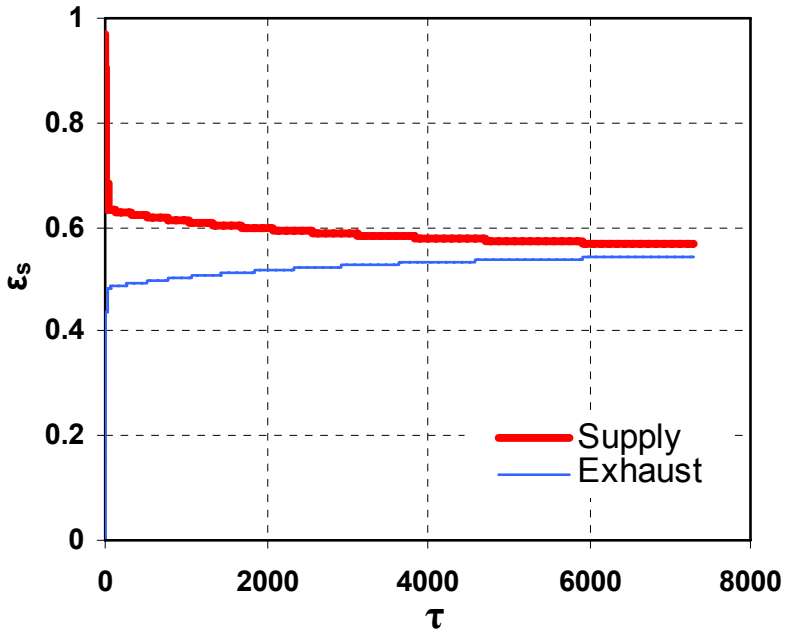

(b)

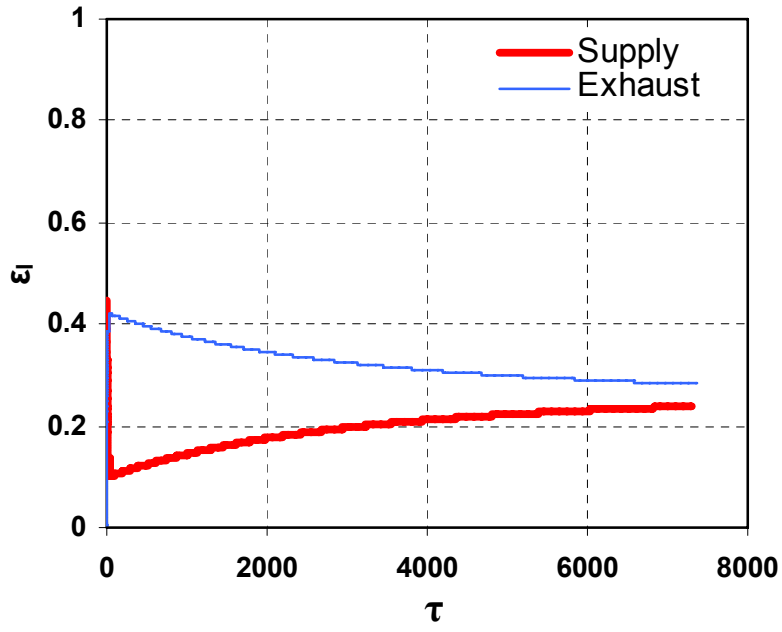

Figure 4-20. System effectiveness versus dimensionless time for AHRI winter condition with $\Delta C_{Salt} = 0.5\%$ (a) sensible and (b) latent transient effectivnesses of the RAMEE system (NTU = 5, $C_{Sol}/C_{Air} = 3$, $\mu = 0.15$, $\sigma = 0$, $0 < \tau < 7281$).

In addition to the numerical model results, similar time delays ($t > 5$ hours) were observed in the laboratory test data for the RAMEE system (See Chapter 3). Thus, a different convergence criterion is defined to identify the large transient response time of the RAMEE system for the case where $\Delta C_{Salt} \neq 0$. As illustrated previously in Chapter 2, this convergence criterion ($\left|\partial\varepsilon/\partial\tau\right| \leq 5\times10^{-6}$) considers only the rate of change in the effectiveness values during the transient period as the salt solution approaches its equilibrium value for each operating condition. When this rate changes very slowly, the system is considered to be in quasi-steady state conditions. Figure 4-21 shows the effect of the using different initial salt solution concentrations on the transient response of the RAMEE system, applying the aforementioned convergence criterion for AHRI winter operation conditions. This figure shows that non-equilibrium initial salt solution concentrations dramatically increase the time to reach quasi-steady state.

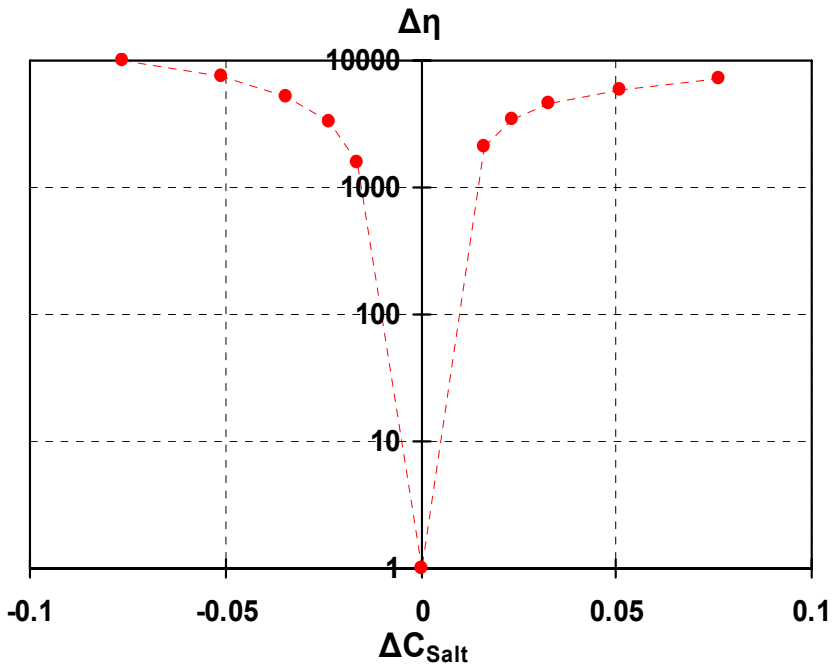

Figure 4-21. Change in the number of liquid desiccant circulations ($\Delta\eta$) to the reach quasi-steady state ($\left|\partial\varepsilon/\partial\tau\right| \le 5\times10^{-6}$) for the RAMEE system due to different initial concentrations that differ from equilibrium ($\Delta C_{Salt} = 0$) (NTU = 5, $C_{Sol}/C_{Air} = 3$, $\mu = 0.15$, $\sigma = 0$, AHRI winter conditions, $\Delta\eta = \eta(\Delta C_{Salt}) - \eta(\Delta C_{Salt} = 0)$.

As illustrated in Figure 4-21, a difference of around 8% between the initial salt solution concentration and its expected steady state value results in the liquid desiccant having to travel about ten thousand more circulations through the system before the steady state concentration is attained. For the specific RAMEE system parameters of Table 2-2 and operating conditions of Figure 4-21, this number of circulations represents a month in real time, which indicates that the system would require almost a month to reach equilibrium. This clearly shows the importance of choosing a salt solution concentration value close to its steady state value for the specific climate being considered to avoid large time delays in practical applications of the RAMEE system. In addition, some system control procedures such as adding water or heat to the liquid

desiccant loop could be used during the operation of the system to move the system toward equilibrium more quickly. This will be the topic of future studies.

4.7 Summary

Chapter 4 presents the transient response of the RAMEE system for step changes provided for the inlet supply air temperature and humidity ratio. Also, the system quasi-steady state operating conditions are predicted as the system approaches its asymptotic operating condition. The effect of various parameters on the transient response are predicted. The number of heat transfer units, thermal capacity ratio, heat loss/gain ratio, storage volume ratio and the normalized initial salt solution concentration have been analyzed in detail. It has been shown that the initial salt solution concentration and the storage volume ratio have significant impacts on the transient response of the system and the heat loss/gain rates from/to the circulated fluid flow can change the system quasi-steady condition substantially.

CHAPTER 5
SUMMARY, CONCLUSIONS AND RECOMMENDATIONS

5.1 Summary

The main objective of this study was to develop and verify a transient numerical model for a run-around membrane energy exchanger (RAMEE) system using cross-flow exchangers with a liquid desiccant as a coupling fluid. The goal is to determine the dynamic performance of a RAMEE system, considering the thermal and mass transfer capacitance effects of the salt solution in the system. To meet this overall objective the following stages have been completed:

1) The numerical/mathematical model that predicts the dynamic behavior of the RAMEE system was developed in chapter 2. The model is two dimensional and transient and includes the effect of the salt solution storage as well as heat loss/gain from/to the liquid desiccant loop. This model of the RAMEE system has been used to predict the sensible, latent and total transient effectivenesses as well as the time required to reach quasi-steady state for different designs and operating conditions. Sensitivity studies were presented which show the importance of input data for the RAMEE system and certain assumptions in the numerical model.

2) The numerical model, presented in Chapter 2 was validated in Chapter 3. The numerical results for the case of only heat transfer for a single heat exchanger were compared to an available analytical solution. The dimensionless bulk outlet temperature of the fluids from the analytical solution and the numerical model agree within 4%. For

the simultaneous heat and moisture transfer in a run-around membrane energy exchanger (RAMEE) a comparison between the numerical results and experimental measurements obtained from laboratory testing of the RAMEE for both sensible and latent effectivenesses was performed at AHRI summer and winter operating conditions. The simulated data could predict the trend of the transient response of the RAMEE system well. The maximum average absolute differences between the measured and simulated transient effectivenesses were 7.5% and 10.3% for summer and winter operating conditions, respectively. These numbers are quite satisfactory due to the fact that the main discrepancy between the simulation and the experiment was observed at initial times. This is due to the fact that it will take time to fill the exchangers with the salt solution and also the exact initial conditions are difficult to determine. The other important reason for this discrepancy is liquid flow mal-distribution within exchangers during testing of the RAMEE system which was not addressed in this study.

3) In Chapter 4, a parametric study was employed to investigate the transient performance of the RAMEE system consisting of two cross flow heat and moisture exchangers. Results were presented for different values of NTU, C_{Sol}/C_{Air}, and μ for balanced air flow rates for sufficient time duration so that quasi-steady state operating conditions can be deduced. As well, a finite heat loss/gain ratio was included in the RAMEE system to study the effect of external heat loss or gain on the performance of the run-around heat and moisture recovery system. Finally, an investigation of the initial salt solution concentration and its impact on the transient response of the RAMEE system was presented.

5.2 Conclusions

The following conclusions can be made from the research presented in this thesis:

1) The numerical model for the transient response of a single heat exchanger and a run-around membrane energy exchanger, developed in this thesis, provides reliable results. This conclusion is based on comparison between the numerical model results and an analytical solution from the literature as well as experimental data from laboratory testing of the RAMEE system.

2) The numerical model in this study can be used to predict the quasi-steady state effectivness values. It is shown for AHRI summer operating conditions the maximum effectiveness of a run-around heat and moisture recovery system occurs approximately at $C_{Sol}/C_{Air} = 3$ which is in agreement with a previous finding (Fan et al., 2006). This value will vary for different operating conditions. Also, it is found that the maximum total effectiveness of the RAMEE system occurs when the mass flow rate of pure salt is equal to the mass flow rate of dry air ($\dot{m}_{Salt}/\dot{m}_{Air} = 1$) for AHRI summer operating conditions. These maximum effectiveness values will occur at different mass flow rate ratios for different operating conditions.

3) The time it takes to reach quasi-steady state is influenced by the operating conditions. The number of desiccant circulations required to reach equilibrium increases with an increase in the heat capacity rate ratio (C_{Sol}/C_{Air}). On the other hand, an increase in number of heat transfer units (NTU) causes a decrease in the required number of salt solution circulations. Contrary trend is observed considering the real time to evaluate the response of the system. It is shown that the real time required to reach a quasi-steady

state condition will decrease with an increase in the heat capacity rate ratio (C_{Sol}/C_{Air}), while this time will increase when NTU increases. Increasing C_{Sol}/C_{Air} from 1 to 10 reduces the transient times by 45%. Decreasing NTU from 15 to 1 reduces the transient times by 81%.

4) The storage volume of the liquid desiccant salt solution has a significant impact on the transient response of the system, implying that the size of the storage tank should be minimized considering the range of operating conditions and the design constraints. For instance, an increase in the volume fraction (μ) from 0.15 (used in the laboratory testing of the RAMEE) to 0.5, which corresponds to a 5.5 times reduction in the size of storage tanks, reduces the response time by 75% for both AHRI operating conditions.

5) The presence of heat loss/gain ratio to/from the surroundings changes the quasi-steady state effectiveness values significantly. This is a quite important parameter in the RAMEE system operation, since 10% heat loss/gain could change effectiveness up to ±6%. Heat loss/gain should be avoided to satisfy energy and mass balances in the system during operating conditions and achieve the same effectiveness values in both the supply and exhaust sides of the system.

6) The initial salt solution concentration plays an important role on the transient response time of the system. In some operating conditions (e.g. AHRI winter operating condition), using an equilibrium salt solution concentration at indoor condition as an initial value (which results in a difference between steady-state and initial concentrations of 7.6%) results in transient delays of up to a month in real time. To reduce this transient response time during the operation of the RAMEE system, the salt solution concentration

should be chosen to be very close to the steady state value that will exist for the specific climate being considered.

5.3 Recommendations for Future Work

There are still many topics that can be studied to design and operate a run-around membrane energy exchanger (RAMEE) in the future. Some of these investigations which should be done to develop and improve a RAMEE system are:

1) The numerical model developed in this thesis can be used to identify operational strategies to minimize transient time delay. Also, the system design can be optimized based on cost (e.g. material, insulation, piping and energy requirement of liquid pumps) and performance through the numerical model.

2) Uniform channel sizes (i.e. air channel spacing) and the same flow rate through each channel were used in this study. A study is recommended for the effect of mal-distributed fluid flows due to variations in the plate spacing on the performance of a run-around system due to manufacturing limitations and pressure variations which may cause the channels to deform.

3) The impact of frosting and fouling on the system performance should be studied. Frosting and fouling may change the permeability of the membrane and as a consequence the heat and moisture transfer rates will change in the system.

4) The transient response of the RAMEE system depends on many dimensionless heat and moisture transfer parameters as well as operating conditions, liquid desiccant storage

volumes and salt solution concentration. Future work should aim to develop correlations between these parameters and the transient response time of the RAMEE system.

5) In this thesis, the performance of $MgCl_2$ as a coupling fluid was examined. However, the behavior of a RAMEE system with various liquid desiccants and mixtures of desiccants should be investigated to determine the best desiccant for a RAMEE system considering the performance and cost. In addition, the impact of salt solution crystallization on the performance of the RAMEE system can be examined which was avoided in this thesis.

LIST OF REFERENCES

ALI, A., VAFAI, K. and KHALED, A.-.A., 2004. Analysis of heat and mass transfer between air and falling film in a cross flow configuration. *International journal of heat and mass transfer,* **47**(4), pp. 743-755.

ANSI/AHRI STANDARD 1060-2005, Standard for Rating Air-to-Air Exchangers for Energy Recovery Ventilation Equipment. Arlington: Air-Conditioning & Refrigeration Institute.

ANSI/ASHRAE STANDARD 55-2004, Thermal environmental conditions for human occupancy. Atlanta: ASHRAE.

ANSI/ASHRAE STANDARD 62.1-2004, Ventilation for acceptable indoor air quality. Atlanta: ASHRAE.

ANSI/ASME PTC STANDARD 19.1-1998, Measurement uncertainty. New York: ASME.

ASHRAE, 2005. ASHRAE Handbook-Fundamentals. Atlanta: American Society of Heating, Refrigerating and Air-Conditioning Engineers, Inc.

ASHRAE, 2004. ASHRAE Handbook-HVAC System and Equipment. Atlanta: American Society of Heating, Refrigerating and Air Conditioning Engineers Inc.

BENNETT, I.J.D., BESANT, R.W., SCHOENAU, G.J. and JOHNSON, A.B., 1994a. Procedure for optimizing coils in a run-around heat exchanger system. *ASHRAE Transactions,* **100**(1), pp. 442-451.

BENNETT, I.J.D., BESANT, R.W., SCHOENAU, G.J. and JOHNSON, A.B., 1994b. Validation of a run-around heat recovery system model. *ASHRAE Transactions,* **100**(1), pp. 230-237.

BESANT, R.W. and SIMONSON, C.J., 2003. Air-to-air exchangers. *ASHRAE J.,* **45**(4), pp. 42-52.

CHARLES, N.T. and JOHNSON, D.W., 2008. The occurrence and characterization of fouling during membrane evaporative cooling. *Journal of membrane science,* **319**(1), pp. 44-53.

CISTERNAS, L.A. and LAM, E.J., 1991. Analytic correlation for the vapour pressure of aqueous and non-aqueous solutions of single and mixed electrolytes. Part II. Application and extension. *Fluid phase equilibria,* **62**(1), pp. 11-27.

DHITAL, P., BESANT, R.W. and SCHOENAU, G.J., 1995. Integrating run-around heat exchanger systems into the design of large office buildings. *ASHRAE Transactions,* **101**(2), pp. 979-991.

ERB, B., 2007. *Run-around membrane energy exchanger prototype 2 testing ,Summer Work Report.* Saskatoon, Saskatchewan: Department of Mechanical Engineering, University of Saskatchewan.

ERB, B., 2006. *Designing and Testing a Run-Around Heat and Moisture Recovery System. Summer Work Report.* Saskatoon, Saskatchewan: Department of Mechanical Engineering, University of Saskatchewan.

FAN, H., 2005. *Modelling a Run-Around Heat And Moisture Recovery System*, *M.Sc. thesis*, Department of Mechanical Engineering, University of Saskatchewan.

FAN, H., SIMONSON, C.J., BESANT, R.W. and SHANG, W., 2006. Performance of a run-around system for HVAC heat and moisture transfer applications using cross-flow plate exchangers coupled with aqueous lithium bromide. *HVAC R research,* **12**(2), pp. 313-336.

FAN, H., SIMONSON, C.J., BESANT, R.W. and SHANG, W., 2005. Run-around heat recovery system using cross-flow flat-plate heat exchangers with aqueous ethylene glycol as the coupling fluid. *ASHRAE Transactions,* **111**, pp. 901-910.

FANG, L., CLAUSEN, G. and FANGER, P.O., 2000. Temperature and humidity: important factors for perception of air quality and for ventilation requirements. *ASHRAE Transactions,* **106**, pp. 503-510.

FAUCHOUX, M., SIMONSON, C.J. and TORVI, D.A., 2007. The effect of energy recovery on perceived air quality, energy consumption and economics of an office building. *ASHRAE Transactions,* **113**(2), pp. 437-449.

FORSYTH, B.I. and BESANT, R.W., 1988a. The design of a run-around heat recovery system. *ASHRAE Transactions,* **94**(2), pp. 511-531.

FORSYTH, B.I. and BESANT, R.W., 1988b. The performance of a run-around heat recovery system using aqueous glycol as a coupling liquid, *ASHRAE Transactions,* **94**(2), pp. 532-545.

HEMINGSON, H., 2005. *Preliminary Testing for Run Around Heat and Moisture Exchanger, Summer Work Report.* Saskatoon, Saskatchewan: Department of Mechanical Engineering, University.

INCROPERA, F.P. and DEWITT, D.P., 2002. Fundamentals of heat and mass Transfer. Fifth edn. New York: John Wiley & Sons.

ISKRA, C., 2007. *Convective mass transfer between a hydrodynamically developed airflow and liquid water with and without a vapor permeable membrane*, *M.Sc. thesis*, Department of Mechanical Engineering, University of Saskatchewan,.

ISKRA, C.R. and SIMONSON, C.J., 2007. Convective mass transfer coefficient for a hydrodynamically developed airflow in a short rectangular duct. Oxford,: Pergamon.

ISO 5167-1, 1991. Measurement of fluid flow by means of pressure differential devices. ISO.

KOSONEN, R. and TAN, F., 2004. The effect of perceived indoor air quality on productivity loss. *Energy and buildings,* **36**(10), pp. 981-986.

LARSON, M.D., 2006. *The performance of membrane in a newly proposed run-around heat and moisture exchanger*, *M.Sc. thesis*, Department of Mechanical Engineering, University of Saskatchewan.

LARSON, M.D., SIMONSON, C.J., BESANT, R.W. and GIBSON, P.W., 2007. The elastic and moisture transfer properties of polyethylene and polypropylene membranes for use in liquid-to-air energy exchangers. *Journal of membrane science,* **302**(1), pp. 136-149.

LIU, X.H., JIANG, Y. and QU, K.Y., 2007. Heat and mass transfer model of cross flow liquid desiccant air dehumidifier/regenerator. *Energy conversion and management,* **48**(2), pp. 546-554.

LONDON, A.L. and KAYS, W.M., 1951. Liquid-coupled indirect-transfer regenerator for gas-turbine plants. *Transactions of the American Society of Mechanical Engineers,* **73**(5), pp. 529-542.

LUO, X. and ROETZEL, W., 1998. Theoretical investigation on cross-flow heat exchangers with axial dispersion in one fluid. *Revue générale de thermique,* **37**(3), pp. 223-233.

MESQUITA, L.C.S., HARRISON, S.J. and THOMEY, D., 2006. Modeling of heat and mass transfer in parallel plate liquid-desiccant dehumidifiers. *Solar energy,* **80**(11), pp. 1475-1482.

MISHRA, M., DAS, P.K. and SARANGI, S., 2008. Dynamic behavior of three-fluid crossflow heat exchangers. *Journal of heat transfer,* **130**(1), pp. 1.

MISHRA, M., DAS, P.K. and SARANGI, S., 2004. Transient behavior of crossflow heat exchangers with longitudinal conduction and axial dispersion. *Journal of heat transfer,* **126**(3), pp. 425-433.

NIU, J.L. and ZHANG, L.Z., 2001. Membrane-based Enthalpy Exchanger: Material considerations and clarification of moisture resistance. *Journal of membrane science,* **189**(2), pp. 179-191.

PARK, M.S., HOWELL, J.R. and VLIET, G.C., 1994. Numerical and experimental results for coupled heat and mass transfer between a desiccant film and air in cross-flow. *International journal of heat and mass transfer,* **37**(1), pp. 395-402.

PATANKAR, S. V., 1980. Numerical Heat Transfer and Fluid Flow, First edn, Taylor & Francis.

RANONG, C.N., HOPKET, J. and ROETZEL, W., 2005. Steady-state and transient behavior of two heat exchangers coupled by a circulating flowstream. *Heat transfer engineering,* **26**(7), pp. 36-50.

ROMIE, F.E., 1994. Transient response of crossflow heat exchangers with zero core thermal capacitance. *Journal of heat transfer,* **116**(3), pp. 775-777.

ROMIE, F.E., 1983. Transient response of gas-to-gas crossflow heat exchangers with neither gas mixed. *Journal of heat transfer,* **105**(3), pp. 563-570.

SHAH, R.K., 1981. In: S. KAKAÇ, A.E. BERGLES and F. MAYINGER, eds, *Thermal design theory for regenerators. In Heat Exchangers: Thermal-Hydraulic Fundamentals and Design.* New York: Hemisphere, pp. 721-763.

SHAH, R.K. and LONDON, A.L., 1987. Laminar Flow Forced Convection in Ducts. New York: Academic Press.

SHANG, W. and BESANT, R.W., 2005. Effects of pore size variations on regenerative wheel performance. *Journal of engineering for gas turbines and power,* **127**(1), pp. 121-135.

SHANG, W. and BESANT, R.W., 2006. Effects of manufacturing tolerances on regenerative exchanger number of transfer units and entropy generation. *Journal of engineering for gas turbines and power,* **128**(3), pp. 585-598.

SIMONSON, C.J. and BESANT, R.W., 1999a. Energy wheel effectiveness: Part II - correlations. *International journal of heat and mass transfer,* **42**(12), pp. 2171-2185.

SIMONSON, C.J. and BESANT, R.W., 1999b. Energy wheel effectiveness: Part I - development of dimensionless groups. *International journal of heat and mass transfer,* **42**(12), pp. 2161-2170.

SIMONSON, C.J. and BESANT, R.W., 1997. Heat and moisture transfer in desiccant coated rotary energy exchangers: Part I. Numerical model. *HVAC R research,* **3**(4), pp. 325-350.

SPARROW, E.M., ABRAHAM, J.P., MARTIN, G.P. and TONG, J.C.Y., 2001. An experimental investigation of a mass exchanger for transferring water vapor and inhibiting the transfer of other gases. *International journal of heat and mass transfer,* **44**(22), pp. 4313-4321.

SPIGA, G. and SPIGA, M., 1987. Two-dimensional transient solutions for crossflow heat exchangers with neither gas mixed. *Journal of heat transfer,* **109**(2), pp. 281-286.

SPIGA, M. and SPIGA, G., 1988. Transient temperature fields in crossflow heat exchangers with finite wall capacitance. *Journal of heat transfer,* **110**(1), pp. 49-53.

SRIHARI, N. and DAS, S.K., 2008. Experimental and theoretical analysis of transient response of plate heat exchangers in presence of nonuniform flow distribution. New York, N.Y.: American Society of Mechanical Engineers.

STEPHANOPOULOS, G., 1984. Chemical process control: An introduction to theory and practice Englewood Cliffs, N.J.: Prentice-Hall.

WELTY, J.R., WICKS, C.E., WILSON, R.E. and RORRER, G., 2001. Fundamentals of Momentum, Heat and Mass Transfer. 4 edn. New York: John Wiley & Sons Inc.

WU, X.P., JOHNSON, P. and AKBARZADEH, A., 1997. Application of heat pipe heat exchangers to humidity control in air-conditioning systems. *Applied thermal engineering,* **17**(6), pp. 561-568.

ZAYTSEV, I.D. and ASEYEV, G.G., 1992. Properties of Aqueous Solutions of Electrolytes. CRC Press, Inc.

ZENG, Y.Y., 1990. *A study of the performance of run-around heat recovery system using aqueous glycol/air as the coupling fluid*, *M.Sc. thesis*, University of Saskatchewan.

ZENG, Y.Y., BESANT, R.W. and REZKALLAH, K.S., 1992. Effect of temperature-dependent properties on the performance of run-around heat recovery systems using aqueous-glycol coupling fluids. *ASHRAE Transactions,* **98**(1), pp. 551-542.

ZHANG, L.Z. and NIU, J.L., 2002. Effectiveness correlations for heat and moisture transfer processes in an enthalpy exchanger with membrane cores. *Journal of heat transfer,* **124**(5), pp. 922-929.

APPENDIX A
PROPERTIES OF MAGNESIUM CHLORIDE SOLUTIONS

A.1 Equilibrium Water Vapor Pressure

In order to solve Equations (2.10) to (2.13) the equilibrium humidity ratio of the $MgCl_2$ is required to be correlated to the mass ratio of the solution (X_{Sol}). For the case of a non-ideal gas and liquid phases, empirical equations are needed to relate the equilibrium values of the two phases. In this study, the correlations developed by (Cisternas, Lam 1991) , are used,

$$\log p_v = KI[A - B/(T - E_s)] + [C - D/T - E_s] \tag{A.1}$$

where

$$A = A_s + 3.60591\times10^{-4}\cdot I + M_s/2303, \tag{A.2}$$

$$B = B_s + 1.382982\cdot I - 0.031185\cdot I^2, \tag{A.3}$$

$$C = C_s - 3.99334\times10^{-3}\cdot I - 1.11614\times10^{-4}\cdot I^2 + M_s\cdot I(1-\chi)/2303, \tag{A.4}$$

$$D = D_s - 0.138481.I + 0.027511\cdot I^2 - 1.79277\times10^{-3}\cdot I^3 \tag{A.5}$$

$$\chi = 2\cdot(\nu_+ + \nu_-)/(\nu_+\cdot Z_+^2 + \nu_-.Z_-^2), \tag{A.6}$$

and

$$I = \frac{1}{2}\sum_i Z_i^{\,2} m_i' \,. \qquad (A.7)$$

where A_s, B_s, C_s, D_s and E_s are constant and depend on the type of solvent, T is the temperature of salt solution (K), I is the ionic strength (mol/kg), m_i' is the molality (mol/kg) of ionic species, M_s is the molecular weight of solvent (i. e., water), K is an electrolyte parameter, ν_+ is the number of moles of cation, ν_- is the number of moles of anion produced by the dissolution of one mole of electrolyte, Z_+ is the charge of cation and Z_- is the charge of anion. The constants required in Equations (A.1) to (A.7) for $MgCl_2$ aqueous solution are as follows (Cisternas, Lam 1991):

Solvent properties (Water):

A_s = -0.021302, B_s = -5.390915, C_s = 7.192959, D_s = 1730.2857, E_s = 39.53and M_s = 18

Salt properties ($MgCl_2$):

ν_+ = 1, ν_- = 2, Z_+ = +2 and Z_- =-1.

Solution properties ($MgCl_2$-Water):

K = 0.37678

A.2 Density

The density of a multi-component solution can be calculated using the modified Ezrokhi equation (Zaytsev, Aseyev 1992):

$$\log(\rho_{Sol} / \rho_w) = \sum_i \frac{D_i}{(1 + X_{Sol,i})}, \qquad (A.8)$$

where ρ_{Sol} (kg/m^3) is the density of multi-component solution ,ρ_w (kg/m^3) is the water density, D_i are empirical coefficients and $X_{Sol,i}$ is the mass fraction of the water per kilogram of pure salt in the solution.

The density of pure water (kg/m^3) is approximated by a polynomial (Zaytsev, Aseyev 1992):

$$\rho_w = 1000 - 0.062 \cdot (T - 273.15) - 0.00355 \cdot (T - 273.15)^2, \qquad (A.9)$$

$$(273.15 \le T \le 373.15K).$$

The coefficients D_i in Equation (A.8) are calculated from the empirical equation:

$$D_i = b_{0i} + b_{1i} \cdot (T - 273.15) + b_{2i} \cdot (T - 273.15)^2, \qquad (A.10)$$

where the b_{ni} coefficients for $MgCl_2$ aqueous solution are as follow:

$b_0 = 3523 \times 10^{-4}$, $b_1 = 34.5 \times 10^{-6}$ and $b_2 = 0$.

A.3 Thermal Conductivity

The thermal conductivity of multi-component solutions can be calculated using the following correlation (Zaytsev, Aseyev 1992):

$$k_{Sol} = k_w \cdot \left[1 - \sum_i \frac{\beta_i}{1 + X_{Sol,i}} \right], \qquad (A.11)$$

where k_{Sol} [W/(m·K)] is the thermal conductivity of the solution, k_w [W/(m·K)] is the thermal conductivity of water, β_i are empirical coefficients, and $X_{Sol,i}$ is the mass content of the water in kilograms per kilogram of pure salt. For $MgCl_2$ the value of β is 0.4779.

Thermal conductivity of pure water is calculated by a following correlation (Zaytsev, Aseyev 1992):

$$k_w = 0.5545 + 0.00246 \cdot (T - 273.15) - 0.00001184 \cdot (T - 273.15)^2, \qquad (A.12)$$

$$(273.15 \le T \le 373.15\,K).$$

A.4 Specific Heat Capacity

The specific heat capacity of solutions is calculated using the following correlation (Zaytsev, Aseyev 1992):

$$c_{pSol} = c_{pw} + \sum_i \frac{B_{1i} + B_{2i} X_i' + B_{3i}(T - 273.15) + B_{4i}(T - 273.15)^2}{1 + X_{Sol,i}}, \qquad (A.13)$$

where c_{pSol} [J/(kg·K)]is the heat capacity of a multi-component solution, c_{pw} [J/(kg·K)]is the heat capacity of water, B_{ni} are coefficients, X_i' is the mass content of i^{th} component in a binary isopiestic solution in kilograms of the substance per kilogram of solution, and $X_{Sol,i}$ is the mass content of the water in kilograms per kilogram of pure salt. The X_i' value is calculated by the following correlation:

$$X_i' = E_i^{-1} \cdot \sum_j \frac{E_j}{1 + X_{Sol,i}}, \qquad (A.14)$$

For one component solution such as $MgCl_2$, above equation is simplified to:

$$X' = \frac{1}{1 + X_{Sol}}. \qquad (A.15)$$

For MgCl2 aqueous solution B_{ni} coefficients are: B_1 = -6304.3, B_2 = 3082.9, B_3 = 7.9 and B4 = -0.0139.

The specific heat capacity [J/(kg·K)] of pure water is calculated by the following correlation (Zaytsev, Aseyev 1992):

$$c_{p_w} = 134225.4(T/100)^{-6.5} + 3490 \cdot (T/100)^{0.14}, \qquad (A.16)$$

$$(273.15 \le T \le 373.15K).$$

A.5 Heat of Solution

The heat of solution of Magnesium Chloride at $T = 323.15\,K$ and various concentrations is tablated in (Zaytsev, Aseyev 1992). In order to calculate the heat of solution, curve fitting is done based on their presented data. The curve fitted and experimental values are shown in Figure A-1.

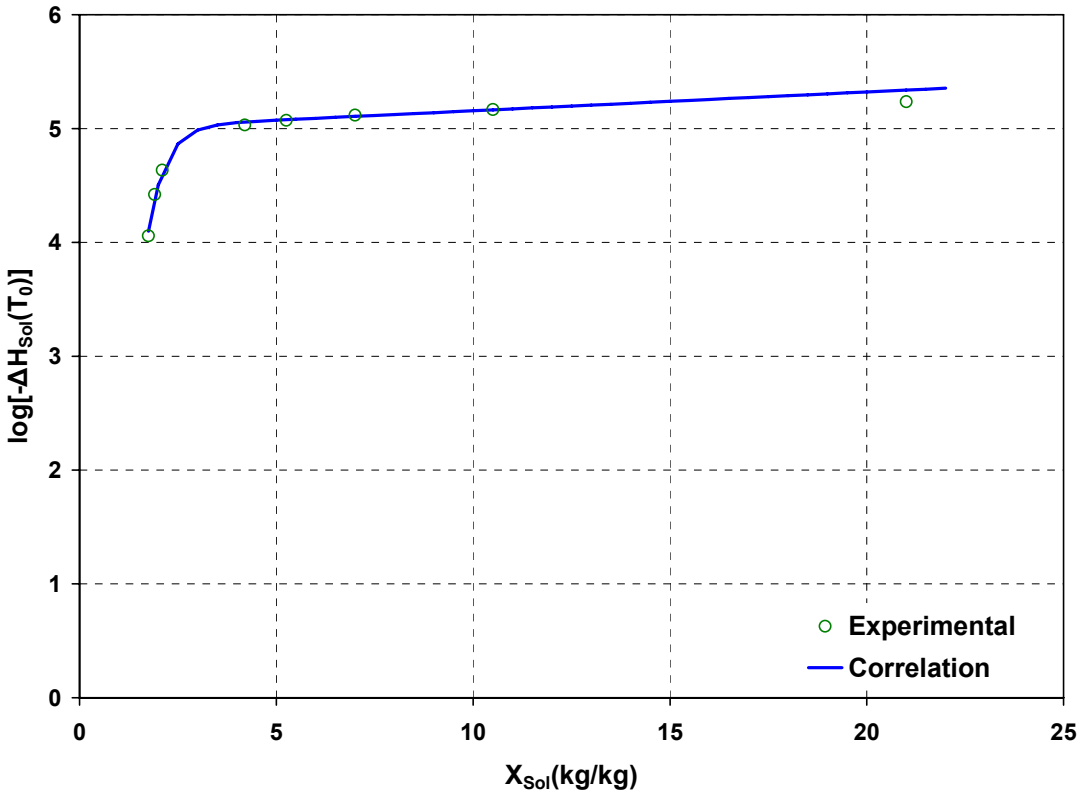

Figure A-1. Heat of solution for $MgCl_2$ as a function of concentration at 323.15 K comparing the experimental data and the fitted curve.

The correlation based on the curve fit is as follow:

$$\log(-\Delta H_{Sol}[T = 323.15\,K]) = (\alpha - \beta)e^{(-\gamma X_{Sol})} + \eta X_{Sol} + \beta \qquad \text{(A. 17)}$$

where α = -45.0438, β = 4.9913, γ = 2.2827 and η = 0.0165. The value of the square sum of the residual at X_{Sol} is 0.0046.

APPENDIX B
DEVELOPMENT OF GOVERNING EQUATIONS FOR A SINGLE LIQUID-TO-AIR MEMBRANE ENERGY EXCHANGER (LAMEE)

To develop the governing equations for the heat and moisture exchanger, a control volume method is used based on coordinates system shown in Figure B-1.

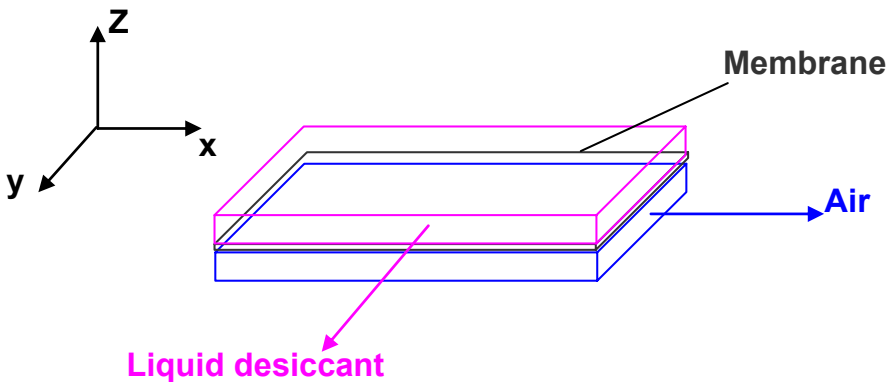

Figure B-1. The coordinate system of the exchanger.

B.1 Mass Transfer Equation

B.1.1 Liquid Side

Considering a stationary infinitesimal control volume within the liquid side of the heat exchanger as shown in Figure B-2 and assuming diffusion only in z direction (neglecting mass diffusion in x and y directions), the mass transfer equations can be developed.

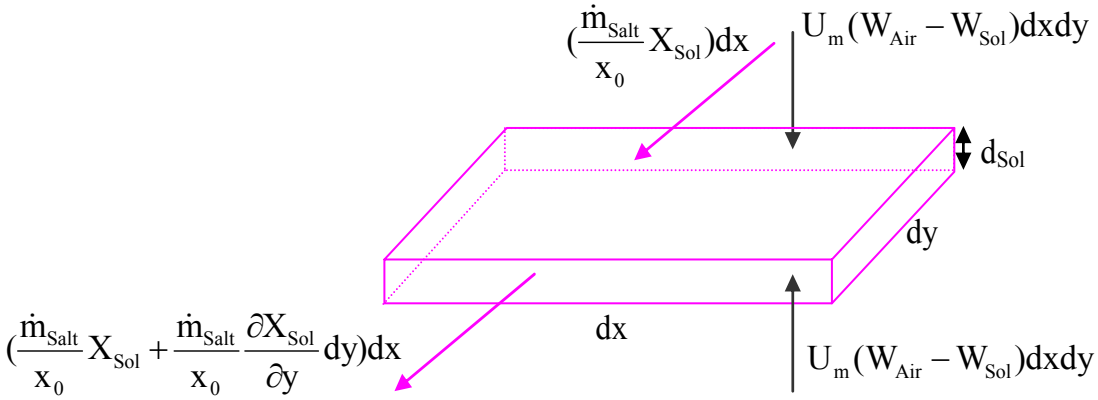

Figure B-2. Control volume of the liquid desiccant flow showing mass input and mass output.

The principle of conservation of mass for water gives:

$$\rho_{Salt} dx dy d_{Sol} \frac{\partial X_{Sol}}{\partial t} = 2U_m(W_{Air} - W_{Sol})dxdy - \frac{\dot{m}_{Salt}}{x_0} \frac{\partial X_{Sol}}{\partial y} dydx\,, \qquad \text{(B.1)}$$

which can be simplified to:

$$\rho_{Salt} d_{Sol} \frac{\partial X_{Sol}}{\partial t} + \frac{\dot{m}_{Salt}}{x_0} \frac{\partial X_{Sol}}{\partial y} - 2U_m(W_{Air} - W_{Sol}) = 0\,. \qquad \text{(B.2)}$$

Letting $t^*_{Sol} = \frac{tV_{Sol}}{x_0}$, $y^* = \frac{y}{y_0}$ and also assuming $V_{Salt} = V_{Sol}$ due to a well mixed solution gives:

$$\frac{\partial X_{Sol}}{\partial t^*} + \frac{\partial X_{Sol}}{\partial y^*} - \frac{2U_m x_0 y_0}{\dot{m}_{Salt}}(W_{Air} - W_{Sol}) = 0\,. \qquad \text{(B.3)}$$

By introducing

$$NTU_{m,Sol} = \frac{2U_m x_0 y_0}{\dot{m}_{Salt}}\,, \qquad \text{(B.4)}$$

gives:

$$\frac{\partial X_{Sol}}{\partial t^{*}_{Sol}} + \frac{\partial X_{Sol}}{\partial y^{*}} - NTU_{m,Sol}(W_{Air} - W_{Sol}) = 0\,. \qquad (B.5)$$

B.1.2. Air Side

Cutting out a stationary infinitesimal control volume within the air side of the heat exchanger as shown in Figure B-3 and assuming diffusion only in the z direction (neglecting mass diffusion in the x and y directions), the mass transfer equation can be developed.

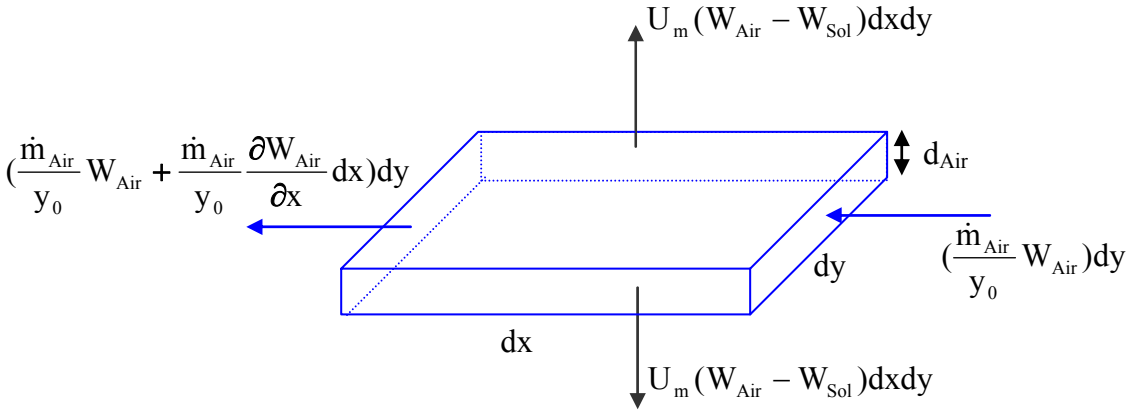

Figure B-3. Control volume of the air flow showing mass input and mass output.

The principle of conservation of mass for water gives:

$$\rho_{Air}dxdyd_{Air}\frac{\partial W_{Air}}{\partial t} = -2U_m(W_{Air} - W_{sol})dxdy - \frac{\dot{m}_{Air}}{y_0}dxdy\frac{\partial W_{Air}}{\partial x}\,, \qquad (B.6)$$

which can be simplified to:

$$\rho_{Air}d_{Air}\frac{\partial W_{Air}}{\partial t} + \frac{\dot{m}_{Air}}{y_0}\frac{\partial W_{Air}}{\partial x} + 2U_m(W_{Air} - W_{Sol}) = 0\,. \qquad (B.7)$$

Letting $t^*_{Air} = \frac{tV_{Air}}{x_0}$ and $x^* = \frac{x}{x_0}$ gives:

$$\frac{\partial W_{Air}}{\partial t^*} + \frac{\partial W_{Air}}{\partial x^*} + \frac{2U_m x_0 y_0}{\dot{m}_{Air}}(W_{Air} - W_{Sol}) = 0, \tag{B.8}$$

By introducing

$$NTU_{m,Air} = \frac{2U_m x_0 y_0}{\dot{m}_{Air}}, \tag{B.9}$$

gives:

$$\frac{\partial W_{Air}}{\partial t^*_{Air}} + \frac{\partial W_{Air}}{\partial x^*} + NTU_{m,Air}(W_{Air} - W_{Sol}) = 0. \tag{B.10}$$

B.2 Heat Transfer Equation

B.2.1 Liquid Side

Cutting out a stationary infinitesimal control volume within the liquid side of the heat exchanger as shown in Figure B-4 and assuming diffusion only in z direction (no heat diffusion in x and y directions), the heat transfer equations can be developed.

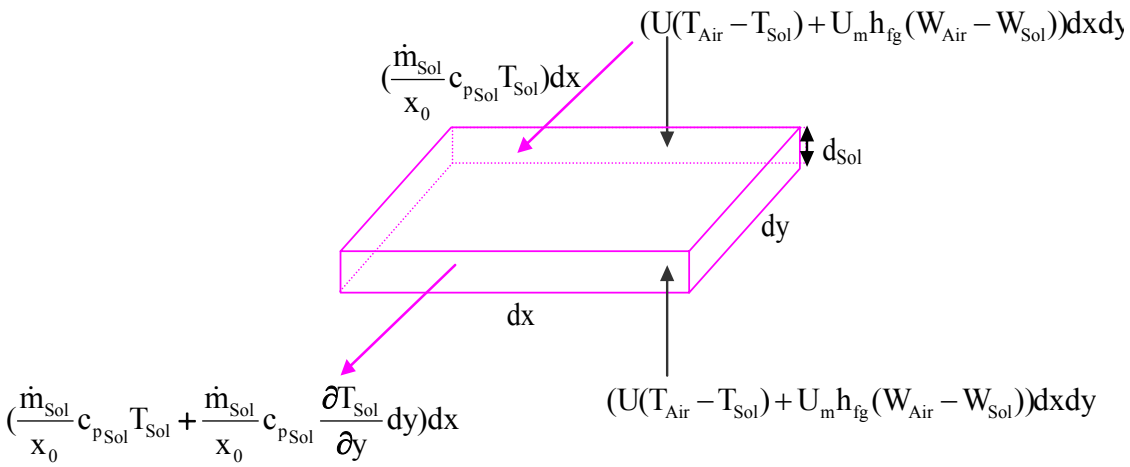

Figure B-4. Control volume of the liquid desiccant fluid showing energy input and energy output.

The principle of conservation of energy:

$$\rho_{Sol} dxdy d_{Sol} c_{pSol} \frac{\partial T_{Sol}}{\partial t} = -\frac{\dot{m}_{Sol}}{x_0} c_{pSol} \frac{\partial T_{Sol}}{\partial y} dxdy + 2U(T_{Air}-T_{Sol})dxdy + 2U_m (W_{Air}-W_{Sol}) h_{fg} dxdy \quad , \quad (B.11)$$

which can be simplified to:

$$\rho_{Sol} d_{Sol} c_{pSol} \frac{\partial T_{Sol}}{\partial t} + \frac{\dot{m}_{Sol}}{x_0} c_{pSol} \frac{\partial T_{Sol}}{\partial y} - 2U(T_{Air}-T_{Sol}) - 2U_m (W_{Air}-W_{Sol}) h_{fg} = 0 . \quad (B.12)$$

Letting $t^*_{Sol} = \frac{t V_{Sol}}{x_0}$, $y^* = \frac{y}{y_0}$ gives:

$$\frac{\partial T_{Sol}}{\partial t^*} + \frac{\partial T_{Sol}}{\partial y^*} - \frac{2U x_0 y_0}{C_{Sol}} (T_{Air}-W_{Sol}) - \frac{2U_m x_0 y_0}{C_{Sol}} (W_{Air}-W_{Sol}) h_{fg} = 0 . \quad (B.13)$$

By introducing:

$$NTU_{Sol} = \frac{2Ux_0y_0}{C_{Sol}}, \tag{B.14}$$

gives:

$$\frac{\partial T_{Sol}}{\partial t^*_{Sol}} + \frac{\partial T_{Sol}}{\partial y^*} - NTU_{sol}(T_{Air} - T_{Sol}) - \frac{NTU_{m,Sol}}{c_{pSol}(1+X_{Sol})} h_{fg}(W_{Air} - W_{Sol}) = 0. \tag{B.15}$$

B.2.2. Air Side

Cutting out a stationary infinitesimal control volume within the air side of the heat exchanger as shown in Figure B-5 and assuming no heat diffusion in the x and y directions (diffusion only in the z direction), the mass trasfer equation can be developed.

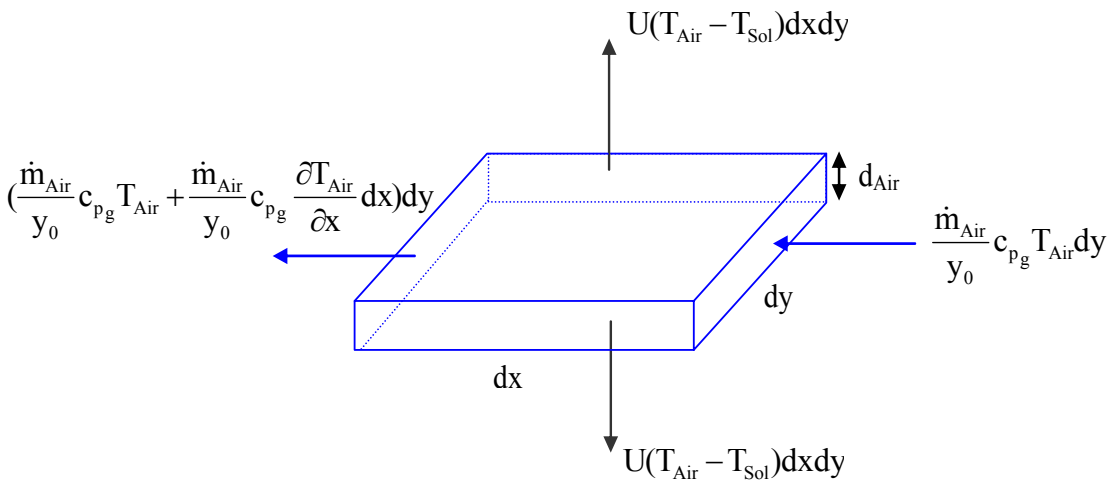

Figure B-5. Control volume of the air flow showing energy input and energy output.

The principle of conservation of energy:

$$\rho_g dxdyd_{Air} c_{p_g} \frac{\partial T_{Air}}{\partial t} = -\frac{\dot{m}_{Air}}{y_0} c_{p_g} \frac{\partial T_{Air}}{\partial x} dxdy - 2U(T_{Air} - T_{Sol})dxdy, \tag{B.16}$$

which can be simplified to:

$$\rho_g c_{p_g} d_{Air} \frac{\partial T_{Air}}{\partial t} + \frac{\dot{m}_{Air}}{y_0} c_{p_g} \frac{\partial T_{Air}}{\partial x} + 2U(T_{Air} - T_{Sol}) = 0. \quad \text{(B.17)}$$

Letting $t^*_{Air} = \frac{tV_{Air}}{x_0}$ and $x^* = \frac{x}{x_0}$ gives:

$$\frac{\partial T_{Air}}{\partial t^*} + \frac{\partial T_{Air}}{\partial x^*} + \frac{2Ux_0 y_0}{C_g}(T_{Air} - T_{Sol}) = 0, \quad \text{(B.18)}$$

where

$$C_g = \dot{m}_{Air}(c_{p_{Air}} + W_{Air} c_{p_v}). \quad \text{(B.19)}$$

By introducing:

$$NTU_{Air} = \frac{2Ux_0 y_0}{C_g}, \quad \text{(B.20)}$$

$$\frac{\partial T_{Air}}{\partial t^*_{Air}} + \frac{\partial T_{Air}}{\partial x^*} + NTU_{Air}(T_{Air} - T_{Sol}) = 0. \quad \text{(B.21)}$$

B.3 Normalized Governing Equations and Boundary Equations

The final governing equations and boundary conditions for the air and liquid are summarized as follows:

B 3.1 Liquid Side

$$\frac{\partial X_{Sol}}{\partial t^*_{Sol}} + \frac{\partial X_{Sol}}{\partial y^*} - NTU_{m,Sol}(W_{Air} - W_{Sol}) = 0, \quad \text{(B.22)}$$

and

$$\frac{\partial T_{Sol}}{\partial t^*_{Sol}} + \frac{\partial T_{Sol}}{\partial y^*} - NTU_{Sol}(T_{Air} - T_{Sol}) - \frac{NTU_{m,Sol}}{c_{p_{Sol}}(1 + X_{Sol})} h_{fg}(W_{Air} - W_{Sol}) = 0. \quad \text{(B.23)}$$

$$W_{Sol}\big|_{x^*=0} = W_{Sol,in}(X_{Sol,in}, T_{Sol,in}), \quad \text{(B.24)}$$

$$W_{Sol}\Big|_{t^*_{Sol}=0} = W_{Sol,Initial}(X_{Sol,Initial}, T_{Air,Indoor}), \tag{B.25}$$

$$T_{Sol}\Big|_{x^*=0} = T_{Sol,in}, \tag{B.26}$$

and

$$T_{Sol}\Big|_{t^*_{Sol}=0} = T_{Air,Indoor}. \tag{B.27}$$

B.3.2 Air Side

$$\frac{\partial W_{Air}}{\partial t^*_{Air}} + \frac{\partial W_{Air}}{\partial x^*} + NTU_{m,Air}(W_{Air} - W_{Sol}) = 0, \tag{B.28}$$

and

$$\frac{\partial T_{Air}}{\partial t^*_{Air}} + \frac{\partial T_{Air}}{\partial x^*} + NTU_{Air}(T_{Air} - T_{Sol}) = 0. \tag{B.29}$$

$$W_{Air}\Big|_{y^*=0} = W_{Air,in}, \tag{B.30}$$

$$W_{Air}\Big|_{t^*_{Air}=0} = W_{Air,Indoor}, \tag{B.31}$$

$$T_{Air}\Big|_{y^*=0} = T_{Air,in}, \tag{B.32}$$

and

$$T_{Air}\Big|_{t^*_{Air}=0} = T_{Air,Indoor}. \tag{B.33}$$

B.4 Discretization of the Normalized Governing Equations

The governing equations for each exchanger presented in section B.3 are discretised using the implicit finite difference technique for the time derivative and the upwind scheme for the first order space derivative. It needs to be mentioned that that (i) refers to the current node, (k) refers to the current time step and (j) refers to iteration number in the discretised equations. The discretized equations for the conservation of water and energy in the salt solution from equations (B.22) and (B.23), respectively are as follow:

$$X_{Sol}^{j,i,k} = \frac{\frac{X_{Sol}^{i,k-1}}{\Delta t^*} + \frac{X_{Sol}^{j,i-1,k}}{\Delta y^*} + NTU_{m,Sol}^{j-1,i,k}\left[W_{Air}^{j-1,i,k} - W_{Sol}^{j-1,i,k}\right]}{\frac{1}{\Delta t_{Sol}^*} + \frac{1}{\Delta y^*}}, \tag{B.34}$$

$$T_{Sol}^{j,i,k} = \frac{\frac{T_{Sol}^{i,k-1}}{\Delta t_{Sol}^*} + \frac{T_{Sol}^{j,i-1,k}}{\Delta y^*} + NTU_{Sol}^{j-1,i,k}T_{Air}^{j-1,i,k} + \frac{NTU_{m,Sol}^{j-1,i,k}}{c_{p,Sol}^{j-1,i,k}(1+X_{Sol}^{j,i,k})}h_{fg}\left[W_{Air}^{j-1,i,k} - W_{Sol}^{j-1,i,k}\right]}{\frac{1}{\Delta t_{Sol}^*} + \frac{1}{\Delta y^*} + NTU_{Sol}^{j-1,i,k}}, \tag{B.35}$$

and the discretized equations for the conservation of water and energy in the air from equations (B.28) and (B.29), respectively are as follow:

$$W_{Air}^{j,i,k} = \frac{\frac{W_{Air}^{i,k-1}}{\Delta t_{Air}^*} + \frac{W_{Air}^{j,i-1,k}}{\Delta x^*} + NTU_{m,Air}^{j-1,i,k}W_{Sol}^{j,i,k}}{\frac{1}{\Delta t_{Air}^*} + \frac{1}{\Delta x^*} + NTU_{m,Air}^{j-1,i,k}}, \tag{B.36}$$

$$T_{Air}^{j,i,k} = \frac{\frac{T_{Air}^{i,k-1}}{\Delta t_{Air}^*} + \frac{T_{Air}^{j,i-1,k}}{\Delta x^*} + NTU_{Air}^{j-1,i,k}T_{Sol}^{j,i,k}}{\frac{1}{\Delta t_{Air}^*} + \frac{1}{\Delta x^*} + NTU_{Air}^{j-1,i,k}}. \tag{B.37}$$

APPENDIX C
DEVELOPMENT OF GOVERNING EQUATIONS FOR STORAGE TANKS

In this section, assumptions and equations to calculate the outlet temperature concentration of storage tanks are presented in detail. As shown in Figure C-1, in order to develop the equations describing the conservation of mass and energy, one exchanger with a storage tank is considered as one control volume and a sub-system. It needs to mention that the exhaust sub-system, which is not shown, is similar to supply sub-system with a similar exchanger, storage tank and circulating pump.

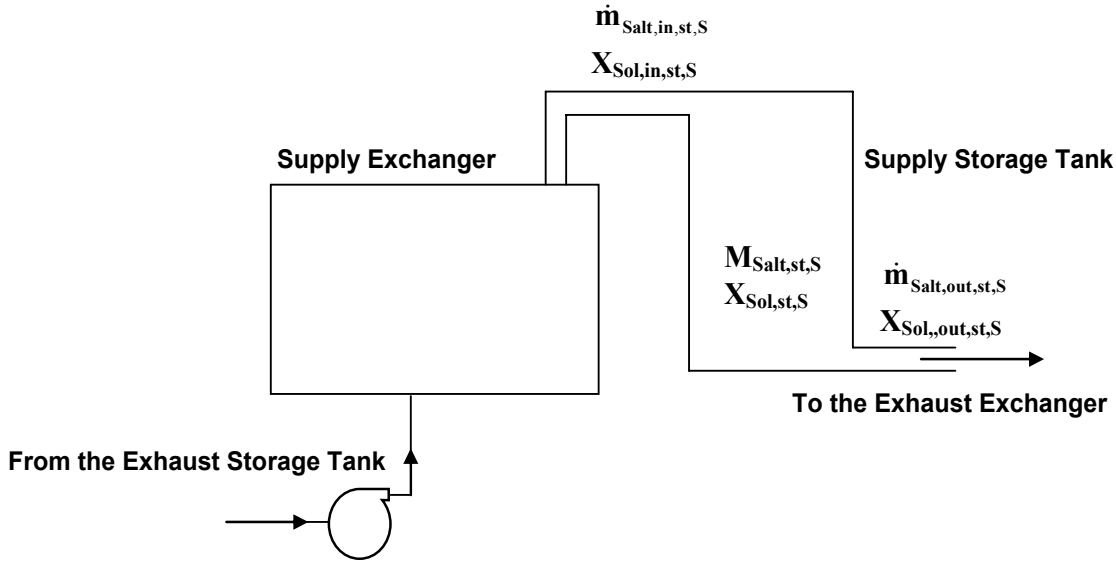

Figure C-1. Schematic of a storage tank and an exchanger showing the water mass fractions for the supply sub-system as a control volume.

C.1 Mass Balance Equation

The assumptions used in the analysis of mass balance for the control volume are as follows:

1. Storage tanks are well mixed, which infers that $X_{Sol,st} = X_{Sol,out,st}$ where $X = \frac{\text{Mass of Water}}{\text{Mass of Salt}}$

2. The total mass of salt in the entire system is constant ($M_{Salt,total}$ = const.).

3. The pump provides constant volume flow rate of salt solution in each sub-system (i.e. $Q_{Sol,S}$ = const.). However, pumps may provide different volume flow rates in each sub-system.

The principle of conservation of mass for water within the reservoir gives:

$$\frac{d}{dt}(M_{Salt,st,S}X_{Sol,st,S}) = \dot{m}_{Salt,in,st,S}X_{Sol,in,st,S} - \dot{m}_{Salt,out,st,S}X_{Sol,out,st,S}. \quad (C.1)$$

From the assumption (1) the above equation can be simplified to:

$$\frac{d}{dt}(M_{salt,st,S}X_{Sol,st,a}) = \dot{m}_{Salt,in,st,S}X_{Sol,in,st,S} - \dot{m}_{Salt,out,st,S}X_{Sol,st,S}, \quad (C.2)$$

Also, the principle of conversation of mass for pure salt within storage gives:

$$\frac{d}{dt}(M_{Salt,st,S}) = \dot{m}_{Salt,in,st,S} - \dot{m}_{Salt,out,st,S}, \quad (C.3)$$

where the mass flow rate of salt which enters to the supply storage tank can be calculated by knowing the volume flow rate of pump in the supply sub-system and change of salt solution concentration due to moisture transfer in the supply exchanger :

$$\dot{m}_{Salt,st,in,S} = (\rho_{Sol,out,ex,S}Q_S)/(1 + X_{Sol,out,ex,S}). \quad (C.4)$$

Besides, the outlet mass flow rate of the salt from the storage tank can be calculated as:

$$\dot{m}_{Salt,st,out,S} = (\rho_{Sol,st,S} Q_E)/(1 + X_{Sol,st,S}) . \quad (C.5)$$

The density of salt solution in Equation (C.5) depends on the temperature and concentration of the salt solution. The implication is that to solve the conservation of mass equations the temperature of salt solution should be known. By solving coupled conservation of mass and energy equations, we will be able to find the concentration and temperature of salt solution in the storage tank. In the next section the conservation of energy equations are presented.

C.2 Energy Balance Equation

In this section, assumptions and equations to calculate temperature and enthalpy of salt solution in the storage tanks are presented. As in the previous section, one exchanger with a storage tank shown in Figure C-2 is considered as one control volume and a sub-system in developing the governing equations.

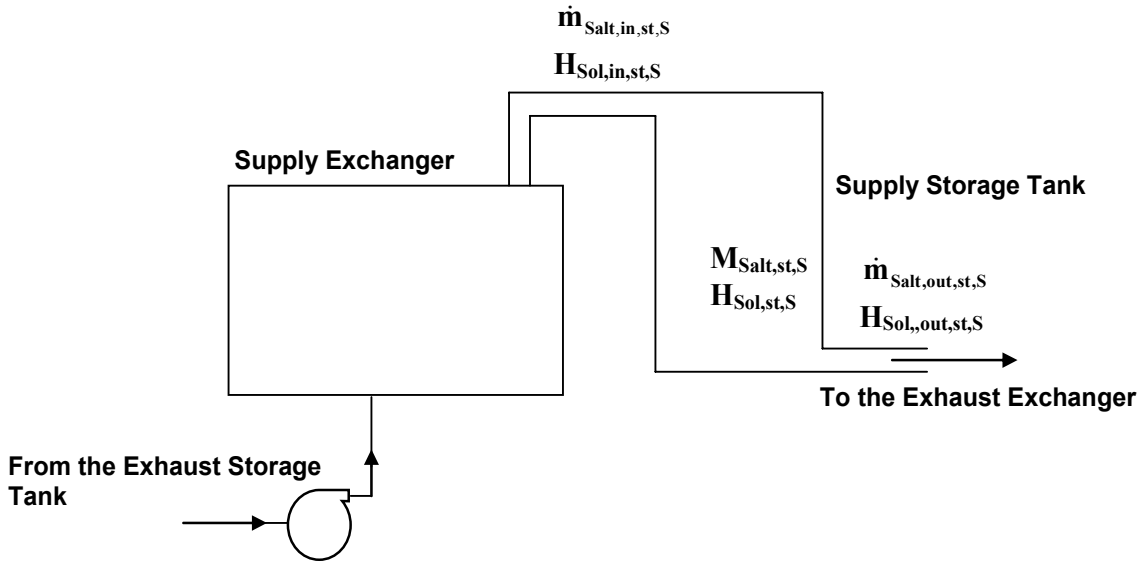

Figure C-2. Schematic of a storage tank and an exchanger showing the enthalpies for the supply sub-system as a control volume.

The assumptions used in the analysis of energy balance for the control volume are as follows:

1. Storage tanks are well mixed ($H_{Sol,st,S} = H_{Sol,out,st,S}$).

2. The heat loss/gain from/to the salt solution line is considered in the energy equation for the storage tank as an additional term.

The principle of conservation of energy for storage tank gives:

$$\frac{d}{dt}(M_{Sol,st,S}H_{Sol,st,S}) = \dot{m}_{Sol,in,st,S}H_{Sol,in,st,S} - \dot{m}_{Sol,out,st,S}H_{Sol,out,St,S} + q\,, \qquad (C.6)$$

From the assumption (1) the above equation can be simplified to:

$$\frac{d}{dt}(M_{Sol,st,S}H_{Sol,st,S}) = \dot{m}_{Sol,in,st,S}H_{Sol,in,st,S} - \dot{m}_{Sol,out,st,S}H_{Sol,st,S} + q\,. \qquad (C.7)$$

where $M_{Sol,st,S}$ is the mass of solution in the storage tank and can be calculated by knowing mass of salt and water content in the reservoir:

$$M_{Sol,st,S} = M_{Salt,st}\,(1 + X_{Sol,st,S})\,. \tag{C.8}$$

Also, the inlet and outlet mass flow rates of salt solution can be calculated as follow by knowing their pertinent concentration

$$\dot{m}_{Sol,in,st,S} = \dot{m}_{Salt,in,st,S}(1 + X_{Sol,in,st,S})\,, \tag{C.9}$$

and

$$\dot{m}_{Sol,out,st,S} = \dot{m}_{Salt,out,st,S}(1 + X_{Sol,st,S})\,. \tag{C.10}$$

The enthalpy of salt solution in the storage tank depends on several parameters (i.e. temperature, heat capacity of solution and reference enthalpy) and can be calculated as (Stephanopoulos 1984):

$$h_{Sol,st,S} = h_{Sol,st,S}(T_0) + c_{p\,Sol,st,S}(T_{Sol,st,S} - T_0)\,, \tag{C.11}$$

as well for inlet salt solution flow:

$$h_{Sol,in,st,S} = h_{Sol,in,st,S}(T_0) + c_{p\,Sol,in,st,S}(T_{Sol,in,st,S} - T_0)\,, \tag{C.12}$$

where T_0 is the reference temperature and at this temperature the enthalpy values are:

$$H_{Sol,st,S}(T_0) = \frac{X_{Sol,st,S}}{1+X_{Sol,st,S}} H_w + \frac{1}{1+X_{Sol,st,S}} H_{Salt} + \frac{1}{1+X_{Sol,st,S}} \Delta H_{Sol,st,S}(T_0)\,, \tag{C.13}$$

$$H_{Sol,in,,st,S}(T_0) = \frac{X_{Sol,in,St,S}}{1+X_{Sol,in,st,S}} H_w + \frac{1}{1+X_{Sol,in,st,S}} H_{Salt} + \frac{1}{1+X_{Sol,in,st,S}} \Delta H_{Sol,in,st,S}(T_0), \quad (C.14)$$

where, H_w and H_{Salt} are the specific enthalpies (joules per kilogram) of water and salt at reference temperature (T_0). Also, $\Delta H_{Sol,}$ is defined as heat of solution per kilogram of salt at the reference temperature. Now by defining:

$$A = \frac{X}{1+X}, \quad (C.15)$$

$$C_{Salt} = \frac{1}{1+X}, \quad (C.16)$$

and substituting Equations (C.11)-(C.14) to Equation (C.7)and rearranging:

$$\begin{aligned}
&\frac{d}{dt}\left[M_{Sol,st,S}\left(C_{Salt,st,S}\Delta H_{Sol,st,S}(T_0) + c_{p_{Sol,st,S}}(T_{Sol,st,S} - T_0)\right)\right] \\
&+ H_w\left[\frac{d}{dt}\left(A_{Sol,st,S}M_{Sol,st,S}\right) - A_{Sol,in,st,S}\dot{m}_{Sol,in,st,S} + A_{Sol,st,S}\dot{m}_{Sol,out,st,S}\right] \\
&+ H_{Salt}\left[\frac{d}{dt}\left(C_{Salt,st,a}M_{Sol,st,S}\right) - C_{Salt,in,st,S}\dot{m}_{Sol,in,st,S} + C_{Salt,st,S}\dot{m}_{Sol,out,st,S}\right] = . \quad (C.17) \\
&\dot{m}_{Sol,in,st,S}\left[C_{Salt,in,st,S}\Delta H_{Sol,in,st,S}(T_0) + c_{p_{Sol,in,st,S}}(T_{Sol,in,st,S} - T_0)\right] \\
&- \dot{m}_{Sol,out,st,S}\left[C_{Salt,st,S}\Delta H_{Sol,st,S}(T_0) + c_{p_{Sol,st,S}}(T_{Sol,st,S} - T_0)\right] + q
\end{aligned}$$

In Equation (C.17) conservation of mass for water and salt in the storage tank indicates that the coefficients of H_w and H_{Salt} are zero. Therefore, the energy equation can be simplified to:

$$\frac{d}{dt}\left[M_{Sol,st,S}\left(C_{Salt,st,S}\Delta H_{Sol,st,S}(T_0)+c_{p_{Sol,st,S}}(T_{Sol,st,S}-T_0)\right)\right]=$$
$$\dot{m}_{Sol,in,st,S}\left[C_{Salt,in,st,S}\Delta H_{Sol,in,st,S}(T_0)+c_{p_{Sol,in,st,S}}(T_{Sol,in,st,S}-T_0)\right]. \qquad (C.18)$$
$$-\dot{m}_{Sol,out,st,S}\left[C_{Salt,st,S}\Delta H_{Sol,st,S}(T_0)+c_{p_{Sol,st,S}}(T_{Sol,st,S}-T_0)\right]+q$$

APPENDIX D
THE ANZELIUS - SCHUMANS FUNCTIONS

In the analytical solution for differential equations of a transient model of a single cross flow heat exchanger developed by (Romie 1994), the Anzelius - Schuman functions, $G_0(\psi, \omega)$ and $F_0(\psi, \omega)$, and their extension were used. These functions are:

$$G_0(\psi,\omega) = \int_0^{\omega} G_{-1}(\psi,\omega')d\omega' = \exp(-\psi-\omega)\sum_{r=1}^{\infty}(\frac{\omega}{\psi})^{r/2} I_r(2\sqrt{\psi\omega}), \qquad (D.1)$$

and

$$F_0(\psi,\omega) = G_0(\psi,\omega) + G_{-1}(\psi,\omega), \qquad (D.2)$$

where

$$G_{-1}(\psi,\omega) = \frac{\partial G_0(\psi,\omega)}{\partial\omega} = \exp(-\psi-\omega)I_0(2\sqrt{\psi\omega}). \qquad (D.3)$$

In the above equations ψ and ω are positive and the I_r are modified Bessel functions of the first kind r^{th} order.

APPENDIX E
THE NUMERICAL MODEL ALGORITHM AND COMPUTER PROGRAM

This appendix presents the basic algorithm of the numerical solution for the Run-Around Membrane Energy Exchanger (RAMEE) using flow charts and the numerical code to simulate the transient behavior of the system.

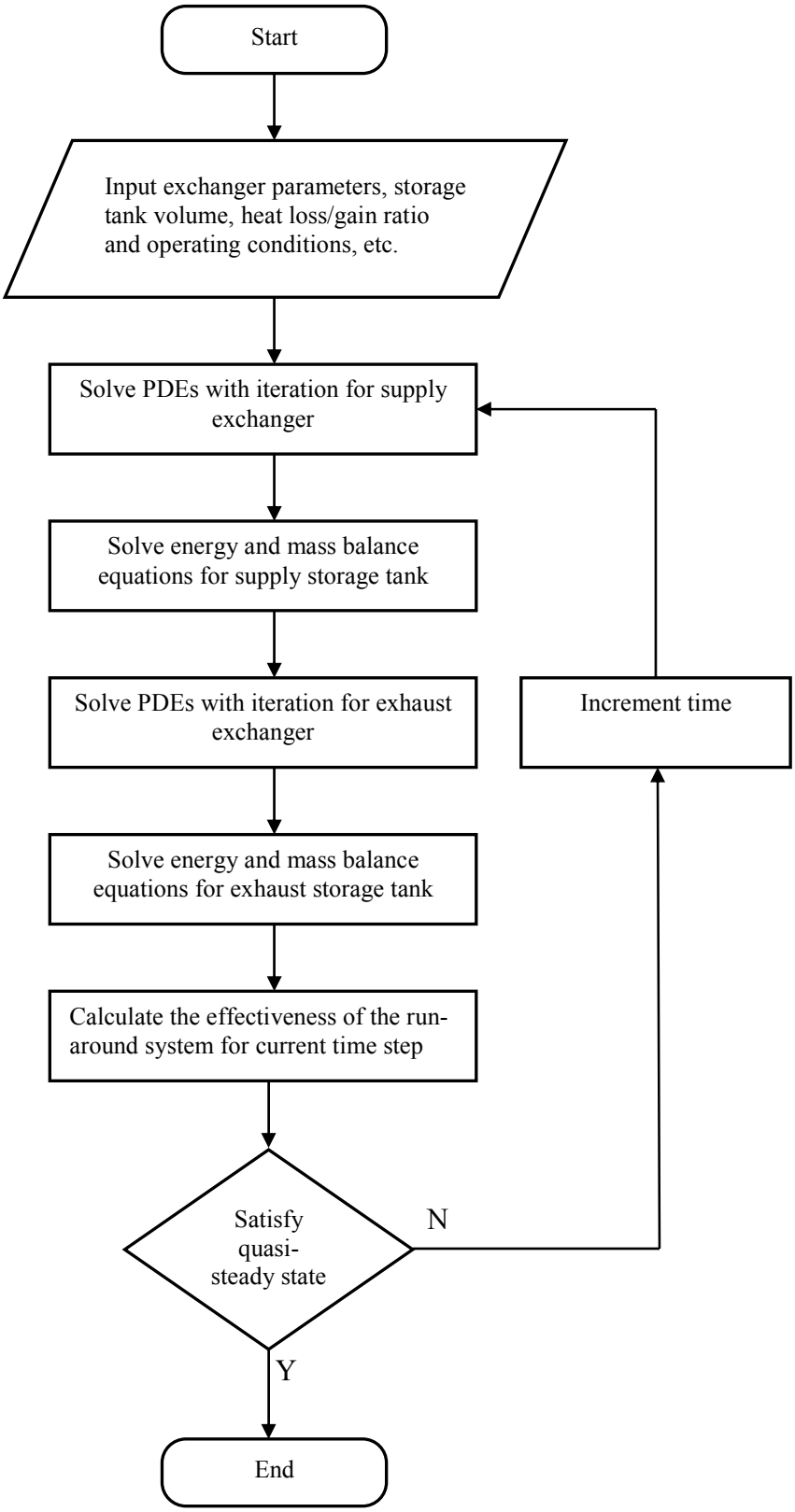
Start
Input exchanger parameters, storage tank volume, heat loss/gain ratio and operating conditions, etc.
Solve PDEs with iteration for supply exchanger
Solve energy and mass balance equations for supply storage tank
Solve PDEs with iteration for exhaust exchanger
Solve energy and mass balance equations for exhaust storage tank
Calculate the effectiveness of the run-around system for current time step
Satisfy quasi-steady state
N
Y
Increment time
End

This numerical code was written using PGI Visual FORTRAN (Microsoft Visual Studio 2005) and is given below:

```
Program RAMEE

  ******! Numerical code to simulate transient behavior of the Run-around Membrane Energy Exchanger (RAMEE) **********
                                  ***! By: Mehran Seyed Ahmadi***
                                  ***! 2007-2008***
Implicit none

!**Nodal parameters**!
integer::i,j
integer::m=100
integer::n=100
!*********************!

!**Time step parameters**!
integer,parameter::NT=3000
integer::N_T
real (8)::delta_t
!************************!

!**Exchanger physical parameters**!
real(8)::x_0,y_0,z_0
real(8)::d_M,d_A,d_S
real(8)::Channel_Num
real(8)::delta_x,delta_y
!*********************************!

!**Air properties**!
real(8)::T_Air_in,T_Air_in_E
real(8)::W_Air_in,W_Air_in_E
real(8)::M_Air
real(8),dimension(m,n)::T_Air,T_Air_E
real(8),dimension(m,n)::W_Air,W_Air_E
real(8),dimension(m,n)::T_Air_P,T_Air_P_E
real(8),dimension(m,n)::W_Air_P,W_Air_P_E
real(8),dimension(1,NT)::T_Air_Show,T_Air_Show_E
real(8),dimension(1,NT)::W_Air_Show,W_Air_Show_E
real(8)::T_Air_Out,W_Air_Out,C_Air_Out
real(8)::T_Air_Out_E,W_Air_Out_E,C_Air_Out_E
real(8),dimension(1,NT)::Error_Mass_Show_E
real(8)::C_Air_in,C_Air_in_E
real(8),dimension(m,n)::C_Air,C_Air_E
real(8)::h_Air
real(8)::h_Air_E
real(8),dimension(m,n)::Den_Air,Den_Air_E
real(8),parameter::h_fg=2501300
real(8)::M_Gas
real(8),dimension(m,n)::M_Gas_E
real(8),dimension(m,n)::Cp_g
real(8),dimension(m,n)::Cp_g_E
```

```
real(8)::X_Air_in,X_Air_in_E
real(8),dimension(m,n)::Den_g
real(8),dimension(m,n)::Den_g_E
!!*************************************!

!**Salt solution properties**!
real(8)::M_Sol
real(8)::M_Sol_E
real(8)::Volume_Sol_Total
real(8)::Q,Q_E
real(8),dimension(m,n)::T_Sol,T_Sol_E
real(8),dimension(m,n)::T_Sol_P,T_Sol_P_E
real(8)::T_Sol_in,T_Sol_in_E
real(8)::T_Sol_Out,T_Sol_Out_E
real(8),dimension(m,n)::X_sol,X_Sol_E
real(8),dimension(m,n)::X_Sol_P,X_Sol_P_E
real(8)::X_Sol_in,X_Sol_in_E
real(8)::X_Sol_Out,X_Sol_Out_E
real(8),dimension(m,n)::W_Sol,W_Sol_E
real(8)::W_Sol_Out,W_Sol_Out_E
real(8),dimension(m,n)::Cp_Sol,Cp_Sol_E
real(8),dimension(m,n)::C_Sol,C_Sol_E
real(8)::C_Sol_in,C_Sol_in_E
real(8)::C_Sol_Out,C_Sol_Out_E
real(8),dimension(m,n)::h_Sol,h_Sol_E
real(8),dimension(m,n)::Den_Sol,Den_Sol_E
real(8)::Den_Sol_in,Den_Sol_in_E
integer::Saturation
real(8),dimension(1,NT)::T_Sol_Show,X_Sol_Show,W_Sol_Show
real(8),dimension(1,NT)::T_Sol_Show_E,X_Sol_Show_E,W_Sol_Show_E
real(8)::Mass_Water,Mass_Water_E
real(8)::Mass_water_p
real(8)::Change_Solution_Water
real(8)::Mass_water_initial
real(8)::Mass_Sol,Mass_Sol_E,Mass_Sol_Total
real(8)::Mass_sol_p
real(8)::Volume_ratio
!*************************************!

!**Pure salt properties**!
real(8)::M_Salt
real(8)::M_Salt_E
real(8),dimension(m,n)::C_Salt
real(8)::Mass_Salt_E,Mass_Salt,Mass_salt_total
real(8)::Mass_salt_st,Mass_salt_st_E
real(8)::Mass_Salt_st_P,Mass_salt_st_P_e
!************************!

!**Pure salt constants**!
integer::SS
real(8)::Mw,Ms
real(8)::Ahta,Kai,Beta
real(8)::As,Bs,Cs,Ds,Es
real(8)::b1,b2,b3,b4
real(8)::d1,d2,d3
real(8)::D_swreal(8)::de1,de2,de3
```

```
real(8)::Salt_density
real(8)::Mol_Co
!**************************!

!**Storage tank properties**!
real(8)::Lo_Pe,Lo_Pe_E
real(8)::Den_Sol_st,Den_Sol_st_E
real(8)::Den_Water,a_c
real(8)::T_Sol_st,T_sol_st_E
real(8)::tc_sol_st,tc_sol_st_E
real(8)::T_sol_st_p,T_sol_st_p_E
real(8)::X_Sol_St,X_Sol_St_E
real(8)::X_Sol_st_P,X_Sol_st_p_E
real(8)::M_salt_in_st,M_salt_in_st_E
real(8)::M_salt_Out_st,M_salt_out_st_E
real(8)::Mass_sol_st,Mass_sol_st_E
real(8)::Mass_sol_st_p,Mass_sol_st_p_E
real(8)::Mass_Water_st,Mass_Water_st_E
real(8)::Mass_Ratio
real(8)::DL_Time,DL_Time_E
real(8),dimension(1,NT)::T_Sol_st_Show,X_Sol_st_Show,T_Sol_st_Show_E,X_Sol_st_Show_E
!**************************!

!**Performance and the system operation parameters**!
real(8)::C_r
real(8)::C_r_S,C_r_S_E
real(8)::Cm_r
real(8)::Cm_r_E
real(8),dimension(m,n)::U_h,U_h_E
real(8),dimension(m,n)::U_m,U_m_E
real(8),dimension(m,n)::NTU_Sol,NTU_Sol_E
real(8),dimension(m,n)::NTU_Air,NTU_Air_E
real(8),dimension(m,n)::NTU_mSol,NTU_mSol_E
real(8),dimension(m,n)::NTU_mAir,NTU_mAir_E
real(8)::NTU_Max,NTU_Max_E
real(8)::NTU_m_Max,NTU_m_Max_E

! Effectiveness values for LAMEEs based on heat and moisture transfer between air and salt solution
real(8)::Sensible_Effs,Sensible_Effs_E
real(8)::Latent_Effs,Latent_Effs_E
real(8)::Total_Effs,Total_Effs_E
real(8),dimension(1,NT)::Sensible_Effs_Show,Latent_Effs_show,Total_Effs_show
real(8),dimension(1,NT)::Sensible_Effs_Show_E,Latent_Effs_show_E,Total_Effs_show_E
!**************************!

! Effectiveness values for the RAMEE system based on heat and moisture transfer between supply and
exhaust air
real(8)::Eff_sensible,Eff_latent,Eff_Total
real(8),dimension(1,NT)::E_Total_Show_S,E_Sensible_Show_S,E_Latent_Show_S,E_Total_Show_E,E_S
ensible_Show_E,E_Latent_Show_E
!**************************!

!**Convergence criteria**!
real(8),parameter::relax_factor=1.
integer::CCa,CCs
integer::CCs_E,CCa_E
```

```
real(8)::residual,Residual_E
integer::me_c
real(8):: res_M,res_M_T,T_sol_old_M,X_sol_old_M
!************************!

!**Energy/mass balance**!
real(8)::Q_Air_E,Q_Sol_E,Q_Sol,Q_Air
real(8)::J_Sol_E,J_Sol
real(8)::error,error_mass
real(8)::Error_E,Error_mass_E
!**********************!

                    !!!!****Starting the main body of program****!!!!

! Choosing the type of salt solution
Print*,"*******Choose the salt solution********"
Print*,"1=LiBr   2=LiCl   3=MgCl2"
print*,"Enter the number:"
read*,SS

! Selecting the appropriate constants for the type of salt chosen
Call
Salt_Solution(SS,Mw,Ms,Ahta,Kai,As,Bs,Cs,Ds,Es,b1,b2,b3,b4,d1,d2,d3,D_sw,Beta,de1,de2,de3,Salt_den
sity,Mol_Co)

! Specifying all input values, initial values, exchanger sizes, nodes, and time step information
Call
Input_Values(T_Air_in,W_Air_in,T_Air_in_E,W_Air_in_E,T_Sol_in,X_Sol_in,x_0,y_0,z_0,m,n,delta_x,
delta_y,delta_t,d_M,d_A,d_S,M_Air,Q,Q_E,Volume_Sol_total,Lo_Pe,Lo_Pe_E)

! Calculating the constant values for mass, volume, mass flow rate, and volume flow rates for the RAMEE
system
Call
Constant_mass_volume_rates(W_Air_in,W_Air_in_E,T_Sol_in,X_Sol_in,x_0,y_0,z_0,d_M,d_A,d_S,M_
Air,M_Gas,M_Gas_E,Channel_Num,Den_Sol_in,Q,Q_E,Volume_sol_total,SS,DL_Time,DL_Time_E,Ma
ss_Sol_Total,Mass_Salt_Total,Volume_ratio)

! Calculating the heat capacity rate for the supply air inlet
Call
C_Air_Inlet(M_Air,W_Air_in,W_Air_in_E,C_Air_in,C_Air_in_E)

! Specifying initial values for all nodes in the surface
do i=1,m
do j=1,n
T_Air(i,j)=T_Air_in_E
T_Sol(i,j)=T_Sol_in
X_Sol(i,j)=X_Sol_in
W_Air(i,j)=W_Air_in_E
T_Air_P(i,j)=T_Air_in_E
T_Sol_P(i,j)=T_Sol_in
X_Sol_P(i,j)=X_Sol_in
W_Air_P(i,j)=W_Air_in_E
end do
end do

! Specifying a step change in the supply exchanger inlet conditions at t=0
```

```
do j=1,n
T_Air_P(1,j)=T_Air_in
W_Air_P(1,j)=W_Air_in
T_Air(1,j)=T_Air_in
W_Air(1,j)=W_Air_in
end do

me_c=0
! The above value is zero until the quasi-steady state is reached.  It is then changed to 1.

Saturation=0
! The above value is zero as long as saturation has not occurred.  It will change to 1 if saturation occurs and
give alarm

                    !****Calculating the RAMEE system properties for each time step****!
do N_T=1,NT

if (Saturation==0) then
! If the salt solution in the system has not reached saturation limit continue loop, otherwise exit

                    !*******Calculating the supply side properties******

residual=0
M_Sol=Q*Den_Sol_in/Channel_Num
M_Salt=M_Sol/(1+X_Sol_in)

Call
C_sol_in(T_Sol_in,X_Sol_in,b1,b2,b3,b4,C_Sol_in,M_Sol,M_Salt)

! Solving PDEs for the supply exchanger
do while (residual==0)
do i=1,m
CCs=0
do while(CCs==0)
! Calculating NTU, NTU_m and other properties for the salt solution in the supply exchanger
Call
NTU_S(SS,d_M,d_A,d_S,NTU_Sol,X_Sol,T_Sol,M_Sol,m,n,x_0,y_0,z_0,h_Sol,h_Air,i,C_Sol,Cp_Sol,De
n_Sol,U_h,M_Salt,W_Air_in,X_Sol_in,NTU_mSol,U_m,D_sw)

! Calculating the salt solution temperature and concentration for the supply exchanger with iteration
Call
GSs_solver(SS,m,n,NTU_Sol,NTU_mSol,U_m,T_Sol,T_Air,M_Sol,T_Sol_in,T_Air_in,X_Sol_in,X_Sol,
W_Air,W_Sol,delta_y,CCs,i,relax_factor,C_Sol,x_0,y_0,Cp_Sol,Den_Sol,d_S,delta_t,T_Sol_P,X_Sol_P,U
_h,M_Salt,Saturation)
end do
end do

do j=1,n
CCa=0
do while(CCa==0)
! Calculating NTU, NTU_m and other properties for air in the supply exchanger
Call
NTU_A(SS,d_M,d_A,d_S,NTU_Air,W_Air,T_Air,T_Sol,X_Sol,M_Air,m,n,x_0,y_0,z_0,j,C_Air,Den_g,C
p_g,M_Gas,U_h,Den_Air,h_Sol,h_air,M_Salt,Cp_Sol,W_Air_in,X_Sol_in,NTU_mAir,D_sw,U_m)

! Calculating the air temperature and humidity ratio for the supply exchanger with iteration
```

```
Call
GSa_solver(m,n,NTU_Air,NTU_mAir,T_Sol,T_Air,W_Sol,W_Air,T_Sol_in,T_Air_in,delta_x,CCa,j,relax
_factor,Den_g,Cp_g,d_A,y_0,T_Air_P,delta_t,M_Air,U_h,Den_Air,W_Air_P,U_m,M_Gas)
end do
end do

! Calculating the residual of PDEs for the supply side exchanger
Call
Res_Finding(d_M,d_A,d_S,m,n,T_Air,T_Sol,W_Air,X_Sol,M_Sol,delta_x,delta_y,U_m,residual,x_0,y_0,
C_sol,W_Sol,h_fg,Den_Sol,Cp_Sol,T_Sol_P,U_h,delta_t,Salt_Density,X_sol_P,M_Salt,Den_g,Cp_g,T_Ai
r_P,W_Air_P,Den_Air,M_Gas,M_Air)

if (residual==1) then
! Assigning calculated properties as properties for previous time step if the residual criteria is met
do i=1,m
do j=1,n
T_Air_P(i,j)=T_Air(i,j)
T_Sol_P(i,j)=T_Sol(i,j)
X_Sol_p(i,j)=X_Sol(i,j)
W_Air_P(i,j)=W_Air(i,j)
end do
end do

! Calculating the average outlet salt solution and air conditions and saving them for show and calculate
energy and moisture balances between solution and air sides for the supply exchanger
Call
Outlet(SS,T_Sol,C_Sol,X_Sol,m,n,T_Sol_Out,C_Sol_Out,X_Sol_Out,M_Salt,W_Sol_Out,Cp_Sol,T_Air,
W_Air,C_Air,T_Air_Out,W_Air_Out,C_Air_Out,M_Air,W_Air_in,X_Sol_in,T_Air_in,T_Sol_in,C_Sol_i
n,Q_Air,Q_Sol,Error,Error_mass,C_Air_in)

T_Sol_Show(1,N_T)=T_Sol_Out
X_Sol_Show(1,N_T)=X_Sol_Out
W_Sol_Show(1,N_T)=W_Sol_Out
T_Air_Show(1,N_T)=T_Air_Out
W_Air_Show(1,N_T)=W_Air_Out

! Calculating the effectiveness for the supply side of RAMEE ONLY (not the system) based on air and
solution heat and moisture transfer
Call
SEE(T_Air_in,T_Sol_in,T_Air_Out,T_Sol_Out,C_Air_Out,C_Sol_Out,Sensible_Effs,C_r_S,SS,W_Air_in
,W_Air_out,X_sol_in,M_Sol,M_Air,M_Salt,X_Sol_Out,Latent_Effs,Total_Effs,X_Air_in,C_Air_in)


! Calculating the total mass of salt in the supply exchanger
Call Salt_Sum(m,n,delta_x,delta_y,Den_sol,d_S,X_sol,Mass_Salt,Channel_Num,Mass_Sol,Mass_Water)

! Calculating the supply storage tank properties

! Specifying initial (1st time step) properties of the supply storage tank
if (N_T==1) then
Den_sol_st_E=Den_Sol_in
X_sol_st_E=X_Sol_in
X_Sol_st_P=X_Sol_in
T_sol_st_p=T_sol_in
Mass_Salt_E=Mass_Salt
Mass_salt_st=(Mass_salt_Total-Mass_Salt_E-Mass_Salt)/2.
```

```
Mass_salt_st_E=(Mass_salt_Total-Mass_Salt_E-Mass_Salt)/2.
Mass_Salt_st_P=Mass_Salt_st
T_sol_st=T_sol_out
Mass_sol_st=Mass_Salt_st*(1+X_Sol_in)
Mass_sol_st_p=Mass_sol_st
end if

res_M=1
res_M_T=1
T_sol_old_M=T_sol_Out
X_sol_old_M=X_sol_out
do while(res_M>1e-15.and.res_M_T>1e-15)
! Calculating the salt solution concentration in the supply storage tank
Call
Storage_tank(X_sol_out,T_sol_out,Den_sol_st_E,X_sol_st_E,Mass_salt_total,Mass_Salt_st_E,Mass_Salt,
Mass_Salt_E,Q,Q_E,X_Sol_st,T_Sol_st,SS,delta_t,X_Sol_st_P,Mass_Salt_st_P,Den_sol_st,Mass_salt_st,T
_sol_st_p,M_salt_in_st,M_salt_out_st,Mass_sol_st_p,Mass_sol_st,M_sol,Channel_Num)

! Calculating the salt solution temperature in the supply storage tank
Call
Storage_Tank_Tem(T_sol_Out,T_sol_St,T_sol_st_p,X_Sol_St,X_Sol_Out,Mass_salt_st,M_salt_in_st,M_s
alt_out_st,Mass_salt_st_p,X_Sol_st_p,delta_t,SS,Q_Sol,Lo_Pe,T_Sol_in,C_Sol_Out,Channel_Num,Mass_
sol_st_p,Mass_sol_st,M_sol)
res_M=abs(X_Sol_st-X_Sol_old_M)/X_Sol_st
res_M_T=abs(T_Sol_st-T_Sol_old_M)/T_Sol_st
T_sol_old_M=T_Sol_st
X_sol_old_M=X_Sol_st
end do

Mass_Salt_st_P=Mass_salt_st
Mass_sol_st_p=Mass_sol_st
tc_Sol_st=T_Sol_st-273.15
Den_Water=1000-0.062*tc_Sol_st-0.00355*tc_Sol_st**2
a_c=de1+(tc_Sol_st*de2)+((tc_Sol_st**2)*de3)
Den_Sol_st=10**(a_c/(1+X_Sol_st))*(Den_Water)
T_sol_st_P=T_Sol_st
X_Sol_st_P=X_Sol_st
T_Sol_st_Show(1,N_T)=T_sol_st
X_Sol_st_Show(1,N_T)=X_sol_st
Mass_sol_st=Mass_salt_st*(1+X_sol_st)
Mass_Water_st=Mass_sol_st-Mass_salt_st
end if
!!End of Calculation of the storage tank properties
end do
                !****************Calculating the exhaust side properties***************

! Assigning the exhaust exchanger inlet conditions the same as supply storage tank conditions
T_Sol_in_E=T_Sol_st
X_Sol_in_E=X_Sol_st
Den_Sol_in_E=Den_Sol_st
M_Sol_E=Q_E*Den_Sol_in_E/Channel_Num
M_Salt_E=M_Sol_E/(1+X_Sol_in_E)

Call
C_sol_in(T_Sol_in_E,X_Sol_in_E,b1,b2,b3,b4,C_Sol_in_E,M_Sol_E,M_Salt)
```

```
! Initiating the exhaust exchanger conditions for first time step
if (N_T==1) then
do i=1,m
do j=1,n
T_Air_E(i,j)=T_Air_in_E
W_Air_E(i,j)=W_Air_in_E
T_Sol_E(i,j)=T_Sol_in
X_Sol_E(i,j)=X_Sol_in
T_Air_P_E(i,j)=T_Air_in_E
T_Sol_P_E(i,j)=T_Sol_in
X_Sol_P_E(i,j)=X_Sol_in
end do
end do
else
! Setting inlet properties for the exhaust exchanger
do i=1,m
T_Sol_E(i,1)=T_Sol_in_E
X_Sol_E(i,1)=X_Sol_in_E
end do

end if

! The same method and subroutines as the supply side are used to calculate the exhaust exchanger and
storage tank properties
Residual_E=0

do while (residual_E==0)
do i=1,m
CCs_E=0
do while(CCs_E==0)
Call
NTU_S(SS,d_M,d_A,d_S,NTU_Sol_E,X_Sol_E,T_Sol_E,M_Sol_E,m,n,x_0,y_0,z_0,h_Sol_E,h_Air_E,i,
C_Sol_E,Cp_Sol_E,Den_Sol_E,U_h_E,M_Salt_E,W_Air_in_E,X_Sol_in_E,NTU_mSol_E,U_m_E,D_sw)

Call
GSs_solver(SS,m,n,NTU_Sol_E,NTU_mSol_E,U_m_E,T_Sol_E,T_Air_E,M_Sol_E,T_Sol_in_E,T_Air_i
n_e,X_Sol_in_E,X_Sol_E,W_Air_E,W_Sol_E,delta_y,CCs_E,i,relax_factor,C_Sol_E,x_0,y_0,Cp_Sol_E,
Den_Sol_E,d_S,delta_t,T_Sol_P_E,X_Sol_P_E,U_h_E,M_Salt_E,Saturation)
end do
end do

do j=1,n
CCa_E=0
do while(CCa_E==0)
Call
NTU_A(SS,d_M,d_A,d_S,NTU_Air_E,W_Air_E,T_Air_E,T_Sol_E,X_Sol_E,M_Air,m,n,x_0,y_0,z_0,j,C
_Air_E,Den_g_E,Cp_g_E,M_Gas_E,U_h_E,Den_Air_E,h_Sol_E,h_air_E,M_Salt_E,Cp_Sol_E,W_Air_in
_E,X_Sol_in_E,NTU_mAir_E,D_sw,U_m_E)

Call
GSa_solver(m,n,NTU_Air_E,NTU_mAir_E,T_Sol_E,T_Air_E,W_Sol_E,W_Air_E,T_Sol_in_E,T_Air_in
_E,delta_x,CCa_E,j,relax_factor,Den_g_E,Cp_g_E,d_A,y_0,T_Air_P_E,delta_t,M_Air,U_h_E,Den_Air_E
,W_Air_P_E,U_m_E,M_Gas_E)
end do
end do
```

```
Call
Res_Finding(d_M,d_A,d_S,m,n,T_Air_E,T_Sol_E,W_Air_E,X_Sol_E,M_Sol_E,delta_x,delta_y,U_m_E,r
esidual_E,x_0,y_0,C_sol_E,W_Sol_E,h_fg,Den_Sol_E,Cp_Sol_E,T_Sol_P_E,U_h_E,delta_t,Salt_Density,
X_sol_P_E,M_Salt_E,Den_g_E,Cp_g_E,T_Air_P_E,W_Air_P_E,Den_Air_E,M_Gas_E,M_Air)

if (residual_E==1) then
do i=1,m
do j=1,n
T_Air_P_E(i,j)=T_Air_E(i,j)
T_Sol_P_E(i,j)=T_Sol_E(i,j)
X_Sol_p_E(i,j)=X_Sol_E(i,j)
W_Air_P_E(i,j)=W_Air_E(i,j)
end do
end do

Call
Outlet(SS,T_Sol_E,C_Sol_E,X_Sol_E,m,n,T_Sol_Out_E,C_Sol_Out_E,X_Sol_Out_E,M_Salt_E,W_Sol_
Out_E,Cp_Sol_E,T_Air_E,W_Air_E,C_Air_E,T_Air_Out_E,W_Air_Out_E,C_Air_Out_E,M_Air,W_Air_
in_E,X_Sol_in_E,T_Air_in_E,T_Sol_in_E,C_Sol_in_E,Q_Air_E,Q_Sol_E,Error_E,Error_mass_E,C_Air_i
n_E)
T_Sol_Show_E(1,N_T)=T_Sol_Out_E
X_Sol_Show_E(1,N_T)=X_Sol_Out_E
W_Sol_Show_E(1,N_T)=W_Sol_Out_E
T_Air_Show_E(1,N_T)=T_Air_Out_E
W_Air_Show_E(1,N_T)=W_Air_Out_E
Error_Mass_Show_E(1,N_T)=Error_mass_E

SEE(T_Air_in_E,T_Sol_in_E,T_Air_Out_E,T_Sol_Out_E,C_Air_Out_E,C_Sol_Out_E,Sensible_Effs_E,C
_r_S_E,SS,W_Air_in_E,W_Air_out_E,X_sol_in_E,M_Sol_E,M_Air,M_Salt_E,X_Sol_Out_E,Latent_Effs
_E,Total_Effs_E,X_Air_in_E,C_Air_in_E)

Sensible_Effs_Show(1,N_T)=Sensible_Effs
Latent_Effs_show(1,N_T)=Latent_Effs
Total_Effs_show(1,N_T)=Total_Effs
Sensible_Effs_Show_E(1,N_T)=Sensible_Effs_E
Latent_Effs_show_E(1,N_T)=Latent_Effs_E
Total_Effs_show_E(1,N_T)=Total_Effs_E

Call
Salt_Sum(m,n,delta_x,delta_y,Den_sol,d_S,X_sol,Mass_Salt,Channel_Num,Mass_Sol_E,Mass_Water_E)
if (N_T==1) then
X_Sol_st_P_E=X_Sol_in
Mass_Salt_st_P_E=Mass_Salt_st_E
T_sol_St_E=T_sol_out_E
T_sol_st_p_E=T_sol_out_E
Mass_ratio=(Mass_salt+Mass_salt_E)/(Mass_Salt_Total)
Mass_sol_st_E=Mass_Salt_st_E*(1+X_Sol_in)
Mass_sol_st_p_E=Mass_sol_st_E
end if

res_M=1
res_M_T=1
T_sol_old_M=T_sol_Out_E
X_sol_old_M=X_sol_out_E

do while(res_M>1e-15.and.res_M_T>1e-15)
```

```
Call
Storage_tank_E(X_sol_out_E,T_sol_out_E,Den_sol_st,X_sol_st,Mass_salt_total,Mass_Salt_st,Mass_Salt,
Mass_Salt_E,Q,Q_E,X_Sol_st_E,T_Sol_st_E,SS,delta_t,X_Sol_st_P_E,Mass_Salt_st_P_E,Den_sol_st_E,
Mass_salt_st_E,T_sol_st_p_E,M_salt_in_st_E,M_salt_out_st_E,Mass_sol_st_p_E,Mass_sol_st_E,M_sol,C
hannel_Num)

Call
Storage_Tank_Tem(T_sol_Out_E,T_sol_St_E,T_sol_st_p_E,X_Sol_St_E,X_Sol_Out_E,Mass_salt_st_E,m
_salt_in_st_Em_salt_out_st_E,Mass_salt_st_p_e,X_Sol_st_p_E,delta_t,SS,Q_Sol_E,Lo_Pe_E,T_Sol_in_E,
C_Sol_Out_E,Channel_Num,Mass_sol_st_p_E,Mass_sol_st_E,M_sol)
res_M=abs(X_Sol_st_E-X_Sol_old_M)/X_Sol_st_E
res_M_T=abs(T_Sol_st_E-T_Sol_old_M)/T_Sol_st_E
T_sol_old_M=T_Sol_st_E
X_sol_old_M=X_Sol_st_E
end do
Mass_Salt_st_P_E=Mass_salt_st_E
Mass_sol_st_p_E=Mass_sol_st_E
tc_Sol_st_E=T_Sol_st_E-273.15
Den_Water=1000-0.062*tc_Sol_st_E-0.00355*tc_Sol_st_E**2
a_c=de1+(tc_Sol_st_E*de2)+((tc_Sol_st_E**2)*de3)
Den_Sol_st_E=10**(a_c/(1+X_Sol_st_E))*(Den_Water)
T_sol_st_P_E=T_Sol_st_E
X_sol_st_P_E=X_sol_st_E
T_Sol_st_Show_E(1,N_T)=T_sol_st_E
X_Sol_st_Show_E(1,N_T)=X_sol_st_E
Mass_sol_st_E=Mass_salt_st_E*(1+X_sol_st_E)
Mass_Water_st_E=Mass_sol_st_E-Mass_salt_st_E
end if
end do

! Calculating the total change in the system water mass during a time step
Change_Solution_Water=Channel_num*M_Salt*(X_Sol_Out-
X_Sol_in)+Channel_num*M_Salt_E*(X_Sol_Out_E-X_Sol_in_E)+(Channel_num*M_Salt*X_Sol_out-
Channel_num*M_Salt_E*X_Sol_in_E)+(Channel_num*M_Salt_E*X_Sol_out_E-
Channel_num*M_Salt*X_Sol_in)

! Checking if the quasi-steady state criteria is satisfied
Call
Balance_check(M_Salt,M_Salt_E,X_sol_in_E,X_Sol_out_E,Q_Air_E,Q_Air,Q_Sol,Q_Sol_E,me_c,M_Air
,W_Air_out_E,W_Air_in_E,X_sol_in,X_Sol_out,W_Air_Out,W_Air_in,N_T,Lo_Pe_E,Lo_Pe,Change_So
lution_Water,Channel_Num,T_Air_in,T_Air_in_E)

! Calculating the RAMEE system supply side effectiveness based on change in the air properties passing
through exchangers
Call
Effectiveness(Channel_Num,T_Air_in,M_Air,W_Air_in,h_fg,W_Air_in_E,T_Air_Out,W_Air_out,T_Air_
in_E,M_Salt,X_Sol_Out,X_Sol_in,C_Air_out,Eff_sensible,Eff_latent,Eff_Total,W_Air_Out_E,T_Air_out
_E)
E_Total_Show_S(1,N_T)=Eff_Total
E_Sensible_Show_S(1,N_T)=Eff_sensible
E_Latent_Show_S(1,N_T)= Eff_latent

! Calculating the RAMEE system exhaust side effectiveness based on change in air properties
Call
Effectiveness_E(Channel_Num,T_Air_in,M_Air,W_Air_in,h_fg,W_Air_in_E,T_Air_Out,W_Air_out,T_A
```

```
ir_in_E,M_Salt,X_Sol_Out,X_Sol_in,C_Air_out,Eff_sensible,Eff_latent,Eff_Total,W_Air_Out_E,T_Air_o
ut_E)
E_Total_Show_E(1,N_T)=Eff_Total
E_Sensible_Show_E(1,N_T)=Eff_sensible
E_latent_Show_E(1,N_T)=Eff_latent

! Assigning the supply exchanger inlet conditions as the exhaust storage tank conditions
T_Sol_in=T_Sol_st_E
X_Sol_in=X_Sol_st_E
Den_Sol_in=Den_Sol_st_E

do i=1,m
T_Sol(i,1)=T_Sol_in
X_Sol(i,1)=X_Sol_in
end do

else

goto 10

end if

! If the system has not reached quasi-steady state continue loop, otherwise exit
if (me_c==1) then
goto 10
end if

end do

10 continue

! Calculating the number of heat and mass transfer of the RAMEE system
Call NTU_Maximum(NTU_Air,NTU_Sol,NTU_Max,m,n)
Call NTU_Maximum(NTU_Air_E,NTU_Sol_E,NTU_Max_E,m,n)
Call NTU_m_Maximum(NTU_mAir,NTU_mSol,NTU_m_Max,m,n,M_Salt,M_Air,Cm_r)
Call NTU_m_Maximum(NTU_mAir_E,NTU_mSol_E,NTU_m_Max_E,m,n,M_Salt,M_Air,Cm_r_E)

! Writing output data on files
open(2,file="Temperature.dat")
do i=1,NT
write(2,100) T_Air_Show(1,i),T_Air_Show_E(1,i),T_Sol_Show(1,i),T_Sol_Show_E(1,i)
end do
close(2)

open(3,file="RelativeHumidity.dat")
do i=1,NT
write(3,200)
W_Air_Show(1,i),W_Air_Show_E(1,i),X_Sol_Show(1,i),X_Sol_Show_E(1,i),W_Sol_Show(1,i),W_Sol_S
how_E(1,i)
end do
close(3)

open(4,file="SupplyEff.dat")
do i=1,NT
write(4,300) Sensible_Effs_Show(1,i),Latent_Effs_show(1,i),Total_Effs_show(1,i)
end do
```

```
close(4)

open(5,file="ExhaustEff.dat")
do i=1,NT
write(5,300) Sensible_Effs_Show_E(1,i),Latent_Effs_show_E(1,i),Total_Effs_show_E(1,i)
end do
close(5)

open(7,file="RAMEE.dat")
write(7,400)NTU_Max,NTU_m_Max,Cm_r,C_r_S,Mass_salt_st,Mass_salt_st_E,Mass_Ratio,DL_Time,D
L_Time_E,Mass_salt_total,check
close(7)

open(8,file="Storage.dat")
do i=1,NT
write(8,100)T_Sol_st_Show(1,i),T_Sol_st_Show_E(1,i),X_Sol_st_Show(1,i),X_Sol_st_Show_E(1,i)
end do
close(8)

open(9,file="EFFSystem.dat")
do i=1,NT
write(9,200)E_Sensible_Show_S(1,i),E_Sensible_Show_E(1,i),E_Latent_Show_S(1,i),E_Latent_Show_E(
1,i), E_Total_Show_S(1,i),E_Total_Show_E(1,i),Error_Mass_Show_E(1,i)
end do
close(9)

100 format(4F16.8)
200 format(7F16.10)
300 format(3F16.8)
400 format(12F16.8)

End program RAMEE
```